REPORT DOCUMENTATION PAGE

Form Approved OMB NO. 0704-0188

1. REPORT DATE (DD-MM-YYYY)	2. REPORT TYPE	3. DATES COVERED (From - To)
29-04-2013	Final Report	-

4. TITLE AND SUBTITLE
Use of Bioresorbable hydrogels and genetic engineering to accomplish rapid stabilization and healing in segmental long bone defects

5a. CONTRACT NUMBER
W911NF-09-1-0040

5b. GRANT NUMBER

5c. PROGRAM ELEMENT NUMBER
8D10AS

6. AUTHORS
Michael H. Heggeness, Steven Stice, Alan R. Davis, Jennifer West, Elizabeth A. Davis, Francis H. Gannon, John Peroni, Eva Sevick

5d. PROJECT NUMBER

5e. TASK NUMBER

5f. WORK UNIT NUMBER

7. PERFORMING ORGANIZATION NAMES AND ADDRESSES
Baylor College of Medicine
Office of Research
Baylor College of Medicine
Houston, TX 77030 -3498

8. PERFORMING ORGANIZATION REPORT NUMBER

9. SPONSORING/MONITORING AGENCY NAME(S) AND ADDRESS(ES)
U.S. Army Research Office
P.O. Box 12211
Research Triangle Park, NC 27709-2211

10. SPONSOR/MONITOR'S ACRONYM(S)
ARO

11. SPONSOR/MONITOR'S REPORT NUMBER(S)
55387-MS-DRP.3

12. DISTRIBUTION AVAILIBILITY STATEMENT
Approved for Public Release; Distribution Unlimited

13. SUPPLEMENTARY NOTES
The views, opinions and/or findings contained in this report are those of the author(s) and should not contrued as an official Department of the Army position, policy or decision, unless so designated by other documentation.

14. ABSTRACT
The "Fracture Putty" project was initiated to develop better, faster and more efficient methods to treat dificult fractures. This contract supported study of hydrogel polymers, which are polymerized under direct control of the operating surgeon, and are also designed for biologic cleavage by osteoclast specific proteases. Processes in bone growth and repair were studied in cell cultrues, mice, rats, sheep, pigs, and feasibility of lymphatic imaging was demonstrated in humans. We believe this system is safe and efficacious and will lead to profound enhancements in

15. SUBJECT TERMS
single-step treatment, long bone fractures, segmental defects

16. SECURITY CLASSIFICATION OF:			17. LIMITATION OF ABSTRACT	15. NUMBER OF PAGES	19a. NAME OF RESPONSIBLE PERSON
a. REPORT	b. ABSTRACT	c. THIS PAGE			Michael Heggeness
UU	UU	UU	UU		19b. TELEPHONE NUMBER 713-986-5730

Report Title

Use of Bioresorbable hydrogels and genetic engineering to accomplish rapid stabilization and healing in segmental long bone defects

ABSTRACT

The "Fracture Putty" project was initiated to develop better, faster and more efficient methods to treat dificult fractures. This contract supported study of hydrogel polymers, which are polymerized under direct control of the operating surgeon, and are also designed for biologic cleavage by osteoclast specific proteases. Processes in bone growth and repair were studied in cell cultrues, mice, rats, sheep, pigs, and feasibility of lymphatic imaging was demonstrated in humans. We believe this system is safe and efficacious and will lead to profound enhancements in patient care.

Enter List of papers submitted or published that acknowledge ARO support from the start of the project to the date of this printing. List the papers, including journal references, in the following categories:

(a) Papers published in peer-reviewed journals (N/A for none)

Received	Paper

TOTAL:

Number of Papers published in peer-reviewed journals:

(b) Papers published in non-peer-reviewed journals (N/A for none)

Received	Paper

TOTAL:

Number of Papers published in non peer-reviewed journals:

(c) Presentations

Number of Presentations: 0.00

Non Peer-Reviewed Conference Proceeding publications (other than abstracts):

Received Paper

TOTAL:

Number of Non Peer-Reviewed Conference Proceeding publications (other than abstracts):

Peer-Reviewed Conference Proceeding publications (other than abstracts):

Received Paper

TOTAL:

Number of Peer-Reviewed Conference Proceeding publications (other than abstracts):

(d) Manuscripts

Received Paper

TOTAL:

Number of Manuscripts:

Books

Received Paper

TOTAL:

Patents Submitted

Patents Awarded

Awards

Graduate Students

NAME	PERCENT_SUPPORTED
FTE Equivalent:	
Total Number:	

Names of Post Doctorates

NAME	PERCENT_SUPPORTED
FTE Equivalent:	
Total Number:	

Names of Faculty Supported

NAME	PERCENT_SUPPORTED
FTE Equivalent:	
Total Number:	

Names of Under Graduate students supported

NAME	PERCENT_SUPPORTED
FTE Equivalent:	
Total Number:	

Student Metrics

This section only applies to graduating undergraduates supported by this agreement in this reporting period

The number of undergraduates funded by this agreement who graduated during this period:	0.00
The number of undergraduates funded by this agreement who graduated during this period with a degree in science, mathematics, engineering, or technology fields:.....	0.00
The number of undergraduates funded by your agreement who graduated during this period and will continue to pursue a graduate or Ph.D. degree in science, mathematics, engineering, or technology fields:.....	0.00
Number of graduating undergraduates who achieved a 3.5 GPA to 4.0 (4.0 max scale):	0.00
Number of graduating undergraduates funded by a DoD funded Center of Excellence grant for Education, Research and Engineering:	0.00
The number of undergraduates funded by your agreement who graduated during this period and intend to work for the Department of Defense	0.00
The number of undergraduates funded by your agreement who graduated during this period and will receive scholarships or fellowships for further studies in science, mathematics, engineering or technology fields:	0.00

Names of Personnel receiving masters degrees

NAME

Total Number:

Names of personnel receiving PHDs

NAME

Total Number:

Names of other research staff

NAME	PERCENT_SUPPORTED

FTE Equivalent:

Total Number:

Sub Contractors (DD882)

Inventions (DD882)

Scientific Progress

See attached.

Technology Transfer

1) **Fracture Putty Report**
    a. W911NF-09-1-0040
    b. Report, 12/15/10 – 02/13/12
    c. Baylor College of Medicine, University of Georgia, Rice University, University of Texas Health Science Center
    d. Michael H. Heggeness, M.D., Ph.D., Principal Investigator
    e. February 13, 2012
2) **The research effort is directed at devising a method for the single-step treatment of long bone fractures with segmental defects.**

Introduction

Extremity trauma is extremely common in war fighter casualties. Unfortunately, the management of high energy injuries, particularly to the lower limb is extremely challenging. Closed fractures of the lower leg (tibia and fibula) without other associated injuries represent formidable clinical challenges, and often fail to heal and ultimately result in an amputation. With more complex injuries, such as those that involve skin penetration or burn or blast injuries, war fighters and civilians usually require several months of treatment, including multiple surgical procedures to have any chance of avoiding an amputation.

The situation is markedly worsened in patients who have lost bone at the site of the injury, in the very best of circumstances, require at least 6 weeks of active treatment per centimeter of missing bone, to accomplish healing of the bone fracture with a missing The additional anatomic challenges of a limited blood supply, compounded by vascular injury, infection, soft tissue loss, and infection leaves us in the unfortunate situation of pursuing lengthy (often over more than a year) treatments only to accomplish a poorly functioning limb, or reluctantly proceed to amputation.

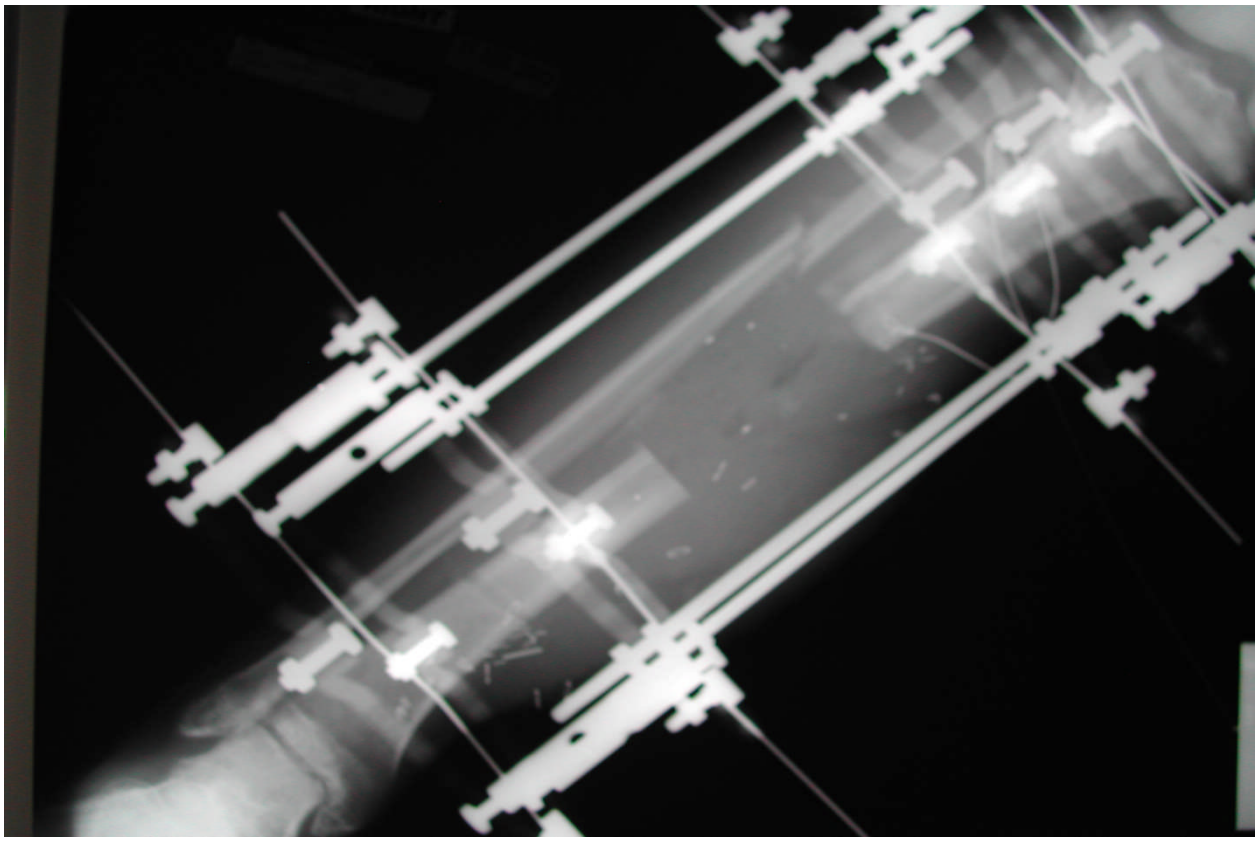

The DARPA “Fracture Putty” project was initiated to allow us to develop better, faster and more efficient methods to treat these difficult fractures, Ideally with a “one step procedure”, allow medical staff to place a “putty” into a fracture site that would rapidly supply stability and rapid bone healing that would hasten recovery, preserve function, and prevent the need for amputation.

Implementation

The Baylor College of Medicine team chose to develop a tissue engineering method that used a non-infectious adenoviral vector to induce very high levels of production of the human gene for Bone Morphogenic Protein 2, in short term (24 hour) cultures of cells. These cells, (which die within 48 hours of implantation, and are cleared from the host in 7 days) produce large amounts of this potent bone growth factor inducing an extremely rapid process of bone formation that is accomplished entirely by the host's cells. For most applications, the cells are embedded in "hydrogel" beads, which protect the cells from an immunologic response as they are producing the BMP2 growth factor. This also allows convenient handling of the material, and allows good control of its location in the body, or within a surgical wound. This method of tissue engineering was developed at the Baylor college of Medicine, with collaboration with Rice University investigators and is summarized as follows.

We tested a two component poly(ethylene glycol)-diacrylate (PEG-DA) hydrogel material, one which is an acellular biodegradable polymer that can provide structural stabilization to the critical defect and a second osteoinductive component to launch the rapid bone healing and soft tissue repair (Figure 1).

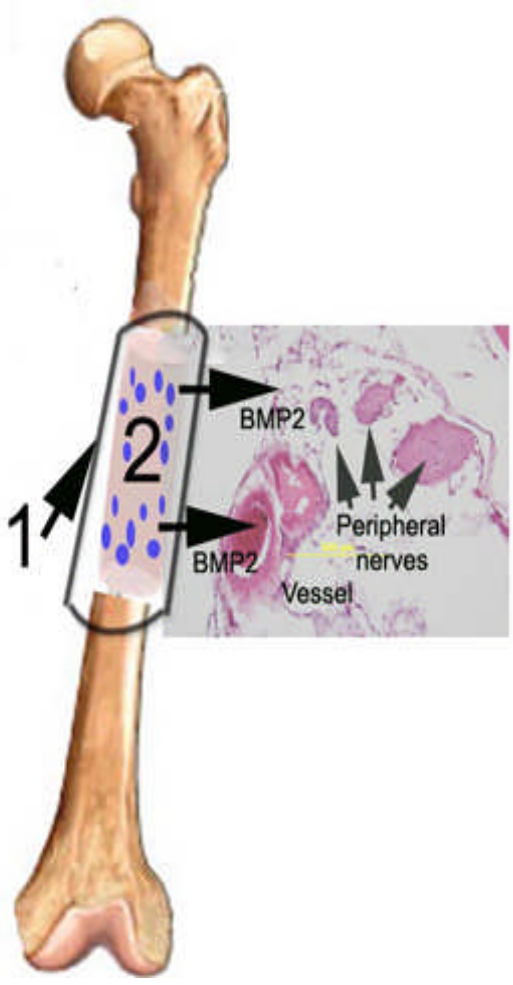

Figure 1. Fracture Putty. We depict our concept of fracture putty and its use in repair of a critical size defect. To first stabilize the bone, we will place a highly cross-linked hydrogel (1) with higher mechanical strength around each end of the bone, However, this hydrogel will not form a complete circle around the bone since a longitudinal slit is left for casting the less cross-linked hydrogel (2), allowing for BMP2 secretion from the gel, which contains BMP2-producing cells. Although the outside hydrogel is not designed for BMP2 secretion, it is designed not only to maintain bone mechanical strength while healing takes place, but is formulated in such a way as to ultimately be degraded by osteoclasts. After the outer hydrogel (1) is poured, the inner one, containing BMP2-producing cells is then poured (2), which is similarly formulated for ultimate degradation. Secretion of BMP2 into the surrounding tissue initiates the complex process of endochonral bone formation. Note that bone can be formed not only by heterotopic ossification as we have previously shown, but also by utilizing stem cells in the periosteum of the fractured bone, since we have intentionally engineered the system to take advantage of the speed of orthotopic ossification as well. We utilize hydrogels for 1) initial support 2) to maintain localized secretion of a powerful biological morphogen (BMP2). However, we also propose the manipulation of a complex biological process (endochondral bone formation) in the adjacent soft tissue to further maximize the speed of healing. For this we propose further engineering of BMP2 in an already powerful system for bone production. Finally, our recent discoveries (see below) of many of the parameters of this process, including the finding that the process recruits pluripotential cells from the sheath of local peripheral

Osteoinductive biomaterials must meet at least 4 criteria before they are considered for clinical orthopedic applications. (1) They must be able to deliver significant levels of osteoinductive agents such as BMP2 locally rather than systemically, (2) the materials must be sequestered within a targeted area, (3) the transduced cells or biomaterial should not elicit a significant immune response (4) the system should be easily degraded without toxicity. Our team has worked extensively to ensure that our system meets the goals of the first three criteria already and ongoing experiments show the feasibility of the fourth.

Briefly, our initial studies on the transduction of human cells with BMP2 expressing adenovirus we used standard adenovirus type 5 vectors [1]. Surprisingly, upon transduction of human mesenchymal stem cells (MSCs), BMP2 was not detectable by Western blotting, whereas high levels of the protein were produced by A549 (human lung carcinoma) cells transduced with the same virus. To account for this discrepancy, we speculated that the human MSCs lacked the receptor for adenovirus type 5, and subsequently, we demonstrated that human MSCs do not express the coxsackie-adenovirus receptor (CAR), accounting for the preceding result with the Ad5BMP2 vector[16]. This finding led us too develop a novel chimeric adenovirus vector, Ad5F35BMP2, which efficiently transduces human mesenchymal stem cells, generating high levels of BMP2. When Ad5BMP2 or Ad5F35BMP2 were compared *in vitro* for their ability to induce BMP2 synthesis in human mesenchymal stem cells and *in vivo* for their ability to stimulate formation of heterotopic bone, mineralized bone was radiologically identified only in the muscle of NOD/SCID mice that received the Ad5F35BMP2-transduced human MSCs[2]. Further our group went on to characterize this bone formation reaction to show that we could produce mineralized bone as rapidly as 7 days after delivery of the BMP2 producing cells [2]. Interestingly, we demonstrated that both the delivery cells [3] as well as the immunological background of the mouse [4] did not affect the progressive nature of this robust reaction, but rather was simply the ability to generate BMP2 within the localized area.

PEG-DA hydrogels are hydrophilic, polymeric networks that when formed from macromolecular precursors > 300, imbibe large quantities of water without dissolution and in doing so impart the physical characteristics of soft tissues. Moreover, the pores or mesh sizes of the hydrogel can be controlled by varying the molecular weight of the PEG-DA polymers so as to mediate the diffusion of gases, nutrients, and metabolites throughout the network [5] while simultaneously preventing interaction with antibodies, complement proteins, and immune cells. In addition, these hydrogels can be photopolymerized in any conformation with the use of biocompatible photoinitiators using visible or long wavelength ultraviolet (UV) light. Thus the cells are maintained at the target site and are unable to diffuse or enter the circulation, thus significantly reducing the risk of serious side effects from circulating cells expressing BMP2. Since BMP2 is known to be essential for acceleration of atherosclerosis, circulating cells expressing high levels of the BMP2 would greatly limit their use in this type of therapy.

In our initial studies, we determined an optimal formulation of PEG-DA hydrogels that would sequester the Ad5F35BMP2 transduced cells and elicit rapid endochondral bone formation [6]. Towards this goal, we first optimized the molecular weight of the polymer, mesh size, and BMP2 release kinetics to determine the molecular weight-cell number combination that yielded maximum BMP2 secretion, cell viability, and mechanical properties. We then demonstrated the ability of the hydrogel encapsulated cells to secrete BMP2 in a localized area, and produce endochondral bone [6]. One of the most significant findings of this study was the lack of any inflammatory response to the biomaterials, within the animal whether loaded with cells or just the material itself [6]. This was in sharp contrast to other biomaterials routinely used such as collagen, ceramics, or mineralized materials which elicit a significant GVHD response to the material. [7]

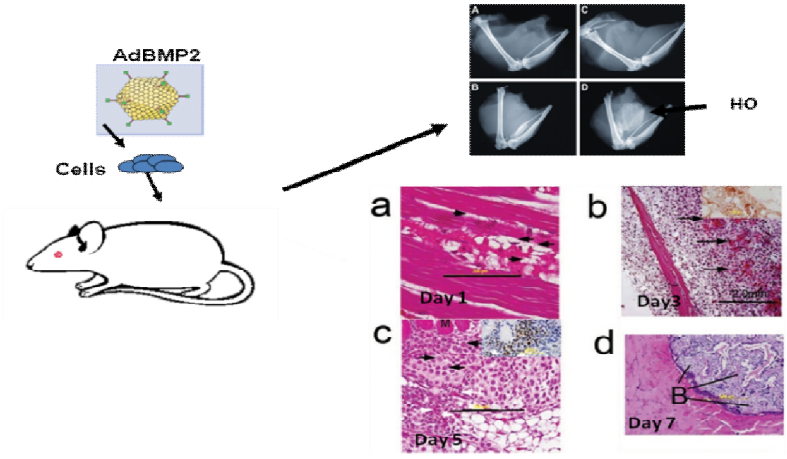

Figure 1: Model of BMP2-mediated bone formation. Ad5BMP2-transduced cells are injected into the quadriceps of a mouse. Heterotopic bone does not form in control anima when no vector (A) or empty vector (B), or Ad5lac (C) are used to transducer the cells. Bone forms rapidly when Ad5BMP2 (D) is used. Endochondra bone formation, where bone is formed by way of cartilage intermediate then ensues (compare Fig to Fig 1d). Specific and synchronous series of stages are achieved in this model. On day 1 brow adipocytes are observed, on day 3 new vessels ar

In Figure 1 we show our model for bone formation. When we inject AdBMP2 transduced cells into the quadriceps of a mouse bone formation begins. Although any cell type can be used, since these cells only serve to produce BMP2, it is important that in immunocompetent animals, these cells be from the same species so that a host versus graft response is not elicited. In some cases cells must be used that do not have the receptor for adenovirus. To overcome this, we have characterized procedures, in collaboration with Dr. Steven Stice, that overcome this roadblock in mice [4] as well as larger animals [10], and do not see why this approach should not be universally applicable. For humans, mesenchymal stem cells prepared from the same individual to be treated would be utilized. We have also previously shown that human mesenchymal stem cells can be efficiently transduced by Ad5F35 vectors to produce BMP2 [2].

One of the first cells that we observe after injection of BMP2-producing cells is the brown adipocyte [18]. This cell serves two purposes, on one side of the cell uncoupled oxidative phosphorylation, mediated by UCP-1, causes a hypoxic microenvironment suitable for chondrogenesis. This is shown in Figure 2 where we note co-staining of markers of hypoxia and UCP-1(not shown) and PGC1-α, both markers of the brown adipocyte. On the other side of the cell, one sees new vessels formation

mediated by VEGF-D (fos-induced growth factor, not shown), an important growth factor in the formation of vessels [19] and also important in lymphangiogenesis [20].

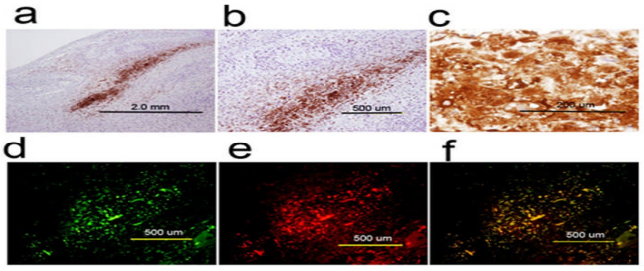

Figure 2. Brown adipocytes generate hypoxia in tissue stimulated with BMP2. Hypoxic regions appear in and near the site of injection. On day 3 after injection of BMP2-producing cells, mice were injected with pimonidazole, which was subsequently detected with an antibody against this compound (Hypoxyprobe monoclonal antibody). One of the hypoxic regions is shown (a, b, c). Sections obtained at day 3 and embedded in paraffin were double-labeled with antibodies against pimonidazole (Hypoxyprobe; d, green) and PGC-1 (e, red). f: merger of d and e shows the close correlation between hypoxia and the brown adipocyte.

We have previously noted that injection of BMP2-producing cells in the mouse quadriceps is totally dependent on recruitment of stem cells from the murine host and that the

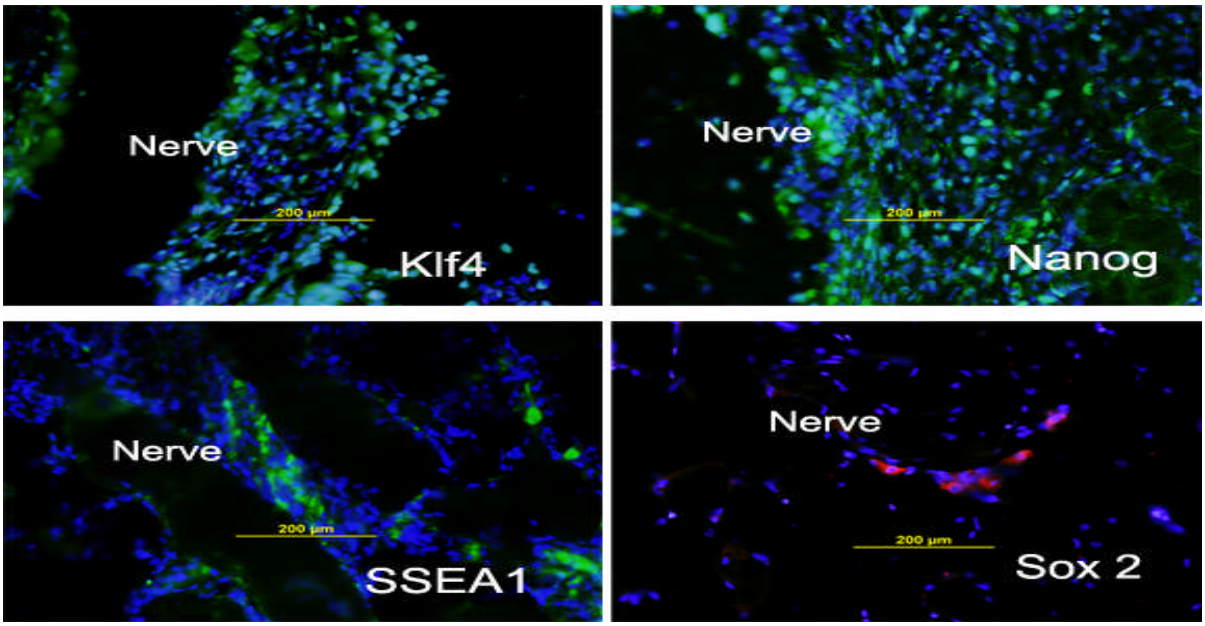

re 3: Expression enes involved in ipotency in HO. ffin sections ined from the limbs of mice 4 after injection MP2 producing were stained mouse oclonal odies against Nanog, SSEA1, ox 2 and then bated with anti-

injected cells play no role in the process [2]. We have noted that these stem cells are housed in the sheath of local peripheral nerves (Figure 3) and express the four markers of pluripotency recently shown to be necessary and sufficient for conversion of somatic cells to embryonic stem cells.

These cells appear to be one of the earliest cell types produced in the tissues after delivery of the BMP, and we hypothesize that they are an essential component to establishing the micro-environment for bone production. This includes, inducing peripheral nerve growth into the newly forming bone, as well as establishment of the vasculature including lymphatics.

In Figures 4 and 5 we note that UCP-1 positive cell (Figure 4) and MMP-9 positive cells are present in peripheral nerves and appear to migrate from the nerves towards the BMP2. Our data suggests that the UCP1 positive cells are critical to oxygen regulation within the tissues, but preliminary data also suggests that these cells are critical to the establishment of the vasculature. They produce VEGFs in response to the BMP as well as appear to assemble into tiny new vessel structures (data not shown). Figure 5 shows the expression of MMP9 in the outlayer of the peripheral nerve cells as they appear to be migrating towards the BMP2. MMP9 plays a major role in establishment of bone the vasculature as well as lymphatics (sinusoidal vessels) essential for homing and delivery of stem cells for tissue repair. Again the data collectively suggests that these nerve sheath cells are essential for establishing early bone formation. These findings are essential to our development of a biomaterial for critical size defect, since the data suggests that extensive soft tissue injury could significantly inhibit the ability for bone to heal. We propose that in understanding the contribution of these tissues we can rapidly recapitulate this even in a scenario of extensive soft tissue loss by delivery of these components ex vivo through the osteoinductive biomaterial. Thus we propose not only to test our second generation hydrogels but to develop even more powerful materials that could be efficacious even in the worst clinical scenarios.

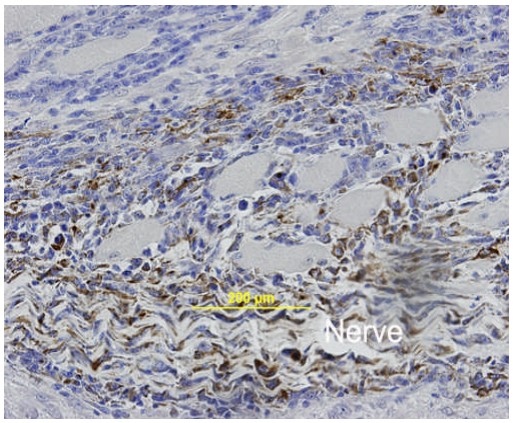

Figure 4. Expression of UCP1 in cells migrating off the sheath of peripheral nerves 3 days after injection of BMP2-producing cells.

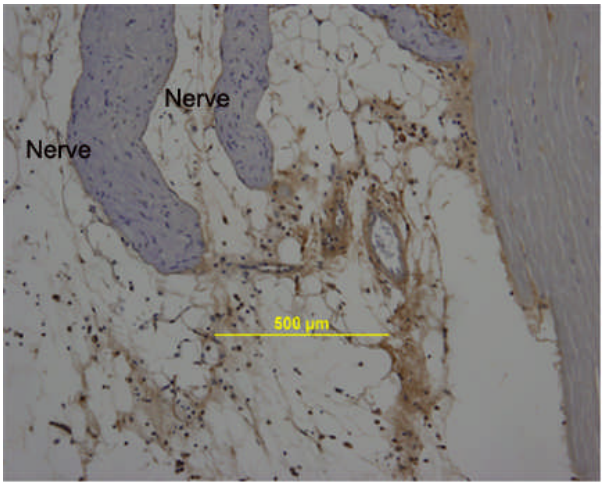

Figure 5: MMP9 expression in peripheral nerve sheath cells

After fracture, the first change is the blood cells within the tissues which are adjacent to the injury site. Soon a hematoma forms which is the beginning of the fracture repair process. It has been shown that the fracture hematoma is essential for the bone repair process[21]. In our experimental model of bone formation, we see in detail, the influence of these inflammatory cells on the process. One of the first is the mast cell. In Figure 6 we see a simple histochemical stain, toluidine blue, for mast cells at various times after injection of BMP2-producing cells. It is obvious that mast cells are predominant in peripheral nerves as well as in and around vessels. In uninjected mice there were no mast cells observed in peripheral nerves and only a very few at other points in the tissue (not shown). These mast cells have previously been shown [22] to be present in the disease fibrodysplasia heterotypica ossificans (FOP) a human disease where heterotopic bone formation is extensive due to the presence of a constitutively active BMP receptor. In addition, mast cells play a key role in the pathogenesis of the peripheral nerve sheath disease neurofibromatosis [23]. The major protein mutated in neurofibromatosis is NF1 and we provide evidence below that NF1 is involved heterotopic bone formation, most likely in modulating movement of stem cells from the nerve sheath. We observed dramatic changes in NF1 expression in our model, during the earliest stages of endochondral bone formation (fig 7)

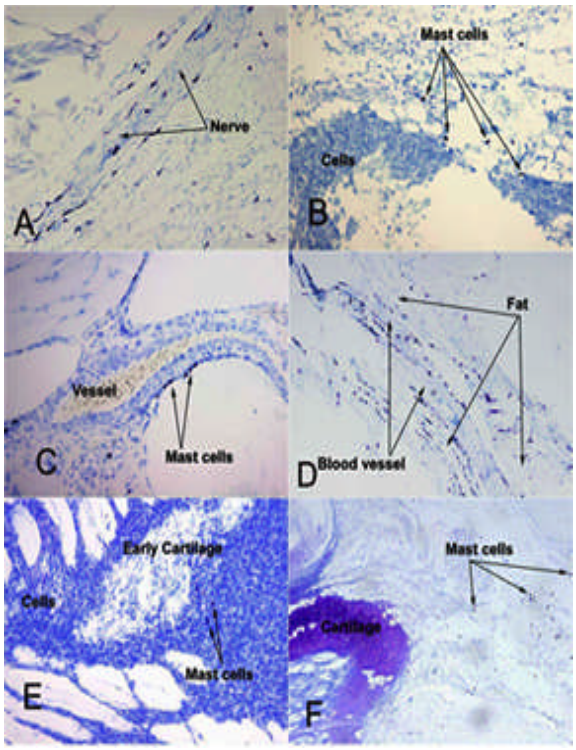

Kinetics of mast cell tion after injection of ducing cells. Mice :ted with BMP2- cells at day 0. Frozen /ere obtained from mice d on day 1, A; day 2, B; lay 5, D; day 6, E; and

Use of imaging and molecularly targeted imaging agents to monitor bone formation. While radiographic imaging can provide images of

progressive calcification, we propose to employ innovative imaging methods to assess implant neovascularization (both angiogenesis and lymphangiogenesis), cellular ingrowth, and bone differentiation by molecularly detecting key steps that can be altered with biological modifiers that can enhance the efficacy of the implant. In addition, since inflammatory responses during biological reabsorption can lead to edema, osteolytic reactions and ultimately, failure, we also develop methods to provide early detection of failures. By applying imaging methods early in the development phase, the opportunity to diagnostically image the progress of fracture putty healing in the battlefield can be readily realized. In this portion of the application, we present methods for imaging key molecular signaling events associated with different stages of osteoconduction that indicate both bone repair and failure in the rat tibia, femur, and sheep metatarsals. Specifically, we focus upon detecting (i) extracellular matrix reorganization provided by key cells providing the earliest steps of ossification, (ii) angiogenesis for blood vascularization within the implant, (iii) lymphangiogenesis both within the implant and in surrounding soft tissues, and (iii) differentiation of osteoblast precursers.

C3a. .Extracellular Matrix reorganization. Recently, in our BMP-2 model, we have identified the influx mast cell and eosinophil infiltration, similar to that reported by [24] in their treatment of calvaria defects treated with collagen sponges. Mast cells uniquely express chymases, or serine proteases, which has been recently shown to process pro-matrix metalloprotease 9 and 2 (pro-MMP-9 and pro-MMP-2) into their active forms (MMP-9 and MMP-2)[25]. MMP-2 and -9 are gelatinases and degrade denatured collagen. Thus the infiltration of mast cells provides a means for regulating gelantinase activity in the ossification process. From screening of peptide libraries, Koivunen *et al.* identified a cyclic CTT peptide c(CTTHWGFTLC) with potent inhibitory activity against MMP-2/9 [26]. However, this peptide is highly susceptible to non-specific degradation *in vivo* [27]. Based upon the CTT peptide, a new cyclic peptide c(KAHWGFTLD)NH_2 targeting MMP-2 was developed through SAR analysis [28].

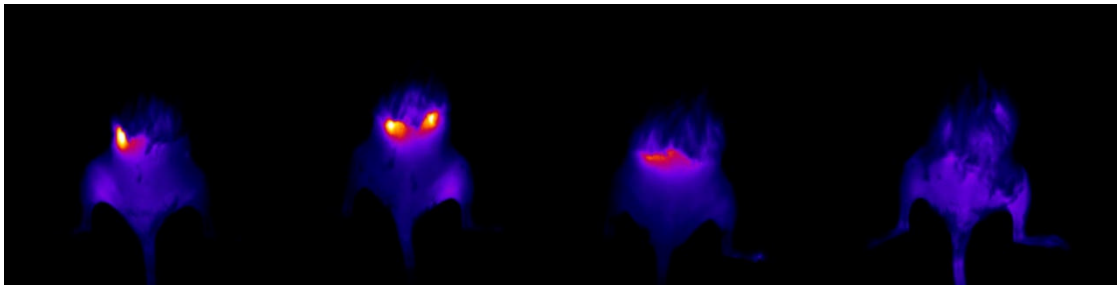

Figure 9. From Left to Right: Typical NIR fluorescence images of the dorsal view of SCID mouse with right hindlimb injected with BMP-2 producing cells and the left hindlimb injected with fibroblasts. At 2 days after injection, there is some MMP-9 expression in control side, but maximal expression in the tissue region 4 days after inoculation with BMP-2 producing cells. Expression diminishes at 6 days. In the case of the scrambled peptide where specificity is expected to be lose, no binding occurs at 4 days after BMP-2 cell injection. (unpublished, Kwon, Sevick, Davis, Olmsted-Davis)

The peptide conjugate, DOTA-SA-K(IRDye800)-c(KAHWGFTLD)NH_2, was dual-labeled with a near-infrared dye, IRDye800, and DOTA for chelation of ^{64}Cu for positron emission tomography imaging. A scrambled peptide was also used as control. MRC5 cells transduced with Ad5F35BMP2 and Ad5F35-control were injected into a hind-leg muscle and the opposite side hind limb as a control in SCID mice. Animals were divided into three groups as 2, 4, and 6 days after injection of BMP2 expressing cells. At 6 hrs after i.v. injection of imaging agents at a dose equivalent to 200 uCi of ^{64}Cu and 5 nmol of IRDye800, fluorescence imaging and PET/computed tomography (CT) scans were performed.
Our in vivo imaging results showed the transient expression of activated MMP-2 and/or -9 in the hindlimb region implanted with the BMP-2 producing cells, with peak expression at 4 days after inoculation (Figure 9).

Since PET is clinically applicable, we also demonstrated localization of the imaging agent with PET imaging (Figures 10 and 11). It is noteworthy that in Figure 10, the MMP imaging agent deposition precedes calcification as seen in x-ray CT.

Figure 10 An example fused x-ray CT and PET (orange) image showing the deposition of the imaging agent in the limb at the site of the arrow.
(unpublished, Kwon, Sevick, Davis, Olmsted-Davis)

Transaxial Coronal

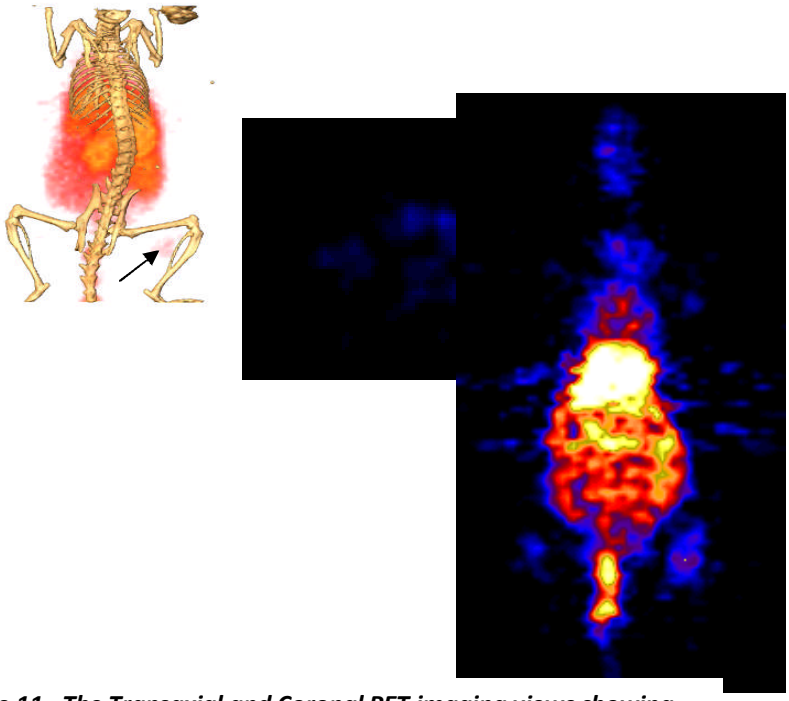

Figure 11. The Transaxial and Coronal PET imaging views showing the tissue region associated with the BMP-2 producing cells will higher contrast from the imaging agent (Arrows). At 6 hours, agent clearance from the animal is not complete, hence the signal in the liver and gut as well as along the bladder and tail (unpublished, Kwon,

The fluorescence and PET images showed that the mean target to background ratio value is the highest in animals 4 days after injection of fibroblasts transduced to express BMP-2 and decreases in mice 6 days after administration. These result correlated well with immunohistochemical staining of tissues isolated from amputated limbs. Our data suggests that molecular imaging of early ossification using specific targeting PET/NIR agent against activated gelatinases.. *In this work, we will use both PET/CT and NIR imaging to follow Mast cell secreted chymase activity to regulate MMP activity in the early ECM remodeling surrounding and invading the implant. We will use PET and NIR imaging for evaluating non-invasively while use frozen sections of tissues to correlate MMP activity with Mast cell location.*

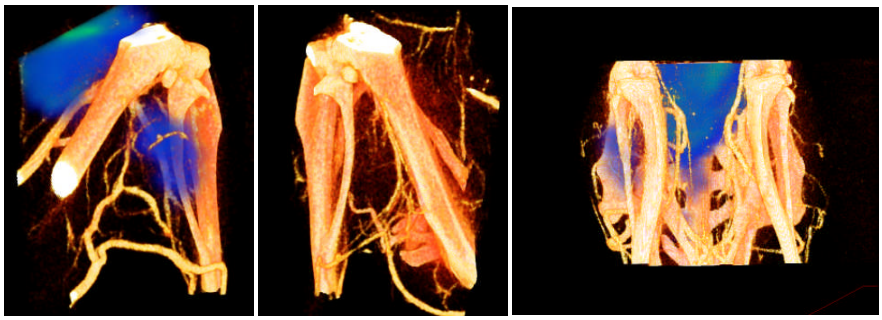

Figure 12: MicroCT and PET overlay of site where (center) control

C3b. Integrin activity. The successful integration of bone graft materials during ossification is well known to depend upon its microvascularization, most notably hemo-angiogenesis. The integrin receptor, $\alpha_v\beta_3$ is strongly expressed in neovascularization and inflammation. A dual labeled imaging agent for NIR/SPECT and gamma imaging, DTPA-Bz-SA Lys(IRDye800)-c(KRGDf), and for NIR/PET imaging DOTA- Lys(IRDye800)-c(KRGDf) targeting integrin $\alpha_v\beta_3$ has recently been developed [29 30]. Using the BMP-2 model of heterotopic bone, we employed anatomical and molecular imaging techniques to assess longitudinally, the progressive changes of early disease associated with integrin receptor, $\alpha_v\beta_3$. In these initial studies (presented herein in brevity for space limitations), we employed CT for bone imaging, CT with Fenestra for vascular contrast, and PET imaging of 61-Cu-DOTA RGD-Cy5.5 for assessing early tissue remodeling. Figure 12 shows the fused PET and Fenestra contrast CT of the hindlimbs of a mouse 9 days after injection of fibroblasts transduced to express BMP-2 (close-up left), fibroblasts transduced with the empty cassette control virus (close-up center) injected with control vector, and entire hind portion for the animal. The microCT shows the lack of mineralization deposits in the muscle, while Fenestra contrast shows dilated and angiogenic vessels that are predominant in the muscle inoculated with BMP2 producing cells. PET imaging with the RGD agent shows the blue "blush" surrounding vessels in the limb injected with BMP2-producing cells (left panel) while none occurs at the control site (center panel). RGD predominantly binds cells undergoing migration and these results show that angiogenesis occurs prior to bone deposition and may be playing an important role in "niche" preparation enabling the construction of "transport" highways for trafficking of progenitor cells.. *These results demonstrate that the early events associated with heterotopic bone formation can be non-invasively and longitudinally imaged in the BMP2 model that progresses to match the clinical endpoint of CT diagnosis of a zonal peripheral bone. More specifically, we already have the capability*

to non-invasively measure the vasculogenesis that is associated with stem cell migration to site of ossification.

C3c. Lymphangiogenesis. The successful integration of bone graft materials during ossification is well known to depend upon its microvascularization, most notably hemo-angiogenesis. Lymphangiogenesis, or the generation of new lymphatic vessels is also associated with wound healing, yet the presence of lymphatics in bone is controversial since the thin-walled, dilated blood vessels (sinusoids) are morphologically similar the lymphatic capillaries. With the recent availability of podoplanin and PROX1 staining to uniquely identify lymphatic endothelial cells (LECS), Edwards and coworkers [31] have shown that normal bone is devoid of lymphatics. However, in the diseases with extensive bone remodeling, (i.e., lymphangioma, Gorham-Stout disease, primary benign and malignant bone tumors, and secondary carcinomas to the bone) lymphangiogenesis occurs within the bone and lymphatics have been identified within cortical tissues. Most recently, Kilian and coworkers [32] showed that the process of lymphangiogenesis occurred within metaphyseal bone defects filled with biodegradable nanoparticles of hydroxyapatite impants within a cylindrical defects of the right femur condyle of mini-pigs. Indeed, clinical evidence also suggests that the lymphatics play a critical role in fracture repair. With normal healing of tibial fracture, foci of ossification are accompanied by immune cell infiltrates, dilated lymphatics, and enlarged lymph nodes in surrounding tissues [33]. Successful implants are also associated with increased lymphatic vessel proliferation at the bone-implant interface in patients undergoing total hip replacement [34] [35] [36] and to be the mechanism of lymphangiogenesis and spurned by lymphangiogenic factors such as PDGF, FBF, and VEGFC. *In this application, we will conduct longitudinal studies of functional lymphatic imaging in animal models to evaluate lymphangiogenesis both in the bone as well as in surrounding soft tissues. We will also employ a novel molecular imaging agent to detect activated LECs that result in lymphatic vessel dilation and sprouting from existing lymphatic vessels.*

C3d. Lymphatic imaging in human subjects. In the ending feasibility study funded by an American Cancer Society Scholar Grant to the P.I., we imaged the arms or legs of 24 normal subjects and 20 subjects with Stage I or II, unilateral lymphedema have been studied with NIR fluorescence enhanced optical lymph imaging following multiple administrations of 25 ug of IC-Green in 0.10 cc at varying sites. Total dose is less than or

equivalent to 400 ug of IC-Green. No adverse events were seen and skin color did not impact imaging results. In the following, we demonstrate results that illustrate for the first time, propulsive lymph flow imaged non-invasively in humans.

In the hands,

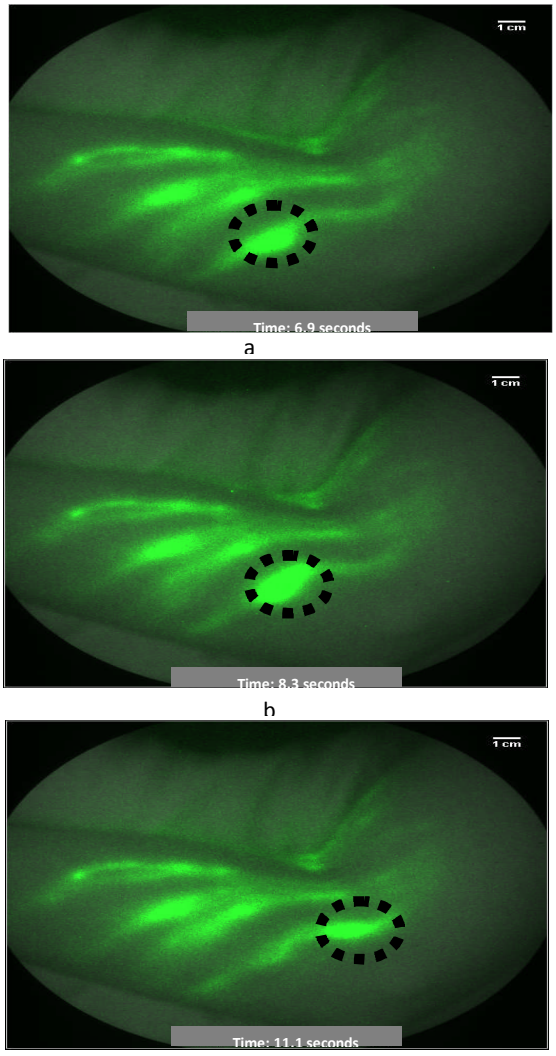

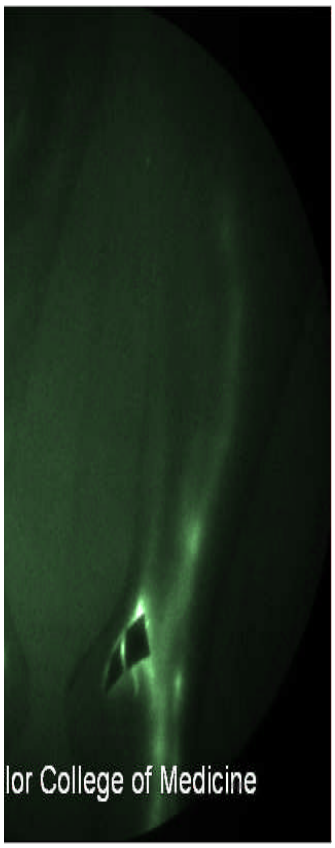

hot from supplemental video
depicting the symmetric
phatic bundles in the lower
old normal female subject
e position. The medial ankle
sites were covered with
opaque plastic to prevent oversaturation of the CCD camera. The apparent "packet" velocity within the ventromedial lymphatic

Figure 13: Set of image frames depicting in vivo lymphatic trafficking of IC-Green in the medial forearm and elbow of a normal 22 year-old Caucasian male resting in a supine position with his arm above his shoulder. The subject was administered four intradermal injections of 25 µg IC-Green diluted in 0.10 cc of saline in the webs

100 µg of IC-Green in 0.40 cc of saline was administered in equal portions interdigitally and along the ankle bone using conventional 27 gauge needles. Almost immediately following administration, trafficking of lymph fluid

"packets" from the site of injections through the radial and ulnar lymphatic bundles could be visualized with fluorescent imaging (Figure 13a-c) heel, on the calf, posteromedially and in the thigh anteromedially showed propulsive lymph flow within the ventromedial lymph bundle of the legs (Figure 14). Deep lymph vessels such as the dorsolateral bundle feeding the popliteal lymph nodes as well as the deep femoral vessels were visualized in thin subjects, but images were particularly diffused owing to tissue scattering properties. In the arms or legs, the lymph propulsion occurred at apparent velocities between 0.4 and 2.6 cm/s and appeared at intervals between 3.2 and 198.8 seconds in the data from 23 normal subjects analyzed thus far. No correlation was found between blood pressure or heart rate and the frequencies or velocities of propelled lymph "packets."

C3e.NIR fluorescence imaging. The ability to follow the processes of endochondral bone formation through non-invasive measures provides us a powerful tool for optimizing and implementing our biomaterials clinically. A major component of this is the ability to identify cellular events through optical imaging by systemic injection of optical dyes. To this end our group under the direction of Dr. Sevick has designed a novel method and instrument for this purpose. Figure 15 illustrates the basics instrumentation design for the optical imagers used in the preclinical and clinical studies in the Sevick laboratory. The system consists of a near infrared laser diode which emits 785 nm light incident upon the tissue surfaces at fluence rates that are less than 1.9 mW/cm^2. Since NIR propagates deeply through tissues, the incident light serves to excite NIR fluorescent agents which we use as contrast agents. The emitted fluorescence is red-shifted from the incident light and passes through a series of optical filters designed to reject scattered excitation light and pass the fluorescent light. The NIR fluorescent light is then collected by the photocathode of a Gen III image intensifier, which converts the NIR fluorescent image on the photocathode to an image a phosphor screen for collection by a 16-bit frame transfer camera. Integration times are between 50 and 800 msecs and the series of images can be combined to generate a movie showing the dynamics of lymphatic trafficking. Our group has also designed systems so that the intensifier and laser diode can be gain modulated for frequency-domain photon migration (FDPM) measurements for tomographic 3-D reconstruction. In this seedling project, we choose not to employ tomography as planar imaging is sufficient to gather the information required for establishing feasibility

or monitoring tissue hydration, and responses to injury and immune challenge. In addition to its tissue penetration capabilities, NIR light does not excite any endogenous fluorophores that could otherwise generate high background levels when visible wavelengths are employed. Thus the NIR system is optimal for deep tissue penetration and low background imaging.

Currently, the only contrast agent available for human NIR fluorescence imaging is indocyanine green (ICG), which is a dark green dye approved for intravenous administration for hepatic and ophthalmological diagnostic tests. Fortuitously, the agent can be excited at 785 nm and the fluorescence at 830 nm and provides a sufficient Stoke's shift to be efficiently collected. ICG has a terrible quantum efficiency of 0.03. The dye, sold as IC-Green (Akorn Pharmaceuticals, Buffalo Grove, IL), is approved for intravenous administration, at 2 mg/kg up to a total maximum of 25 mg, for use in hepatic clearance as well as assessing retinopathy studies. However, ICG does not have a functional group for conjugation to molecularly targeting entities such as antibodies, aptamers, or peptides. Instead, the agent associates with albumin in the blood and provides a unique opportunity to translate NIR instrumentation into vascular imaging. Recently a number of NIR excitable fluorophores with functional groups for conjugation have become commercially available, (i.e., AlexaFluor750 from InVitrogen, Carlsbad CA; IRDye 800CW, Li-Cor, Lincoln Nebraska, and Cy7.5, Amersham/GE Healthcare) thus expanding the opportunities for NIR molecular imaging. Unfortunately, none are approved for human use. We are currently working with Li-Cor to employ their IRDye800 CW imaging agent which has a 30 fold increase in quantum efficiency, for human studies. We have conducted safety and toxicity studies on the IRDye800 CW and find that like ICG, it is rapidly eliminated from the body. Future work will involve securing FDA approval for a lymph

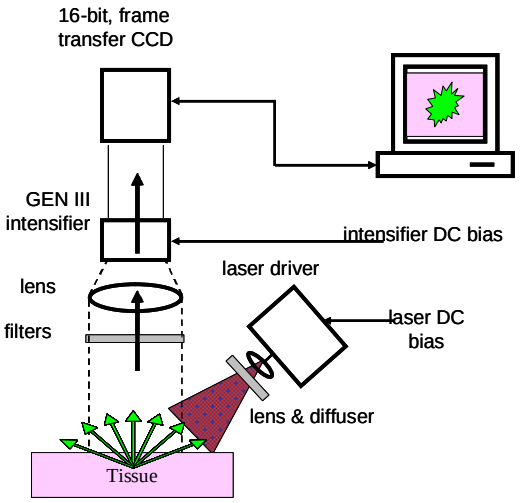

Figure 15: Schematic of NIR optical imaging system.

imaging agent based upon IRDye800 CW.

C3f: Summary. This data collectively demonstrates the team's ability to develop and translate molecular imaging into the clinic. We propose to continue the development of both the lymph and vasculature to provide a non-invasive method for following the earliest stages of bone formation including establishment of the microenvironment, the necessary vasculature, and recruitment of the stem cell populations. This will allow us to monitor the rapid bone formation, potential infection, and healing of soft tissues through tracking of single animals, rather than previous methodologies would require large numbers of animals to look at various stages of development. Another major advancement is that we can now target molecular processes that are unique to bone, rather than a generalized phenomena such as mineral desposition. This allows us to not only identify new bone much earlier, but ensure that we are looking at osteoid rather than mineral. Perhaps one of the greatest aspects of optical imaging is the ability to avoid the significant radiation associated with computational tomography (CT). Our own studies using microCT clearly show the ablation of early bone formation after exposure to the high doses of radiation (often which can be in the range of sub-lethal ablation for bone marrow transplantation). Thus imaging once, can ablate the newly recruited progenitors and stem cells, which disrupts bone healing. Thus following bone formation through these types of processes would not be possible. Alternatively, with the optical-PET imaging, we readily follow the processes and use the results to guide the further development of our materials to improve healing in difficult clinical scenarios.

Based on these studies, new methods for the repair of segmental bone loss in long bone fractures developed within this application were evaluated using two different animal models, the rat and the sheep. Simultaneous experiments were carried out on both species for the entire duration of the funding period. It is well appreciated that the ultimate target for these applications is the human military casualty, and that the large animal model may more directly reflect human injury. However, the rodent models offer a means to quickly and inexpensively pilot new methodology and will be strategically implemented immediately prior to analogous experiments in the sheep.

RAT FEMUR MODEL: Complete healing in 2 weeks

CONTROL: NO CELLS

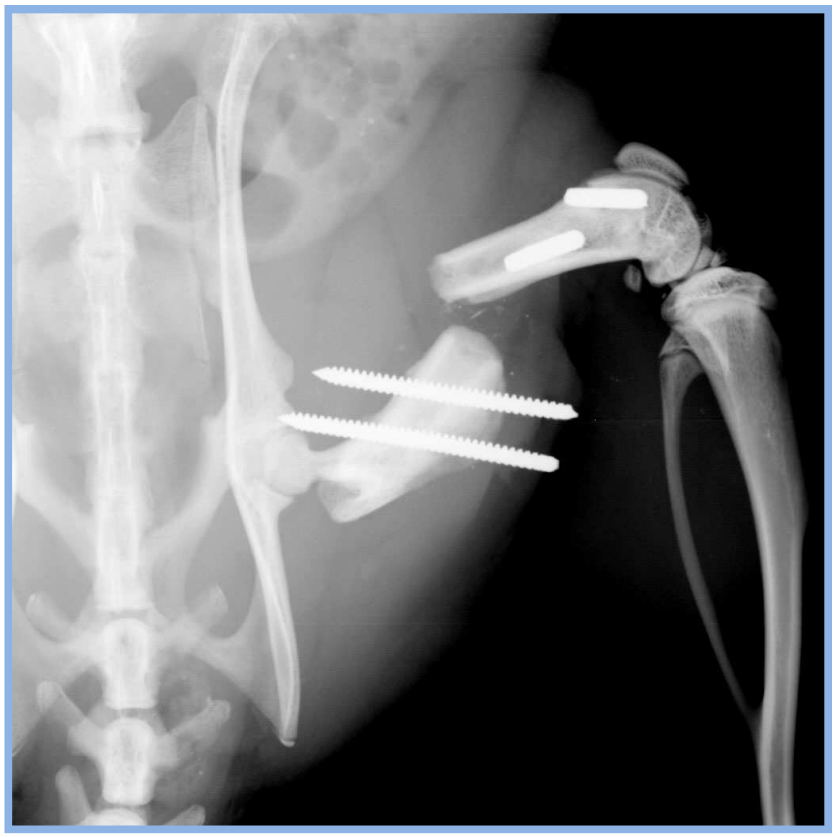

BMP2 producing cells in hydrogel: 2 weeks

3 weeks (external fixator removed at 2 weeks)

As a result of these investigations, several peer-reviewed articles have resulted. These are included in Appendix A for reference.

Large Animal studies

The large animal work has been performed at the University of Georgia, by Drs, John Peroni DVM. And Stephen Stice PhD. Initial work on the sheep tibia and femur fracture models was disappointing. In what seemed to be an immunity based problem, the techniques that had worked so well in rodents were unreliable in the sheep. The action of BMP2 in sheep is known to present special challenges, and indeed other investigators have noted that sheep have a diminished biologic response to the BMP2, as compared to rodents. This may, in part be due to the fact that rodents are biologically closer to humans, than to sheep. It is also suspected that the sheep, perhaps related to their barnyard living environment have an increased immunity to viruses similar to the one that is being used as a vector in our present system. Indeed, inflammatory reactions have been noted histologically. We would note that the method has resulted in the successful induction of bone by these investigators in both sheep and swine, but is not yet quite optimized.

With this project we propose to investigate the option of repairing a bone defect in sheep and pigs with a material that is not the traditional metallic implants but rather a biological material composed of cells and other proteins that are responsible for the promotion of rapid bone healing. This material is referred to as "fracture putty" because it is made of a gel (hydrogel) within which stem cells can survive and proliferate and very quickly form large amounts of bone. A lot of preliminary work done in rats and mice indicates that this biological material is very effective for this purpose and with this proposal we hope to validate the technique using a large animal model in order to then move onto the difficult task of approval for human use.

Using sheep we tested our material in 3 different bone defect models.

1. Metacarpal notch.

Description.

After induction of anesthesia sheep were placed in lateral recumbency with the operated forelimb uppermost. After clipping and aseptic preparation of the circumference of the third metacarpal region a drape was placed to delineate the surgical field. A 5 cm incision was made to the bone on the lateral aspect of the limb. An oscillating bone saw was used to create a partial "notch" defect of the mid-metacarpal region was created removing a 3 by 2 cm segment of cortical bone.. "Hydrogels" will be placed in either defect and allowed to cure for 5 minutes. Subcutaneous and skin tissues will be closed with respectively a continuous and an interrupted suture pattern. The limb will be bandaged with non-adhesive padding and placed in a fiberglass cast extending from the digit to the base of the carpus.

Results.

Bone formation demonstrated in 3 out 32 sheep. Please see “DARPA SLIDES 1” for related images.

Metacarpal defect

- Sheep (32 sheep)
  - 64 defects

Metacarpal defect

Control – untreated

11/2/09 (19 days) **11/13/09 (28 days)**

Metacarpal defect

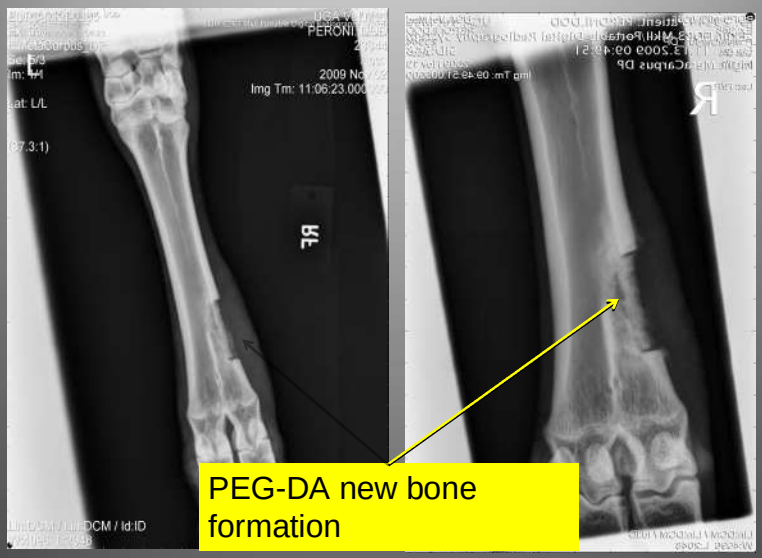

11/2/09 (17 days) **11/13/09 (28 days)**

Metacarpal defect

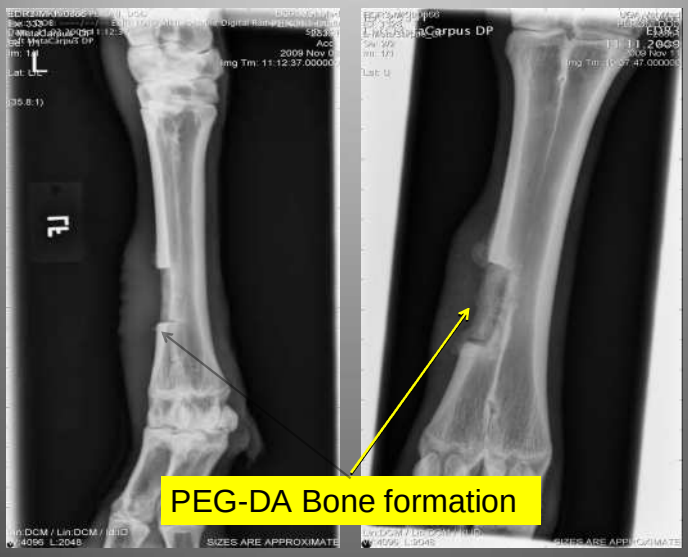

11/2/09 (17 days) **11/13/09 (26 days)**

2. Tibia corticomedullary drill hole defect.

Description.

After induction of anesthesia sheep were placed in lateral recumbency with the operated hindlmb uppermost. After clipping and aseptic preparation of the circumference of the tibail shaft a drape was placed to delineate the surgical field. A 5cm linear incision was made over the medial aspect of the tibia and the bone penetrated using a 4.0mm cortical drill bit. "Hydrogels" will be placed in either defect and allowed to cure for 5 minutes. Subcutaneous and skin tissues will be closed with respectively a continuous and an interrupted suture pattern.

Results.

Bone formation demonstrated in 2 out 12 sheep.

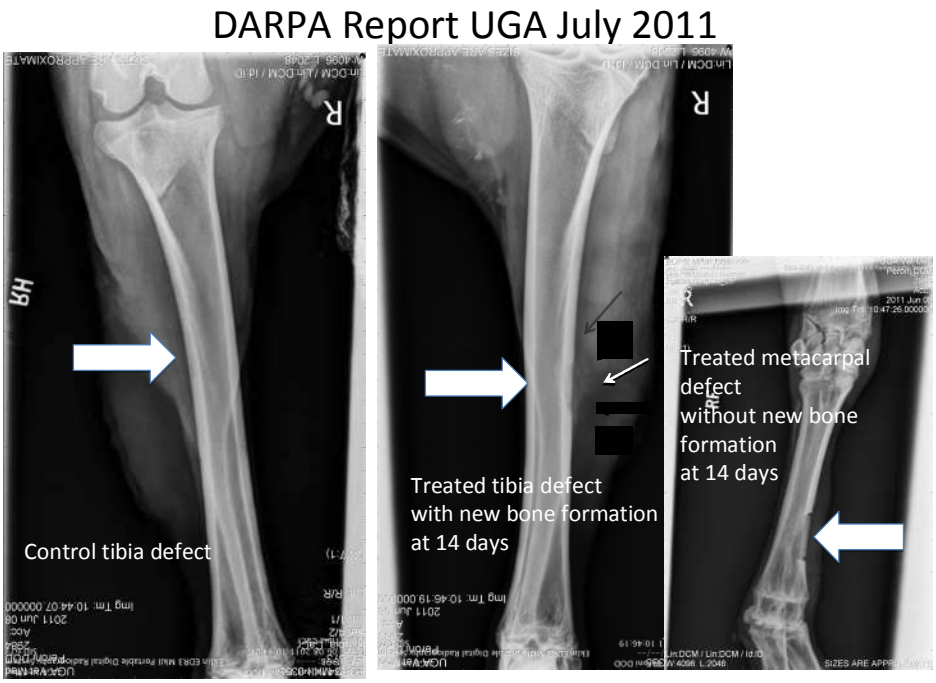

DARPA Report UGA July 2011

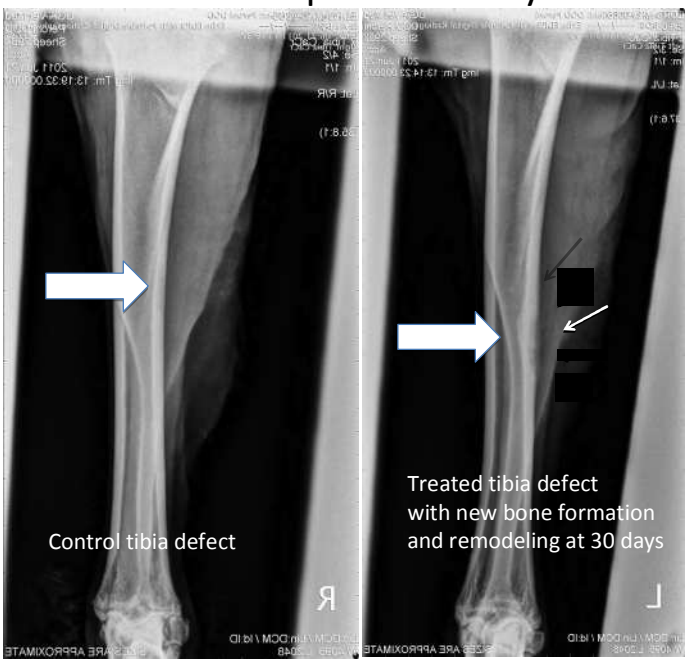

DARPA Report UGA August 2011

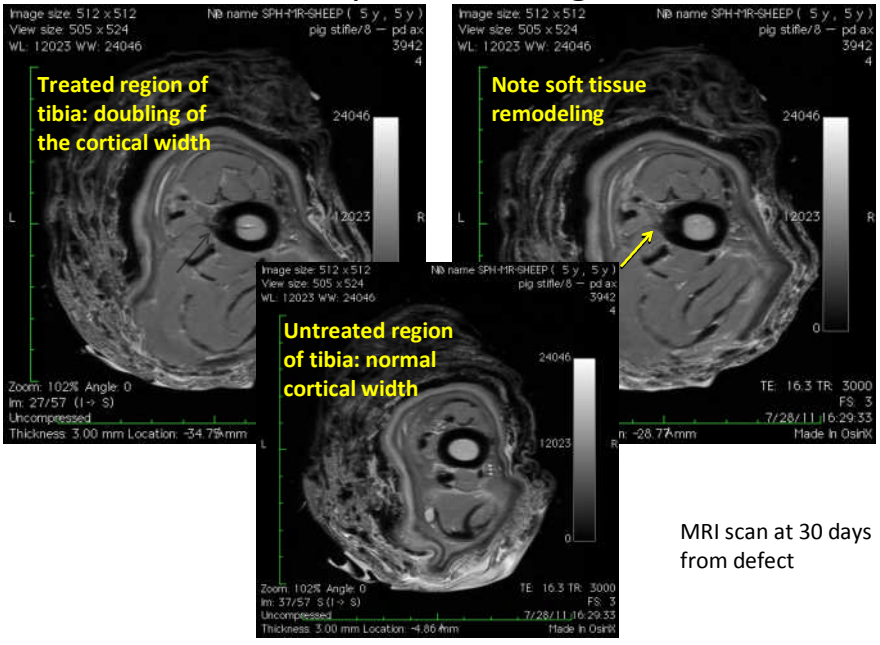

MRI scan at 30 days
from defect

DARPA Report UGA August 2011

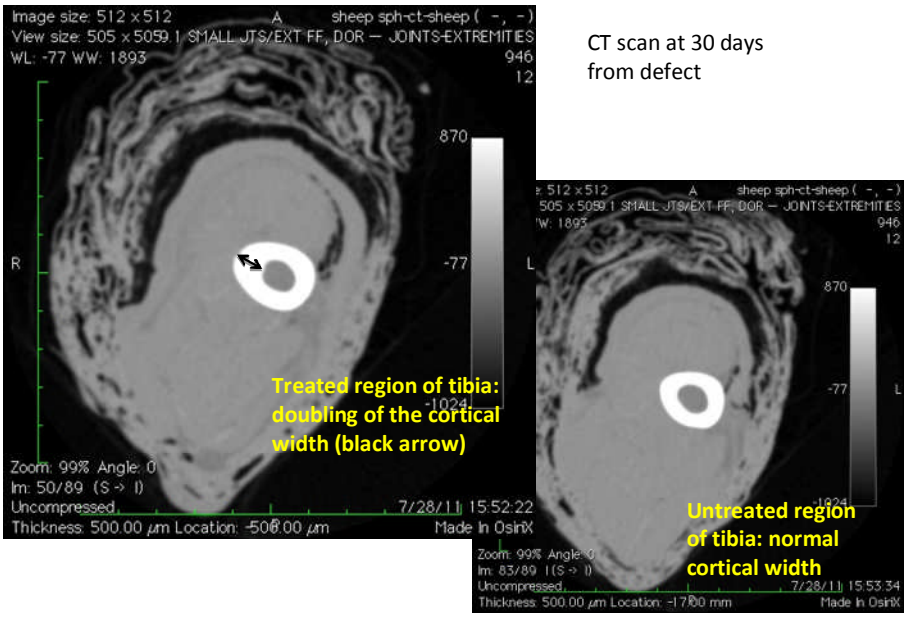

CT scan at 30 days from defect

3. <u>Tibia corticomedullary oscillating saw defect with soft tissue disruption.</u>

Description.

After induction of anesthesia sheep were placed in lateral recumbency with the operated hindlmb uppermost. After clipping and aseptic preparation of the circumference of the tibail shaft a drape was placed to delineate the surgical field. A 5cm linear incision was made over the medial aspect of the tibia and the bone penetrated using a 4.0mm cortical drill bit. "Hydrogels" will be placed in either defect and

allowed to cure for 5 minutes. Subcutaneous and skin tissues will be closed with respectively a continuous and an interrupted suture pattern.

Results.

Bone formation demonstrated in 2 out 11 sheep. Please see “DARPA SLIDES 3” for related images.

We attempted to use similar techniques in pigs which yielded less obvious bone formation but than that shown in the sheep but with more consistency we were able to image a fibrous reaction with small islands of bone forming in the defects.

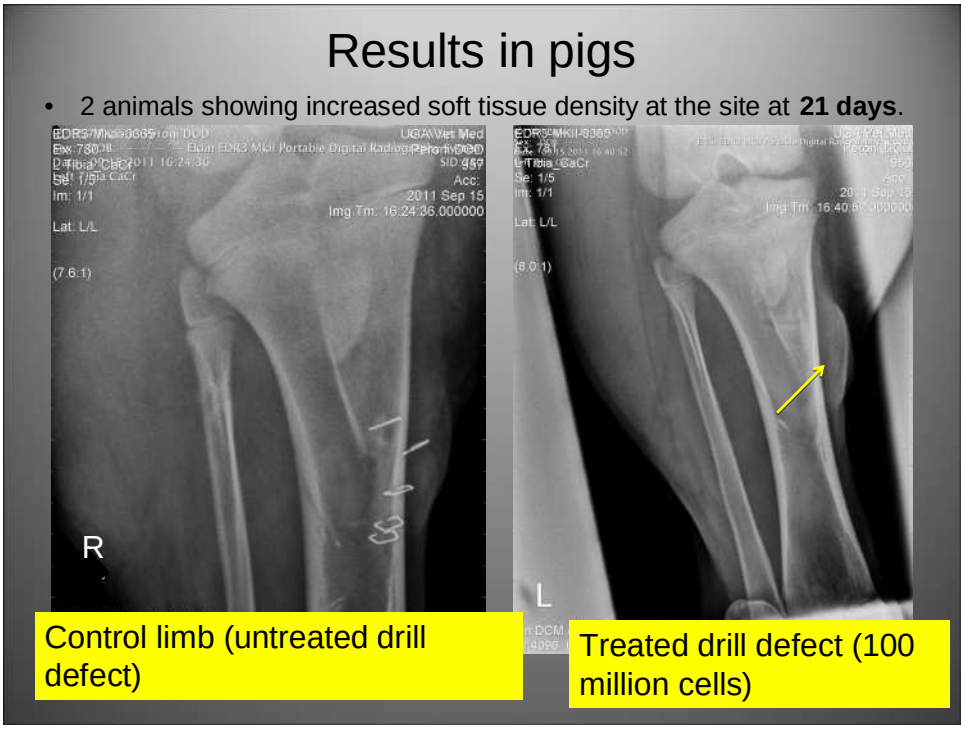

Results in pigs

- 2 animals showing increased soft tissue density at the site at **21 days**.

Control limb (untreated drill defect)

Treated drill defect (100 million cells)

21 days

Conclusions.

We were able to make bone in sheep with more consistency when soft tissue disruption accompanied the bone defect. Also the metacarpal notch related bone formation was less obvious radiographically than that seen in the tibia, possibly as a result of more aggressive trabecular bone penetration in the latter cases.

Human Applications

We have kept the goal of human fracture healing foremost in our thoughts as this work has continued. It is important to not that in the course of performing this work to date; our group has also made important discoveries about how BMP2 actually induced bone. This is a much more complex process than previous BMP2 investigators had appreciated. The process involves the interaction of the molecule with small peripheral nerves within the tissue, the release of local stem cell populations that result in cells (brown fat) that lower oxygen tension, fostering the differentiation of cartilage which ultimately is converted to bone. These observations are novel and new, and have changed the way all of us look at the biology of fracture healing. It should also be noted that examination of pathology specimens from human trauma victims treated by Baylor faculty, the cellular sequences seen in the animals are confirmed to also occur in human fracture healing.

Commercially produced BMP2 has been in clinical use for several years now. The commercial preparation is a freeze dried protein that is reconstituted in the operating room, and placed in a surgical wound after it is soaked into a collagen sponge. The BMP2 is manufactured by production in commercial scale cell culture using Chinese hamster ovary cells that release the BMP into the culture medium, from which it is then purified. This is a very expensive process and ultimately results in a product that costs between $5,000 and $10,000 per use. Advantages of this method are primarily related to the at times astonishingly effective stimulation of new bone formation. Drawbacks to this method include the loss of a high percentage of the BMP2, which becomes bound and inactivated by the collagen sponge (adding to expense), as well as difficulty in controlling the diffusion of the BMP2 eluted from the sponge out of its desired location into areas where bone formation can be harmful to the patient.

Recently a number of serious complications associated with this product have been reported, including new onset of sciatica, retrograde ejaculation, and heterotopic ossification. At the time the commercial product was released for use, the mechanism of action of BMP2 was incorrectly thought to be by direct stimulation of mesenchymal stem cells, and inducing these cells to differentiate into osteoblasts. We now know, based in large part on the observations of the Baylor college of Medicine group here funded by DARPA, that the true action of BMP2 involves direct stimulation of the small nerves in the area, causing a sequence of release of stem cells from the nerve, differentiation of brown fat to create hypoxia, subsequent differentiation of cartilage cells, and substitution of the cartilage by bone. This recapitulates the endochondral ossification steps seen in a bone growth plate. What is remarkable is the rapidity that these several step take place. (In our hands this can take as little as 6 days!).

Many of the complications associated with the commercial product are consistent with the unknowing use of the BMP2 in proximity to the sympathetic chain, nerve roots, and major nerves. With the now better understood effects of BMP2 on nerves, we believe that the vast majority of these complications can be avoided.

We would stress that with the use of hydrogels, as in our present method, the unwanted migration of active bone formation outside of the desired location has not been observed, nor have we encountered neurologic complications.

Safety Concerns

In assessing risks for our proposed gene therapy to enhance and augment fracture callus formation, we examined the possibilities of both short term and long term exposure to the virus particles. Study subjects in gene therapy trials are at risk for developing adverse effects based on a number of factors.

Factors likely to increase the risk of adverse reactions include persistence of the viral vector, integration of the viral genetic material to the host genome, prolonged expression of the transgene, and altered expression of the host genes.

This adenovirus construct has been used in many experiments using several hundred animals of the course of the last decade without significant adverse effects but we would like to comment on each of the risk factors noted above.

Persistence of a viral vector, in many cases, would lead to an adverse outcome if the transgene is continually expressed, especially in the case of such a powerful morphogen as BMP2. In out system the vector is incorporated into cells which are then transplanted into the host to allow for expression of the transgene locally. Our studies indicate that the infected cells are cleared from the host within 7 days thus limiting the exposure of the host to the transgene. The resulting bone formation that occurs after this 7 day period is not mediated by the transgene but by the normal host osseous reparative response as once the bone formation cascade is started by the adenoviral vector BMP the process is self sustaining.

To date, there has been no detection of viral integration into the host genome of any of the animals tested. This is likely due to the fact that the transgene product is manufactured within the transduced

cells and only that product is secreted, not the virus particles themselves. Additionally, in the current system, the cells are held within a volume of hydrogels that inhibit the cellular diffusion making it extremely unlikely that the viral particles would escape to then integrate in the host genome. All of the animals that have received the transduced cells have shown no evidence of bone formation at sites distant from the site of inoculation further indicating that this is a local process without significant risk of widely disseminated viral particles.

The BMP molecules as a whole have a half life in minutes given their powerful nature to affect the surrounding tissues. We have further engineered the system to allow only the transduced cells to produce the BMP molecules and these are further confined to the surrounding hydrogel matrix. The bone formation observed has only been in the area of the injection sites and there is even no evidence of bone formation in the areas adjacent to the exterior edges of the hydrogel matrix indicating that the BMP molecules produced have no significant risk to be found in locations other than the injection sites. Given that the transduced cells are cleared from the hosts within 7 days there is essentially no risk that the transgene will be expressed for longer than that period.

The three factors noted above indicate that our system limits the viral particles to a well defined local site and negligible risk of wandering viral particles hence the risk to altering the host genome is extremely low.

We believe this system is safe an efficacious and will lead to profound enhancements in patient care.

Next Steps

There is continued work on the large animal models still underway at the University of Georgia, using the small amount of remaining funds, which are predicted to run out in April of 2012. One frustration that we are experiencing is that we know with confidence that the human BMP2 molecule works very efficiently indeed in humans. An (expensive) commercially purified BMP2 product has been in very wide use for over 5 years. There have been some significant complications reported, generally due in our view, to the fact that the biology of the way this molecule works had been misunderstood prior to the work of our group, so generously supported by DARPA. We feel strongly that this method will have a very central place in the future management of major trauma, in both the warfighter and in the civilian arena.

Appendix A

Vessel Formation Is Induced Prior to the Appearance of Cartilage in BMP-2-Mediated Heterotopic Ossification

Christine Fouletier Dilling ,[1] Aya M Wada,[2] Zawaunyka W Lazard,[1] Elizabeth A Salisbury ,[1]
Francis H Gannon,[3] Tegy J Vadakkan,[2] Liang Gao,[2] Karen Hirschi ,[1,4] Mary E Dickinson ,[2] Alan R Davis ,[1,5] and Elizabeth A Olmsted-Davis[1,5]
[1]Center for Cell and Gene Therapy, Baylor College of Medicine, Houston, TX, USA
[2]Departments of Molecular Physiology and Biophysics and Medicine, Baylor College of Medicine, Houston, TX, USA
[3]Department of Pathology, Baylor College of Medicine, Houston, TX, USA
[4]Department of Pediatrics, Pediatrics-Nutrition, Baylor College of Medicine, Houston, TX, USA
[5]Department of Pediatrics, Hematology-Oncology, Baylor College of Medicine, Houston, TX, USA

ABSTRACT

Heterotopic ossification (HO), or endochondral bone formation at nonskeletal sites, often results from traumatic injury and can lead to devastating consequences. Alternatively, the ability to harness this phenomenon would greatly enhance current orthopedic tools for treating segmental bone defects. Thus, understanding the earliest events in this process potentially would allow us to design more targeted therapies to either block or enhance this process. Using a murine model of HO induced by delivery of adenovirus-transduced cells expressing bone morphogenetic protein 2 (BMP-2), we show here that one of the earliest stages in this process is the establishment of new vessels prior to the appearance of cartilage. As early as 48 hours after induction of HO, we observed the appearance of brown adipocytes expressing vascular endothelial growth factors (VEGFs) simultaneous with endothelial progenitor replication. This was determined by using a murine model that possesses the VEGF receptor 2 (Flk1) promoter containing an endothelial cell enhancer driving the expression of nuclear-localized yellow fluorescent protein (YFP). Expression of this marker has been shown previously to correlate with the establishment of new vasculature, and the nuclear localization of YFP expression allowed us to quantify changes in endothelial cell numbers. We found a significant increase in Flk1-H2B::YFP cells in BMP-2-treated animals compared with controls. The increase in endothelial progenitors occurred 3 days prior to the appearance of early cartilage. The data collectively suggest that vascular remodeling and growth may be essential to modify the microenvironment and enable engraftment of the necessary progenitors to form endochondral bone. _ 2010 American Society for Bone and Mineral Research.

KEY WORDS: BONE MORPHOGENTIC PROTEIN TYPE 2; HETEROTOPIC OSSIFICATION; VESSEL FORMATION

Introduction

Endochondral bone formation is thought to proceed through an ordered series of events starting with the proliferation and ‘‘condensation’’ of presumptive mesenchymal cells to form avascular cartilage. Hence it is presumed that the lack of vasculature and associated cellular replication creates the hypoxic environment necessary for chondrogenic differentiation. Using a murine model that possesses the VEGF receptor 2 (Flk1) promoter containing an endothelial cell enhancer driving the expression of YFP,(1) we confirmed recent data from our laboratory using a model of heterotopic ossification that suggested that vessels may play an essential role in the induction of chondrogenesis.(2) It has been well established that vessel formation plays a key role in late events during the process of bone formation. Vessels invade the perichondrium and hypertrophic zone and are required for the replacement of cartilage by bone.(3) The angiogenic factor vascular endothelial growth factor (VEGF) promotes vascular invasion via specific receptors, including Flk1 (VEGF receptor 2) expressed in endothelial cells, in the perichondrium or surrounding tissue.(4,5) These events of cartilage matrix remodeling and vascular invasion are necessary for the migration and differentiation of osteoblasts and osteoclasts,

which remove mineralized cartilage matrix and replace it with bone. However, much less is known about the role of vessel formation prior to the appearance of the precartilage tissue. During normal wound repair, a series of cell signaling events is induced by the hypoxic state of the tissues, resulting in upregulation of hypoxia inducible factor (HIF1), which, in turn, upregulates a series of factors including several VEGFs (A, B, and

ORIGINAL ARTICLE JBMR Received in original form March 29, 2009; revised form September 30, 2009; accepted October 15, 2009. Published online October 17, 2009. Address correspondence to: Alan R Davis, Center for Cell and Gene Therapy, One Baylor Plaza, Houston, TX 77030, USA. E-mail: ardavis@bcm.tmc.edu C Fouletier Dilling and AM Wada contributed equally to the work. Journal of Bone and Mineral Research, Vol. 25, No. 5, May 2010, pp 1147–1156 DOI: 10.1359/jbmr.091031 _ 2010 American Society for Bone and Mineral Research 1147

D), leading to vessel formation. Hypoxia-induced angiogenesis has been proposed to be necessary for creating specialized vessels that facilitate progenitor homing and engraftment into damaged tissues.(6) Little is known about whether such a process plays a key role in the repair of bone. Using a model of de novo bone formation to identify the earliest events in this process, we have demonstrated that myelomesenchymal stem cells are recruited to the tissues to form the early cartilage.(7) One of the earliest events in this model is the appearance of brown adipocytes. These cells are capable of using their uncoupled aerobic respiration to reduce localized oxygen tension and effectively pattern the newly forming cartilage condensations.(8) This is consistent with in vitro data showing that bone marrow–derived mesenchymal stem cells can undergo chondrogenesis in the presence of bone morphogenetic protein 2 (BMP-2) and low oxygen.(9) We also observed the appearance of vessels lining the edges of the perichondrial region, separated only by brown adipose tissue, suggesting that perhaps the reduction in oxygen tension coordinately activates new vessel formation in the region.(8) Thus these progenitors may indeed be recruited to the site of new bone formation through the vasculature. In this study we focused on defining this tentative early vessel formation. To determine this, we chose to employ a transgenic mouse model that expresses the fusion protein human histone H2B with enhanced yellow fluorescent protein (EYFP) (H2B:YFP) in endothelial cells under the regulation of a Flk1 promoter/ enhancer fragment (Flk1-H2B::YFP).(1) Recent improvements in genetically encoded fluorescent protein expression in animal models, along with advances in optical imaging and image analysis software, have enabled the analysis of many aspects of tissue development at a cellular level.(10) Previous studies using this transgenic animal indicates that Flk1-H2B::YFP expression is restricted to endothelial cells of smaller and/or newly forming vessels,(8) thus providing a mechanism for quantification of new vessels.

Here we demonstrate new vessel formation within the tissues prior to the appearance of the presumptive cartilage. Quantification of the number of endothelial cells shows that one of the first steps of bone formation is to induce additional endothelial cell proliferation. Histologic analysis shows that increases in endothelial cell numbers are evident just prior to the influx of chondrocytic progenitors. Immunohistochemical analysis of the tissues prior to the mesenchymal condensations revealed a rapid and transient expression of VEGF-A and -D from the brown adipocytes. The data collectively suggest that the brown adipocytes may play a key role in establishing patterning of the cartilage via regulation of oxygen tension within the tissues through induction of both aerobic respiration and early angiogenesis.

Materials and Methods

Cell culture

A murine C57BL/6-derived cell line (MC3T3-E1) was obtained from American Type Culture Collection (Manassas, VA), propagated in a modified essential medium (a-MEM) supplemented with 10% FBS (Hyclone, Logan, UT, USA), 100 U/mL penicillin, 100 mg/mL streptomycin, and 0.25mg/mL amphotericin B (Life Technologies, Inc., Gaithersburg, MD, USA). Briefly, the cells were grown in DMEM supplemented as described earlier and cultured at a subconfluent density to maintain the phenotype. All cell types were grown at 378C and 5% CO_2 in humidified air. Transduction of cells with adenovirus in the presence of GeneJammer adenoviruses Replication defective first-generation human type 5 adenovirus (Ad5) deleted in regions E1 and E3 was constructed to contain the cDNA for BMP-2 in the E1 region of the viral genome.(11) The virus particle (vp) to plaque-forming unit (pfu) ratios were 55 and 200 for Ad5-BMP-2 and Ad5-empty, respectively, and all viruses were shown to be negative for replication-competent adenovirus. The C57BL/6 cell line, or MC3T3-E1 (1_10^6), was transduced with Ad5-BMP-2 or Ad5-empty cassette control virus at a concentration of 5000 vp/cell with 1.2% GeneJammer, as described previously.(12)

Heterotopic bone assay

The transduced cells were resuspended at a concentration of 5_10^6 cells/100 mL of PBS and then delivered through intramuscular injection into the hind limb quadriceps muscle of Flk1 mice. Animals were euthanized at daily intervals, and hind limbs were harvested, embedded, and stored at _808C. All animal studies were performed in accordance with standards of the Baylor College of Medicine, Department of Comparative Medicine, after review and approval of the protocol by the Institutional Animal Care and Use Committee (IACUC).

Histologic analysis and staining analysis

Soft tissues encompassing the site of new bone formation were isolated from the rear hind limbs of the mice. Both the skin and skeletal bone were removed from the tissues prior to freezing. Serial sections (15mm) were prepared that encompassed the entire tissue (approximately 50 sections per tissue specimen). We then performed hematoxylin and eosin staining on every fifth slide, which allowed us to locate the region containing either our delivery cells or the

newly forming endochondral bone. Serial unstained slides were used for immunohistochemical staining (either single- or double-antibody labeling). For double-antibody labeling, samples were treated with both primary antibodies simultaneously, followed by washing and incubation with respective secondary antibodies, used at 1:500 dilution, to which Alexa Fluor 488, 594, or 647 was conjugated. Primary antibodies were used as follows: SMA mouse monoclonal used at 1:200 dilution (Sigma Chemical Company, St Louis, MO, USA), CD31 rat monoclonal used at 1:75 dilution (BD Pharmingen, San Diego, CA, USA), Flk1 goat polyclonal used at 1:100 dilution (R&D Systems, Minneapolis, MN, USA), Ki67 rat monoclonal used at 1:100 (Dako, Carpinteria, CA, UDA), and VEGF-D goat polyclonal used at 1:100 dilution (Santa Cruz Biotechnology, Inc., Santa Cruz, CA, USA). Stained tissue sections were examined by confocal microscopy (LSM 510 META, Zeiss, Inc., Thornwood, NY, USA) using a 20_/0.75NA objective lens.

Flk1-positive cell quantification in BMP-induced tissues

To quantify the increase in YFP-positive cells in the BMP-induced tissues, frozen sections across these tissues were counterstained with 4,6-diamidino-2-phenylindole (DAPI), and the YFP expression was compared with that obtained in the control tissues. First, a series of low-magnification (5.4_ and 12_) bright-field images of a tissue section was taken and overlapped to reconstruct the tissue section using Adobe Photoshop CS3 (San Jose, CA, USA). The reconstructed montage image was used to measure the area of the tissue section using a manual contour-tracing method (Zeiss Axiovision). The area of each of the frozen sections was calculated in a similar manner. Area measurements are used to determine the density of labeled cells, as indicated below. High-resolution (10_/NA0.45, 1024_1024 pixels) dual-channel images of tissue sections nuclear stained with DAPI were taken using a confocal microscope (Zeiss LSM 510 META). In each image, the number of nuclei in the DAPI and YFP channels was counted using a modified watershed segmentation algorithm (FARSIGHT, Farsight Image Segmentation Software, courtsey of Badri Roysam, RPI, Troy, NY), which makes use of both intensity and volume thresholds to distinguish two nuclei as separate. All the nuclei counted using the software were $DAPI_þ$. The fraction of DAPI-stained nuclei marked by YFP was counted as $YFP_þ$. The density of $YFP_þ$ cells in a tissue section was defined as the ratio of the number of $YFP_þ$ nuclei in the tissue section measured from the high-magnification images to the area of the tissue section measured from the low-magnification images. The density of the $YFP_þ$ nuclei was calculated for a number of control and BMPtreated tissues at 2 and 4 days after injection. The ratios then were averaged over the various control and BMP-2-treated tissues. The p values were calculated using a Student's t test.

Flk1-$YFP_þ$ cell association analysis

To characterize the cell type(s) that express YFP in the adult muscle tissue, we performed immunoflourescence studies using endothelial cell marker CD31 and Flk1 antibodies; for vascular smooth muscle cells, we used smooth a actin (SMA). Association of cells expressing YFP with immunolabeled cells was analyzed using (FARSIGHT, RPI) and a custom program written in MATLAB (MathWorks, Natick, MA, USA). After identification of each nucleus by DAPI staining, $YFP_þ$ and YFP_ cells then were analyzed for association with the fluorescent signals of each antibody. An intensity threshold was applied to the red channel in each image to identify a cell positive or negative for the immunofluorescent signal. Each identified nucleus and overlapping red channel were counted as $CD31_þ$, $Flk1_þ$, or $SMA_þ$ and then as either YFP_ and $YFP_þ$. Colocalization percentages are shown in the supplemental data section (Table S-1) and described in detail the $YFP_þ$ cell types. The number of $YFP_þ$/ $Ki67_þ$ nuclei in an area of the tissue was calculated by adding the $YFP_þ/Ki67_þ$ in each of the confocal images taken within the area. The area fraction of $YFP_þ/Ki67_þ$ was defined as the total number of $YFP_þ/Ki67_þ$ in the images taken within the area divided by the number of images. The area fraction was measured for five different areas, and the average area fraction was calculated for control and BMP-treated tissues for every fifth slide sectioned throughout the entire hind limb. The area fractions of $YFP_þ$/ $Ki67_þ$ nuclei in the control and the BMP-treated tissues on day 2 were 3.97_2.96 and 6.11_1.76, respectively. The area fractions for day 4 were 5.04_0.72 and 6.41_1.41 in the control and the BMP-treated tissues. Based on the Student's t test, the p value for the day 2 data was .21, and that for the day 4 data was .10. Taken together, the data support the trend that the $YFP_þ/Ki67_þ$ population increases on day 2 and day 4 after the BMP treatment.

qRT-PCR

Nonskeletal tissues (n¼4 per group) surrounding the site of injection of the Ad5-BMP-2 or Ad5-control transduced cells were isolated at daily intervals for 7 days and prepared as total RNA using a Trizol reagent (Life Technologies, Carlsbad, CA, USA) in accordance with the manufacturer's specifications. The two groups of RNAs were subjected to qRT-PCR analysis in parallel, and the C_t values obtained normalized to both internal 18S ribosomal RNA used in multiplexing and to each other to remove changes in gene expression common to both the BMP-2 and control tissues by using the method of DDC_t along with Taqman primers and probes (Applied Biosystems, Carlsbad, CA, USA) as described previously.[8]

Results

Upregulation of vessel markers prior to the onset of chondrogenesis

We have previously described a model of rapid endochondral bone formation[13] in which mineralized bone is observed 7 days after the initial induction with BMP-2. Observation of vessels lining the newly forming perichondrium suggests that vessels may undergo replication prior to chondrogenesis. To confirm this hypothesis, we examined tissues, at 24-hour intervals over the period leading up to chondrogenesis (day 5), for the presence or absence of endothelial cell replication. Figure 1 shows the coexpression of the endothelial cell–specific factor von Willibrand factor (vWF) (red) and Ki67 (green), a marker of cellular replication,[14] in the vessels from tissues that received Ad5- BMP-2-transduced cells starting at 24 hours and

going to 5 days (panels A–E, respectively). As can be seen in Fig. 1B, we did observe overlap of these two markers (yellow) in tissues receiving the Ad5- BMP-2-transduced cells, whereas no replicating endothelial cells were observed in the control tissues (Fig. 1F). We did not attempt to quantify the amount and apparent timing of replication using this method because vWF is an extracellularmatrix protein. Instead, we employed the Flk1-H2B::YFP model for quantifying endothelial progenitor replication over the course of early bone formation.

Flk1-H2B::YFP in vessels

We next determined if there was a significant increase in the number of Flk1þ endothelial progenitors during bone induction, consistent with new vessel formation, prior to chondrogenesis. We chose to use the Flk1-H2B::YFP mouse model,(1) in which new vessel formation could be readily quantified within the muscle tissues. Flk1 is a VEGF receptor transiently expressed on endothelial cells and is thought to contribute to VEGF-induced endothelial cell replication.(15) Therefore, quantification of the nuclear YFP expression within tissues from animals receiving VESSELS FORM PRIOR TO CARTILAGE Journal of Bone and Mineral Research 1149 either Ad5-BMP-2- or Ad5-empty-transduced cells allowed us to to quantify increases in the number of endothelial progenitors within the muscle prior to cartilage formation. We previously quantified the association of Flk1-H2B::YFP mouse model with other endothelial cells markers such as CD31 and found them to be 95% overlapping (see Supplemental Data below). Frozen sections were prepared by serial sectioning from Flk1-H2B::YFP adult hind limb soft tissue (n¼4 per group) consisting of three groups, those receiving (1) cells transduced with Ad5-BMP-2, (2) cells transduced with Ad5-empty cassette control virus, and (3) normal mouse muscle. To ensure uniform quantification and adequate sampling, the entire region of soft tissues in the hind limb was sectioned, and approximately every fifth section was analyzed for YFP expression. To quantify differences in the number of endothelial progenitors, the number of YFPþ cells per the total number of DAPIþ cells was determined using automated segmentation methods (see Materials and Methods). The total YFPþ cells also was quantified per total area of the tissue section to ensure that there was no bias in the fields of view chosen for image analysis (see Materials and Methods). The total area of each tissue section was determined using a montage of images that were collected using wide-field microscopy (Fig. 2A, F). As can be seen in Fig. 2, we found Flk1-H2B::YFPþ cells in both tissues receiving Ad5- empty-transduced cells (Fig. 2B–E) and Ad5-BMP-2-transduced cells (Fig. 2G–O). These panels are higher-magnification confocal images of the region within the corresponding white box on the lower-magnification high-resolution wide-field montage of the entire tissues (Fig. 2A, control; Fig. 2F, BMP-2). The results of the quantification (Fig. 3) shows the average number of Flk1- H2B::YFPþ cells on days 2 and 4. Analysis of the entire soft tissue within several mice showed a significant elevation in tissues receiving the Ad5-BMP-2-transduced cells (p¼.017, day 2, Fig. 3A and p¼.006, day 4, Fig. 3B) compared with control on both days 2 and 4. The peak was approximately 2 days after induction of bone formation, with no statistically significant difference between these results and those obtained in tissue sections isolated 4 days after induction.

Endothelial progenitors undergo replication in tissues receiving Ad5-BMP-2-transduced cells

In the tissues receiving cells transduced with a control adenoviral vector we observed randomly scattered YFPþ cells along the vessel structures, whereas in the tissues receiving Ad5-BMP-2- transduced cells we saw clustering of the YFPþ cells (Fig. 2). This prompted us to question whether the Flk1-H2B::YFP progenitors could be replicating, so we next quantified the number of Flk-H2B::YFPþ cells in these tissues. Representative images used for quantification of YFPþ cell proliferation activity are shown in Fig. 4. Replicating endothelial progenitors were defined as nuclei positive for both Flk1-H2B::YFP (yellow) and the cell proliferation marker Ki67 (red; Fig. 4). In both control and treated animals, we also observed proliferating cells positive for Ki67 that did not overlap with Flk1-H2B::YFP. Quantification of cells positive for both Flk1-H2B::YFP and Ki67 (Fig. 4) indicates a large number of replicating endothelial progenitors in both control and BMP-2- treated tissues at 2 days after induction. Therefore, the percentage of dual-positive cells was not significant at this early time point compared with control. However, by 4 days after induction with BMP-2, we observed much fewer replicating Flk1- H2B::YFP cells in the control group and significantly more in the experimental group (Fig. 4). This difference was found to be statistically signifcant.

Vascular endothelial growth factor (VEGF) mRNA expression

Endothelial progenitor replication appeared to start within 48 hours of induction with BMP-2. This correlated with a significant elevation in VEGF-D [also termed fos-induced growth factor (FIGF)] and VEGF-A RNA expression (Fig. 5). Figure 5 shows the changes in VEGF mRNA expression from day 1 after injection of Ad5-BMP- 2-transduced cells until day 6, as determined by real-time RT-PCR (qRT-PCR). Both VEGF-A and VEGF-D mRNA expression was significantly increased on days 2 and 4 after induction of bone formation. VEFG-B and VEGF-C RNA, however, remained on the same level throughout the time course. Although the data cannot differentiate between expansion of cells expressing VEGF-A and -D and elevated transcription within cells residing in the area, the results suggest that these potent endothelial growth factors are rapidly and transiently increased within the site of new bone formation prior to the onset of cartilage.

Role of brown adipose in vessel formation

The data collectively suggest that vessel replication is occurring simultaneously with elevated expression of VEGFs within the tissues. Since one of the earliest events observed in our model is the recruitment and expansion of brown adipocytes,(8) we next chose to determine if these cells might be expressing the VEGFs. Immunohistochemical analysis of Flk1-H2B::YFP tissues that received either Ad5-BMP-2- or Ad5-empty-transduced cells Fig. 1. Immunohistochemical analysis of endothelial cell replication in tissues isolated at daily intervals after induction of bone formation with cells expressing BMP-2. (A–E) On days 1, 2, 3, 4, and 5, respectively, after injection of BMP-2-producing cells, paraffin sections were prepared and stained with an antibody against

Ki67, followed by a secondary antibody conjugated to Alexa fluor 488 (green) mixed with an anti–von Willibrand Factor (vWF) antibody, followed by a secondary antibody conjugated to Alexa fluor 547 (red). (F) A representative image, similar staining, taken from tissues isolated from mice injected with cells transduced with a control vector (Ad5-empty). showed colocalization of VEGF-D (green, Fig. 6c) and the brown adipocyte-specific marker uncoupling protein 1 (UCP1; red, Fig. 6d) (day 2). As can be seen in Fig. 6e, expression of UCP1 overlaps expression of VEGF-D in cells that are adjacent to the Flk1-H2B::YFPþ endothelial progenitors, suggesting that the brown adipocytes may be contributing to the new vessel formation. We observed additional fluorescence within the surrounding muscle that appears to be punctate and not cellassociated. This staining may represent VEGF-D protein secreted in the tissues. To confirm the cell-specific expression Fig. 2. Wide-field and confocal images of whole tissue sections and quantification of Flk1-H2B::YFP cells. (A, F) Representative montages of lowmagnification gray-scale images (1 pixel¼0.003mm) used for calculating total area for tissue sections. A single representative tissue section is depicted after the entire hind limb muscles that encompassed the injection site were isolated 2 days after receiving an intramuscular injection of cells transduced with either Ad5-empty control vector (A) or Ad5-BMP-2 (B) and sectioned at 15 mm thickness. Although every fifth section across the entire tissue was analyzed, we show only a single representative image of each type. The corresponding regions with positive YFP signal, shown by the boxed areas, were imaged by confocal microscopy (B–E, G–O) for counting the YFPþ cell numbers. of VEGF-D in the brown adipocytes, we performed additional immunostaining (Fig. 6f). Positive expression of VEGF-D (brown staining) was observed only in the brown adipocytes, again suggesting that these cells may play a role in the regulation of new vessels.

Discussion

Similar physiologic steps lead to bone formation during embryonic development and in adult organisms, for instance, in fracture repair or heterotopic ossification. In both cases, bone formation begins with mesenchymal condensation and ends with maturation of the growth plate, recruitment of osteoblasts, and the production of bone. Vascularization has been shown to play a critical role in this process through infiltration into cartilage to form vascularized bone.(16) Here we present data that show that vessels play a much earlier role in patterning of the cartilage and bone. The results show the presence of new vessel formation prior to the onset of mesenchymal condensation and cartilage. We have previously reported the presence of brown adipocytes within the tissues 2 days after the initial induction. We also have shown that these cells regulate localized oxygen tension through their unique metabolism.(8) In this study we extend our knowledge of the functional role of brown adipocytes to include their rapid and transient expression of the potent angiogenic factors VEGF-A and -D. Interestingly, a similar rapid and transient expression of VEGF-D also has been demonstrated in limb development and has been shown to be critical for patterning.(17) We observed a biphasic expression pattern for VEGF-A and -D, suggesting multiple roles for this factor in bone formation. The second peak of expression correlates nicely with the transition of cartilage to bone formation, which has been clearly documented.(16,18) However, the first phase is less well studied, and in our model it appears to correlate with the establishment of new vessels just prior to the onset of chondrogenesis. Zelzer and colleagues also reported a similar biphasic expression of VEGF-A during embryonic bone formation.(19) In these studies, the authors showed two functional roles for VEGF-A, one prior to cartilage and one during the transition of cartilage to bone, similar to our own observation in our model. The data collectively suggest that the brown adipocytes may induce the synthesis of new vessels as a component for patterning the newly forming cartilage. In the proposed model, the brown adipocytes induce new vessels, facilitating the recruitment of chondrogenic precursors, while at the same time lowering localized oxygen tension to allow for chondrogenic differentiation. In support of this mechanism, we show in this study the presence of brown adipocytes expressing VEGF-D only in areas adjacent to our newly expanding vessels, as marked by Flk1-H2B::YFP. Using a model of rapid endochondral bone formation, we show the immediate expansion of vessels within the tissues in response to delivery of BMP-2. Although BMP-2 and -4 play a critical role in the patterning of cartilage and bone in the embryo,(20) much evidence now links the BMPs to a host of other earlier physiologic functions, including vascularization of the early embryo.(21) Thus it may not be surprising that the earliest stage of bone formation in our model is the induction of new vessel formation. On BMP-2 stimulation, the Flk-1-H2B::YFP endothelial progenitors expand as the total number of positive cells per tissue area increases. The Flk1-H2B::YFPþ cells are clustered along individual vessels, suggesting that these vessels are extending or remodeling in response to BMP-2. At this point, we cannot determine whether this increase occurs via replication of tissueresident endothelial progenitors or the recruitment of progenitors to the site of new bone formation. Our data suggest that the expansion of these progenitors, at least in part, is due to replication because we observed an increase in the area of replicating endothelial cells within the tissues receiving Ad5- BMP-2-transduced cells on day 4 compared with control tissues. However, we cannot rule out the possibility that at least some of these cells are recruited from either the circulation or surrounding tissues. Interestingly, their were significant clusters of replicating Flk1-H2B::YFP cells on day 2 in tissues receiving both the Ad5-BMP-2- and the Ad5-empty-transduced cells, suggesting that perhaps the initial inflammatory reponse may be somewhat masking the significance of the replication at this early time point. Alternatively, the increase in replication of the Flk1-H2B::YFP cell population at 4

days after induction of bone formation may represent the need for vascularization to recruit Fig. 3. Increase in Flk-H2B::YFP$_þ$ cells in BMP-2-induced tissue on days 2 and 4. Quantification of Flk1-H2B::YFP$_þ$ cells within the tissues 2 and 4 days after induction with Ad5-BMP-2-transduced or control cells. YFP$_þ$ nuclei were counted and reported as a ratio of the total area of the tissue section determined using the wide-field montage. Flk-H2B::YFP$_þ$ cells were significantly elevated in the tissues receiving BMP-2 compared with controls. The graph depicts the average number of Flk-H2B::YFP$_þ$ cells in five sections for day 2 control, 7 sections for day 2 BMP, 8 sections for day 4 control, and 6 sections for day 4 BMP. The number of images taken in each section ranged from 4 to 22. _Denotes a significant difference as determined by the Student's t test. new chondro-osseous progenitors because this coincides with the appearance of these cells within the tissues.(22) However, recruitment from the surrounding tissue is equally likely because recently Kaplan and colleagues(34) showed local stem and progenitor cell contribution to heterotopic bone formation in a murine model of stem cell transplantation, and this process may require new vessel formation for establishment of these cells. VEGFs have been shown to be essential to expansion of both endothelial cells and vascular smooth muscle cells that assemble to form the vessel structure. Although VEGF-A most commonly has been shown to be responsible for angiogenesis in most systems, recent studies in murine muscle have found VEGF-D to be an extremely potent angiogenic factor.(23) This family member is better known for its critical role in the expansion of lymphatic vasculature.(23) In our model we see both factors highly expressed in the tissues receiving the Ad5-BMP-2-transduced cells compared with those receiving control cells. Again, the rapid but transient elevation in VEGF expression suggests that these factors may be driving the endothelial cell replication. Knockout studies have confirmed that BMPs regulate vasculogenesis during embryonic development.(24) Functional deletion of BMP-4 and the BMP I receptor in mice leads to impaired mesoderm precursors required for vascular development.(25,26) It also has been shown that addition of BMPneutralizing antibodies or noggin suppresses endothelial cell formation during development, whereas addition of rhBMP-4 promotes it.(27) We and others have recently shown the chondrocyte to be of myeloid origin, and it circulates to the site of new bone formation.(22,28) These cells then must recruit and pass from the vessels into the tissues, through a process known as extravasation.(29) This process has been shown to require small vasculature that has a reduced blood flow.(29) Thus it is conceivable that Fig. 4. Quantification of YFP$_þ$ cell proliferation. Representative images of Flk1-H2B::YFP and the cell proliferation marker Ki67. Colocalization of Flk1- H2B::YFP (yellow) and Ki67 (red) was detected in BMP-2-treated and control tissues. Graphs show the total number of YFP$_þ$/Ki67$_þ$ cells in the images taken within the area divided by the number of images analyzed. The area fraction was measured for nine at day 2 and five at day 4 BMP and eight at day 2 and four at day 4 control different areas, and the average area fraction was calculated for control and BMP-treated tissues. The area fractions of YFP$_þ$/Ki67$_þ$ nuclei in the control and the BMP-treated tissues on day 2 were 7.32_3.26 and 10.20_6.95, respectively. The area fractions for day 4 were 6.97_2.32 and 11.26_2.58 in the control and the BMP-treated tissues. Based on the Student's t test, the p value for the day 2 data was .29 and that for the day 4 data was .035. Taken together, the data showed significant YFP$_þ$/Ki67$_þ$ population increases by day 4 after the BMP treatment, but on day 2 there were no significant differences in dividing YFP cell population between control and BMP-treated tissues. VESSELS FORM PRIOR TO CARTILAGE Fig. 5. Expression of VEGF-D during the early stages of endochondral bone formation. Results of qRT-PCR analysis of VEGF-A, -B, -C, and -D mRNA levels in tissues surrounding the lesional site that received either the Ad5-BMP-2- or Ad5-empty-transduced cells isolated at daily intervals for up to 7 days after initial injection. Four biologic replicates were run in triplicate, and the averages were normalized against an internal standard (ribosomal RNA). The samples receiving Ad5-BMP-2-transduced cells then were compared with those obtained from the tissues receiving cells transduced with Ad5-empty cassette virus. Therefore, the graph depicts the fold changes in VEGF RNAs in the BMP-2 samples over time compared with control tissues. Error bars depict_1 SD unit. _Denotes samples that had a statistically significant ($p<.05$) difference from all other samples by the ANOVA test. Fig. 6. Immunohistochemical staining for brown adipocytes expressing VEGF-D (green, c) in tissues isolated from the Flk1-H2B::YFP mice 4 days after receiving MC3T3 cells transduced with Ad5-BMP-2. Brown adipocytes were identified as cells expressing uncoupling protein 1 (UCP 1; red, d) and yellow (b) represents the Flk-yfp$_þ$ endothelial cells within the muscle. The tissues also were stained with VEGF-D antibodies (c) and counterstained with DAPI (blue, a), which stains the nucleus of cells. A merger of these stains (UCP-1, VEGF-D, and YFP) is shown in panel e. In panel f, a paraffin section taken 4 days after injection of BMP-2-producing cells was stained with an antibody against UCP1, and staining was visualized using 3,3'-diaminobenzidine (DAB) as described previously.(8) No staining was observed on a paraffin section taken 4 days after injection of cells transduced with the empty control vector Ad5-HM4 (data not shown). brown adipocytes express the VEGFs to form new vessels that are capable of permitting recruitment of chondrocytic progenitors to the correct location for endochondral bone formation. Since vascular invasion of the growth plate has been well documented to precede the recruitment of osteoblast progenitors to form the new bone,(16,18,29,30) it would not be surprising to have an earlier phase of this process that recruited the chondrocytic progenitors. We have shown previously that the brown adipocytes are capable of inducing hypoxia in the local environment, which in the presence of BMP-2 has been shown to induce chondrogenesis.(8) Thus we propose that the brown adipocytes are capable of patterning the newly forming cartilage by inducing new vessel formation while simultaneously removing oxygen through uncoupled aerobic respiration. Once the progenitors differentiate into

chondrocytes, they then express a number of anti angiogenic proteins to prevent in the growth of new vessels, thus momentarily attenuating this early wave of angiogenesis.(31–33,35) Thus the results presented in this study extend our knowledge about the critical role vascularization plays not only in bone formation but also in cartilage formation as well. The data collectively show a novel process for patterning of new endochondral bone in adult organisms. Further, this is one of the first studies that attempts to understand the biology of tissue engineering of cartilage. Surprisingly, one of the critical components we have identified is contradictory to our current dogma that cartilage does not require vessels. This study suggests that brown adipose may play a pivotal role in establishing new vessels, essential for recruitment of chondrogenic progenitors and patterning of the tissues. These findings ultimately may play an important role in our efforts to replace damaged cartilage through tissue engineering.

Disclosures

All the authors state that they have no conflicts of interest.

Acknowledgments

This study was funded in part by Grants RO1EB005173-01, USMRMC 06135010, USMRMC 06136005 (DOD), and IW911NF- 09-1-0040 (DARPA).

References

1. Fraser ST, Hadjantonakis AK, Sahr KE, et al. Using a histone yellow fluorescent protein fusion for tagging and tracking endothelial cells in ES cells and mice. Genesis. 2005;42:162–171. 2. Shafer J, Davis AR, Gannon FH, et al. Oxygen tension directs chondrogenic differentiation of myelo-monocytic progenitors during endochondral bone formation. Tissue Eng. 2007;13:2011–2019. 3. Colnot C, Lu C, Hu D, Helms JA. Distinguishing the contributions of the perichondrium, cartilage, and vascular endothelium to skeletal development. Dev Biol. 2004;269:55–69. 4. Maes C, Stockmans I, Moermans K, et al. Soluble VEGF isoforms are essential for establishing epiphyseal vascularization and regulating chondrocyte development and survival. J Clin Invest. 2004;113:188– 199. 5. Gerber HP, Vu TH, Ryan AM, Kowalski J, Werb Z, Ferrara N. VEGF couples hypertrophic cartilage remodeling, ossification and angiogenesis during endochondral bone formation. Nat Med. 1999;5:623– 628. 6. Li J, Zhang YP, Kirsner RS. Angiogenesis in wound repair: angiogenic growth factors and the extracellular matrix. Microsc Res Tech. 2003;60:107–114. 7. Fouletier-Dilling CM, Gannon FH, Olmsted-Davis EA, et al. Efficient and rapid osteoinduction in an immune-competent host. Hum Gene Ther. 2007;18:733–745. 8. Olmsted-Davis E, Gannon FH, Ozen M, et al. Hypoxic adipocytes pattern early heterotopic bone formation. Am J Pathol. 2007;170:620–632. 9. Shen M, Yoshida E, Yan W, et al. Basic helix-loop-helix protein DEC1 promotes chondrocyte differentiation at the early and terminal stages. J Biol Chem. 2002;277:50112–50120. 10. Hadjantonakis AK, Dickinson ME, Fraser SE, Papaioannou VE. Technicolour transgenics: imaging tools for functional genomics in the mouse. Nat Rev Genet. 2003;4:613–625. 11. Olmsted EA, Blum JS, Rill D, et al. Adenovirus-mediated BMP2 expression in human bone marrow stromal cells. J Cell Biochem. 2001;82:11–21. 12. Fouletier-Dilling CM, Bosch P, Davis AR, et al. Novel compound enables high-level adenovirus transduction in the absence of an adenovirus-specific receptor. Hum Gene Ther. 2005;16:1287– 1297. 13. Olmsted-Davis EA, Gugala Z, Gannon FH, et al. Use of a chimeric adenovirus vector enhances BMP2 production and bone formation. Hum Gene Ther. 2002;13:1337–1347. 14. Gerdes J, Schwab U, Lemke H, Stein H. Production of a mouse monoclonal antibody reactive with a human nuclear antigen associated with cell proliferation. Int J Cancer. 1983;31:13–20. 15. Sato Y, Kanno S, Oda N, et al. Properties of two VEGF receptors, Flt-1 and KDR, in signal transduction. Ann NY Acad Sci. 2000;902: 201-5; discussion 205–207. 16. Reddi AH. Bone and cartilage differentiation. Curr Opin Genet Dev. 1994;4:737–744. 17. Trelles RD, Leon JR, Kawakami Y, Simoes S, Belmonte JC. Expression of the chick vascular endothelial growth factor D gene during limb development. Mech Dev. 2002;116:239–242. 18. Reddi AH. Regulation of cartilage and bone differentiation by bone morphogenetic proteins. Curr Opin Cell Biol. 1992;4:850–855. 19. Zelzer E, McLean W, Ng YS, et al. Skeletal defects in VEGF(120/120) mice reveal multiple roles for VEGF in skeletogenesis. Development. 2002;129:1893–1904. 20. Li X, Cao X. BMP signaling and skeletogenesis. Ann N Y Acad Sci. 2006;1068:26–40. 21. Hogan BL. Bone morphogenetic proteins in development. Curr Opin Genet Dev. 1996;6:432–438. 22. Shafer J, Gannon DA, Fouletier-Dilling FH, et al. Oxygen tension directs chondrogenic differentiation of myelo-monocytic progenitors during endochondral bone formation. Tissue Eng. 2007;13:2011– 2019. 23. Rissanen TT, Markkanen JE, Gruchala M, et al. VEGF-D is the strongest angiogenic and lymphangiogenic effector among VEGFs delivered into skeletal muscle via adenoviruses. Circ Res. 2003;92:1098– 1106. 24. Moser M, Binder O, Wu Y, et al. BMPER, a novel endothelial cell precursor-derived protein, antagonizes bone morphogenetic protein signaling and endothelial cell differentiation. Mol Cell Biol. 2003;23:5664–5679. VESSELS FORM PRIOR TO CARTILAGE Journal of Bone and Mineral Research 1155 25. Mishina Y, Suzuki A, Gilbert DJ, et al. Genomic organization and chromosomal location of the mouse type I BMP-2/4 receptor. Biochem Biophys Res Commun. 1995;206:310–317. 26. Winnier G, Blessing M, Labosky PA, Hogan BL. Bone morphogenetic protein-4 is

required for mesoderm formation and patterning in the mouse. Genes Dev. 1995;9:2105–2116. 27. Kelly MA, Hirschi KK. Signaling Hierarchy Regulating Human Endothelial Cell Development. Arterioscler Thromb Vasc Biol. 2009. 28. Zhao Y, Glesne D, Huberman E. A human peripheral blood monocytederived subset acts as pluripotent stem cells. Proc Natl Acad Sci U S A. 2003;100:2426–2431. 29. Ruster B, Gottig S, Ludwig RJ, et al. Mesenchymal stem cells display coordinated rolling and adhesion behavior on endothelial cells. Blood. 2006;108:3938–3944. 30. Otsuru S, Tamai K, Yamazaki T, Yoshikawa H, Kaneda Y. Bone marrowderived osteoblast progenitor cells in circulating blood contribute to ectopic bone formation in mice. Biochem Biophys Res Commun. 2007;354:453–458. 31. Pufe T, Petersen WJ, Miosge N, et al. Endostatin/collagen XVIII–an inhibitor of angiogenesis–is expressed in cartilage and fibrocartilage. Matrix Biol. 2004;23:267–276. 32. Oshima Y, Sato K, Tashiro F, et al. Anti-angiogenic action of the Cterminal domain of tenomodulin that shares homology with chondromodulin- I. J Cell Sci. 2004;117:2731–2744. 33. Hayami T, Funaki H, Yaoeda K, et al. Expression of the cartilage derived anti-angiogenic factor chondromodulin-I decreases in the early stage of experimental osteoarthritis. J Rheumatol. 2003; 30:2207–2217. 34. Kaplan FS, Glaser DL, Shore EM, et al. Hematopoietic stem-cell contribution to ectopic skeletogenesis. J Bone Joint Surg Am. 2007;89:347–357. 35. Shukunami C, Iyama K, Inoue H, Hiraki Y. Spatiotemporal pattern of the mouse chondromodulin-I gene expression and its regulatory role in vascular invasion into cartilage during endochondral bone formation. Int J Dev Biol. 1999;43:39–49.

Musculoskeletal Pathology

Hypoxic Adipocytes Pattern Early Heterotopic Bone Formation

Elizabeth Olmsted-Davis,*†‡ Francis H. Gannon,§ Mustafa Ozen,¶ Michael M. Ittmann,¶ Zbigniew Gugala,_ John A. Hipp,‡ Kevin M. Moran,‡ Christine M. Fouletier-Dilling,* Shannon Schumara-Martin,* Ronald W. Lindsey,_ Michael H. Heggeness,‡ Malcolm K. Brenner,‡ and Alan R. Davis*†‡ *From the Center for Cell and Gene Therapy * and the Departments of Pediatrics,† Orthopedic Surgery,‡ and Pathology,¶ Baylor College of Medicine, Houston, Texas; the Department of Orthopedics and Rehabilitation,_ University of Texas Medical Branch, Galveston, Texas; and the Department of Bone Biology,§ Armed Forces Institute of Pathology, Washington, DC* **The factors contributing to heterotopic ossification, the formation of bone in abnormal soft-tissue locations, are beginning to emerge, but little is known about microenvironmental conditions promoting this often devastating disease. Using a murine model in which endochondral bone formation is triggered in muscle by bone morphogenetic protein 2 (BMP2), we studied changes near the site of injection of BMP2- expressing cells. As early as 24 hours later, brown adipocytes began accumulating in the lesional area. These cells stained positively for pimonidazole and therefore generated hypoxic stress within the target tissue, a prerequisite for the differentiation of stem cells to chondrocytes and subsequent heterotopic bone formation. We propose that aberrant expression of BMPs in soft tissue stimulates production of brown adipocytes, which drive the early steps of heterotopic endochondral ossification by lowering oxygen tension in adjacent tissue, creating the correct environment for chondrogenesis. Results in *misty* gray lean mutant mice not producing brown fat suggest that white adipocytes convert into fat-oxidizing cells when brown adipocytes are unavailable, providing a compensatory mechanism for generation of a hypoxic microenvironment. Manipulation of the transcriptional control of adipocyte fate in local softtissue environments may offer a means to prevent or treat development of bone in extraskeletal sites.** ***(Am J Pathol 2007, 170:620–632; DOI: 10.2353/ajpath.2007.060692)***

Heterotopic ossification, defined as the formation of bone in abnormal anatomical locations, can be clinically insignificant or devastating, depending on the site and duration of new bone formation.[1] Besides its high morbidity in total joint arthroplasty, there are many additional causes of heterotopic ossification, including soft-tissue trauma, central nervous system injury, vasculopathies, arthropathies, and inheritance. Fibrodysplasia ossificans progressiva is a rare genetic disorder in which disabling ectopic ossification progresses in a typical anatomical pattern until most or all major joints of the axial and appendicular skeleton are affected[2]; it has recently been found to be attributable to a mutation in ACVRI.[3] Arterial ossification and cardiac valve ossification seem to be highly regulated processes, possibly mediated by bone morphogenetic proteins (BMPs).[4] Attempts to prevent or treat aberrant bone formation have been restricted by the complexity and multiple causes of the disorder. Nonetheless, new therapies are being devised to target the inductive molecules that may trigger the process, the participating progenitor cells, and local tissue environments conducive to osteogenesis. [1] Gene therapy with BMP antagonists seems especially promising because overexpression of BMP4 and underexpression of physiological BMP antagonists are common findings in some forms of heterotopic ossification. [5] Because angiogenesis is absolutely required for endochondral bone formation and is a prominent feature of embryonic bone formation, fracture callus formation, and the preosseous

lesions in fibrodysplasia ossificans progressiva, targeting new blood vessel formation with anti-angiogenic agents may slow or inhibit the production of heterotopic bone.[6] To gain a more complete understanding of the factors that drive heterotopic ossification, we focused on the microenvironmental conditions needed to induce mesenchymal stem cells to differentiate to chondrocytes, which form the cartilaginous matrix essential to osteoblast recruitment and normal osteoid mineralization during endo-

Supported by the Department of Defense (grants PR0 33166 to E.O.D. and PR0 33169 to A.R.D.). Accepted for publication October 24, 2006. Address reprint requests to Alan R. Davis, Baylor College of Medicine, One Baylor Plaza, Houston, TX 77030. E-mail: ardavis@bcm.tmc.edu. *The American Journal of Pathology, Vol. 170, No. 2, February 2007* *DOI: 10.2353/ajpath.2007.060692*

Cell-Based Gene Therapy for Repair of Critical Size Defects in the Rat Fibula

ZaWaunyka W. Lazard,[1] Michael H. Heggeness,[2] John A. Hipp,[2] Corinne Sonnet,[1] Angie S. Fuentes,[2] Rita P. Nistal,[1] Alan R. Davis,[1,2,3] Ronke M. Olabisi,[4] Jennifer L. West,[1,4] and Elizabeth A. Olmsted-Davis[1,2,3]*

[1]Center for Cell and Gene Therapy, Baylor College of Medicine, Houston, Texas 77030
[2]Department of Orthopedic Surgery, Baylor College of Medicine, Houston, Texas 77030
[3]Department of Pediatrics–Hematology Oncology, Baylor College of Medicine, Houston, Texas 77030
[4]Department of Bioengineering, Rice University, 6500 Main St. MS 142, Houston, Texas 77030

ABSTRACT More than a decade has passed since the first experiments using adenovirus-transduced cells expressing bone morphogenetic protein 2 were performed for the synthesis of bone. Since this time, the field of bone gene therapy has tackled many issues surrounding safety and efficacy of this type of strategy. We present studies examining the parameters of the timing of bone healing, and remodeling when heterotopic ossification (HO) is used for bone fracture repair using an adenovirus gene therapy approach. We use a rat fibula defect, which surprisingly does not heal even when a simple fracture is introduced. In this model, the bone quickly resorbs most likely due to the non-weight bearing nature of this bone in rodents. Using our gene therapy system robust HO can be introduced at the targeted location of the defect resulting in bone repair. The HO and resultant bone healing appeared to be dose dependent, based on the number of AdBMP2-transduced cells delivered. Interestingly, the HO undergoes substantial remodeling, and assumes the size and shape of the missing segment of bone. However, in some instances we observed some additional bone associated with the repair, signifying that perhaps the forces on the newly forming bone are inadequate to dictate shape. In all cases, the HO appeared to fuse into the adjacent long bone. The data collectively indicates that the use of BMP2 gene therapy strategies may vary depending on the location and nature of the defect. Therefore, additional parameters should be considered when implementing such strategies. J. Cell. Biochem. 112: 1563–1571, 2011. _ 2011 Wiley-Liss, Inc.

KEY WORDS: HETEROTOPIC OSSIFICATION; CRITICAL SIZE DEFECT; BONE REPAIR

Successful bone repair of non-unions remains a complex challenge in orthopedics today. Segmental bone loss resulting from trauma, cancer progression and various bone diseases are treated with bone grafting procedures that occur approximately 500,000 times annually in the United States [Laurencin et al., 2006]. Around 11% of the non-fatal injuries in the United States involve long bone fractures [Vyrostek et al., 2004] and on average nonunion rates occur in about 10% of these cases, varying with the intervention treatment and type of long bone involved [Giannoudis and Atkins, 2007; Tzioupis and Giannoudis, 2007]. All of these factors contribute to a significant toll on the patients, through lengthy recovery times, changes in quality of life, and enormous expense associated with the course of treatment. Bone distraction osteogenesis, free vascularized bone transfer, limb shortening, and autologous bone grafts are common methods used to manage post-traumatic segmental bone defects in any of the long bone

segments. Specific conditions like mechanical instability, axial deviation, bone defect size, and presence of infection must be addressed with the treatment being customized to each specific case. Distraction osteogenesis, with either the lengthening or bone transport technique, uses the Ilizarov apparatus to stabilize the limb and treat very large defects, up to 30 cm. However, this procedure is plagued with long treatment duration and numerous complications including delayed union at the docking site and devascularization of the transport segment [DeCoster et al., 1999]. The complication rate (major and minor) associated with the Ilizarov technique has been

Biochemistry 112:1563–1571 (2011) Grant sponsor: DAMD; Grant number: W81XWH-07-1-0215; Grant sponsor: DARPA; Grant number: W911NF-09-1- 0040. *Correspondence to: Dr. Elizabeth Olmsted-Davis, PhD, One Baylor Plaza Alkek N1010, Houston, TX 77030. E-mail: edavis@bcm.edu Received 2 February 2011; Accepted 4 February 2011 _ DOI 10.1002/jcb.23068 _ _ Published online 22 February 2011 in Wiley Online Library (wileyonlinelibrary.com). reported to reach as high as 87% [Motsitsi, 2008].

Vascularized bone transplantation can be performed with iliac crest, fibula, or rib but it has significant drawbacks involving donor site morbidity and increased fracture risk [DeCoster et al., 2004]. Limb shortening is restricted to bone defects less than 3 cm and has the shortest treatment time, but it is also associated with excessive soft tissue swelling and loss of limb function [Watson et al., 1995]. Today the gold standard of care for segmental bone loss has become autologous bone graft, but it is limited by graft material availability. Therapies are also plagued with a plethora of complications and drawbacks. Infection, implant failure, dysfunctional limb, unplanned additional surgical procedure, high cost, and prolonged treatment time are only a few of the shortcomings associated with these treatments [Finkemeier, 2002; DeCoster et al., 2004; Sen and Miclau, 2007]. A 30% failure rate is associated with the surgical treatments for segmental bone defects [Sorger et al., 2001]. Bone graft materials are selected based on their osteogenic, osteoinductive, and osteoconductive qualities that would produce the best healing and mechanical stability for each individual case. Osteoinduction refers to the ability of the material to stimulate the host precursor cells to form new bone through their differentiation into chondroblasts or osteoblasts. The osteoinductive capacity of a graft depends on the amount and type of growth factors and cytokines present. One of the most promising growth factors currently being tested is bone morphogenetic protein 2 (BMP2), which can induce both orthotopic and de novo bone formation at targeted locations. Recombinant human rhBMP-2 and rhBMP-7 are approved for clinical application and are commercially available, although neither has been determined to be efficacious in long bone repair by the FDA. One problem associated with the use of the recombinant proteins, beyond the expense and extremely high amount that must be delivered for any effect, is their extremely short half lives in vivo at approximately 24 h [Winn et al., 2000; Jeon et al., 2007]. Further, because of their short retention at the target site additional carrier materials must be implanted as well, thus increasing the risk of infection and making placement of the material difficult [Hollinger et al., 1998; Haidar et al., 2009]. Many have attempted to deliver the BMP2 through gene therapy means in order to overcome delivery of protein that has limited efficacy. These approaches employ either retroviral-transduced cells or the direct use of adenovirus with both methods having serious limitations. The delivery of retroviral-transduced cells, which carry 1–2 copies of the BMP2 gene, provide low levels of the protein locally and allow for these genetically modified cells expressing BMP2 to be incorporated into the bone which increases the overall risk of unwanted long-term adverse reactions [Moutsatsos et al., 2001]. Researchers have also attempted to introduce non-integrating vectors, such as adenovirus or adeno-associated virus [Lieberman et al., 1998; Gafni et al., 2004], directly into the animal which has a large number of associated problems, including poor transduction efficiencies [Olmsted et al., 2001] and diffusion of the free virus expressing BMP2 to other tissues such as the liver and lungs [Baltzer et al., 2000; Gelse et al., 2001]. The injection of the free virus results in limited to no efficacy along with undetectable amounts of protein being expressed at the desired site, as well as significant risk to other tissues such as the liver. To circumvent these problems we have employed a cell-based gene therapy approach, which eliminates the use of free virus in the organism and ensures reliable, efficient transduction, and/or expression of the BMP2 at the target site. Further, the BMP2 transgene cannot integrate into the chromosome, and with the use of a first generation vector the transduced cells are rapidly cleared by the immune system [Fouletier-Dilling et al., 2007].

Again, because the cells are transduced ex vivo, with a replication defective adenovirus, the resultant cells are not considered to be infectious or contain any infectious material, thus there is minimal risk associated with the use of this gene therapy system. Additionally, this system provides a sufficient local concentration of the BMP2 at the target site but the transgene does not integrate into the chromosome, so there is no long-term risk associated with chronic BMP2 expression, or other gene disruption from the insertion. Finally, in our previous studies of heterotopic ossification (HO), we have determined that the cells do not incorporate into the final bone structures and are only acting to deliver the BMP2. This importantly avoids potential longterm adverse reactions arising from the inclusion of the foreign materials in the skeletal bone. In the studies presented here, we are harnessing the bone induction capability of recombinant adenoviral-transduced cells to safely and efficaciously deliver BMP2. This cell-based gene therapy system provides sufficient BMP2 protein in vivo at a specific targeted location to induce rapid repair of a critical size defect introduced into the rat fibula. This circumvents the need for releasing carriers and supraphysiological concentrations of BMP2. Furthermore, the rat fibula model is somewhat unique in that it is fused at the ends to the adjacent tibia, thus creating a non-weight bearing environment. We have noted that even a simple fracture introduced into the fibula does not heal, but rather undergoes extensive resorption leaving an approximate 10mm size defect. Thus, repair of this bone would represent an extremely challenging environment. In the studies presented here, we demonstrate the parameters required by this system for bone healing and find that complete healing occurred by 6 weeks in 100% of the animals. Further, we followed the animals for an additional 6 weeks beyond this point to confirm that the fibula was stable and no additional changes resulted post-healing.

MATERIALS AND METHODS

CELL CULTURE A human fibroblast cell line (MRC5) was acquired from the American Type Culture Collection (Manassas, VA) and propagated in Dulbecco's modified Eagle's medium (DMEM). The medium was supplemented with 10% fetal bovine serum (FBS; Hyclone, Logan, UT), penicillin (100 U/ml), streptomycin (100 mg/ml), amphotericin B (0.25mg/ml; Invitrogen Life Technologies, Gaithersburg, MD), and tetracycline (3 mg/L; Sigma, St. Louis, MO). MRC5 cells are not capable of inducing bone formation before transduction. W20-17, a murine stromal cell line, was obtained as a gift from Genetic Institute (Cambridge, MA) and was propagated as described by Thies et al. [1992]. The W20-17 cells were briefly grown in

supplemented DMEM and cultured at a subconfluent density in order to maintain the phenotype. All cell types were grown at 378C and 5% CO_2 in humidified air. ADENOVIRUS TRANSDUCTION A replication-defective E1- to E3-deleted human adenovirus type 35 fiber protein (Ad5F35) were constructed to contain cDNAs for BMP2 in the E1 region of the virus [Olmsted-Davis et al., 2002] or did not contain any transgene in this region, AdEmpty. The resultant purified viruses, AdBMP2, and AdEmpty cassette, had viral particle (VP)-to-plaque-forming unit (PFU) ratios of 1:77 and 1:111, respectively, and all viruses were confirmed to be negative for replication-competent adenovirus [Olmsted-Davis et al., 2002]. Cells were transduced as previously described with AdBMP2 or AdEmpty cassette at a viral concentration of 2,500 VP/cell [Olmsted-Davis et al., 2002; Fouletier-Dilling et al., 2007]. MRC5 cells were transduced with either AdEmpty or AdBMP2 in DMEM supplemented with 2% FBS at a concentration of 2,500 VP/cell. Adenovirus was allowed to incubate overnight at 378C, humidified atmosphere, 5% CO_2. QUANTIFICATION OF BMP2 BMP2 protein was measured in culture supernatant taken from cells 72 h after transduction with AdBMP2 and culture supernatant was collected and assayed for BMP2 protein using a Quantikine BMP2 immunoassay ELISA kit (DBP200; R&D Systems, Minneapolis, MN). BMP2 protein activity was quantified in culture supernatant collected from cells after transduction with AdBMP2 or AdEmpty cassette or no virus, and a portion incubated with W20-17 bone marrow stromal cells, which rapidly increases alkaline phosphatase expression. Alkaline phosphatase activity is readily quantified [Blum et al., 2001]. Briefly, W20-17 cells were plated in 24-well plates at subconfluent densities (5_10_4 cells/cm_2) and 24 h later the media was replaced with 200ml of fresh media and 200 ml of conditioned culture media from various cells doses. W20-17 cells were then assayed for alkaline phosphatase activity 72 h after the addition of conditioned culture supernatant using a chemiluminescence procedure [Olmsted et al., 2001]. Cellular alkaline phosphatase was extracted by washing the cells with PBS and cells were lysed with three cycles of freeze thaw in 100 ml/cm_2 of 25mM Tris– HCl, pH 8.0, and Triton X-100. For detection of alkaline phosphatase 2ml of $CSPD_1$ ready-to-use with Sapphire II enhancer (Tropix, Bedford, MA) in an eppendorf tube, vortexed, and incubated at room temperature for 30 s. The light output from each sample was integrated for 10 s after a 2-s delay by a Glomax 20/20 luminometer (Promega, Madison, WI). Alkaline phosphatase detection signal was recorded in relative luminescence units (RLU). CRITICAL SIZE DEFECT MODEL The critical size defect was introduced into the rat fibula. Adult homozygous Athymic RNU Nude rats weighing (200–300 g) were administered buprenorphine at 0.5 mg/kg by subcutaneous injection into the right thigh 1 h prior to surgery. The rats underwent general anesthesia through the use of an animal vaporizer that dispensed isoflurane at 2–4% initial induction and 1–

2% throughout the surgery. Each animal was shaved, disinfected with Hibiclens and isolated to a sterile surgical field that included a surgical drape that allowed only the left hind limb to be exposed. A lateral incision in the skin of about 2 cm was performed on the lower leg, along with a smaller incision into the gastrocnemius muscle. This muscle was retracted in order to expose the fibula and an osteotomy was performed to create a 2–4mm segmental defect on the diaphysis of the fibula. Cells were then introduced into the defect void by placement into a sutured muscle pocket. Animals (n¼8) were euthanized and tissues isolated at various time points as indicated in the text. All animal studies were performed in accordance with the standards of Baylor College of Medicine, Department of Comparative Medicine, after review and approval of the protocol by the Institutional Animal Care and Use Committee (IACUC). RADIOGRAPHIC ANALYSIS OF THE NEW BONE Hind limbs were harvested and radiographically analyzed using an XPERT model faxitron (Kubtec, Fairfield, CT) in biplanar projections. Samples were set at an exposure time of 15 s and acceleration voltage of 30 kV. Bone healing was evaluated with radiographs at the termination of each study. Qualitative radiographic analyses were performed using microcomputed tomography (MicroCT) system (eXplore Locus SP: GE Healthcare, London, ON, Canada) at 14 mm resolution. Bone density was determined with a density calibration phantom. Threedimensional reconstructions and cross-sections of the hind limb were generated to identify the defect void and new bone. HISTOLOGICAL ANALYSIS OF THE NEW BONE Animals (n¼8) were euthanized at weekly intervals starting at 2 weeks and ending at 12 weeks. Hind limbs were isolated; formalin fixed, and decalcified paraffin embedded. Serial sections (5 mm) were prepared that encompassed the critical defect site. Hematoxylin and eosin staining was performed on every fifth slide to locate the newly forming endochondral bone. All sections were analyzed by light microscopy.

RESULTS

MODEL OF CRITICAL SIZE DEFECT Varying sizes of bone were removed from the rat fibula starting with a simple fracture (1 mm), and systematically increasing in 1mm increments to a maximum of 10 mm. The rat fibula was selected over other potential bones because unlike in humans, in rodents this bone is uniquely fused to the adjacent tibia. Therefore, a critical defect can readily be introduced without need for additional fixation. After 2 weeks bone healing was radiologically evaluated using microcomputational tomography (mCT). Surprisingly, in all cases 1, 2, 5, and 10mm defects (Fig. 1A–D, respectively) we observed a similar size defect of approximately 10mmor the maximum size introduced into the bone, and the bone ends appeared to be pointed, suggesting that the bone was undergoing significant resorption. Rotation of the mCT images indicated that the bone ends were healed with no apparent sign of an open bone marrow cavity. This indicates that in all cases the bone was not only unable to repair, but that it no longer could maintain normal bone remodeling and had initiated resorption. These results imply that any defect introduced into this model is a significant challenge for bone repair. DOSE RESPONSE TO ADBMP2-TRANSDUCED CELLS We next defined the dose of AdBMP2-transduced cells required to provide optimal healing of the bone defect. Fibroblasts were transduced with AdBMP2 at 2,500 vp/cell [Gugala et al., 2003] and BMP2 protein as well as activity was quantified 72 h later. Total BMP2 protein within the culture supernatant was approximately 18.6 ng per 1_10^6 cells (Fig. 2A). Cells transduced with AdEmpty, as well as untransduced cells, did not produce BMP2. Interestingly, a standard dose of recombinant BMP2 protein used to induce bone formation in a rat critical size defect was approximately 12 mg [Endo et al., 2006]. Since 5_10^6 BMP2-producing cells is adequate to heal the bone completely (Fig. 3A), and we have determined that the transduced cells are present at a maximum of 5 days [Fouletier-Dilling et al., 2007]. This means that a maximum of 93 ng is sufficient to completely heal the bone in this model. This is 130 times less than the amount of protein used in other rat defect studies with recombinant BMP2 suggesting that the prolonged local generation of BMP2 is critical to success due to the short half life of the protein [Endo et al., 2006]. Further, BMP2 protein activity, as determined by the elevation in the BMP2 responsive protein alkaline phosphatase [Blum et al., 2001], showed that this BMP2 being made is active (Fig. 2B). At no time did we observe either BMP2 activity or protein in culture supernatant isolated from the AdEmpty cassette cells or cells alone. Various numbers of the AdBMP2-transduced cells were next injected simultaneously with the introduction of a 3mm bone defect in the fibula. The cells were injected into the void region, and surrounding muscle tissues of the rats (n¼5), and potential bone formation allowed to progress for 2 weeks. Representative images of Fig. 1. Representative three-dimensional reconstructions of rat fibulas through microcomputational analysis. Varying sizes of defects (1–10 mm) were surgically introduced into rat fibulas and 2 weeks later analyzed for the presence of bone repair. The results depicted show an approximately 10mm defect independent of the original defect size (A) 1 mm, (B) 2 mm, (C) 5 mm, and (D) 10 mm. Fig. 2. Quantification of BMP2 protein and activity from adenovirus-transduced cells. A: BMP2 activity in culture supernatant collected 72 h after transduction with AdBMP2- or AdEmpty cassette-transduced cells (2,500 vp/cell) was quantified using an ELISA. BMP2 protein is represented as total protein produced by 5_10^6 cells. Error bars represent means_SD for n¼5. A Student's t-test was applied to demonstrate significance. B: Alkaline phosphatase activity in W20-17 cells after addition of conditioned media from AdBMP2- or AdEmpty cassette-transduced cells (2,500 vp/cell). To demonstrate endogenous levels of alkaline phosphatase we included the cells alone. Alkaline phosphatase activity is depicted as the average relative chemiluminescence units (RLU),

where n¼3. Error bars represent means_SD for n¼3. A Student's t-test was applied to demonstrate significance. the resulting new bone are shown in Figure 3. As seen in Figure 3A, the new bone formation varied drastically with cell numbers. At no time did we observe bone formation or healing in the samples receiving 5_10^4 cells, suggesting that there is a threshold amount of BMP2 required for inducing bone formation. Alternatively, there was no statistical difference between the two highest cell numbers or doses (Fig. 3B), indicating that there is a maximum bone formation response that can be achieved with this system. No bone formation was observed in with the 5_10^4 cell dose, whereas there is a significant 10-fold change in bone volume between the 5_10^5 and 5_10^7 cell doses. There was a significant difference between the highest doses 5_10^6 and 5_10^7 suggesting that this may be a maximum response to BMP2. For that reason, we used this dose for all subsequent experiments. BONE HEALING OF THE FIBULA DEFECT We next determined the ability of the therapy to heal the critical size defect over 12 weeks. Figure 4 shows there is substantial bone formation at 2 weeks using this dose of cells, which appears to quickly resorb and by 4 weeks the new bone more closely resembles the fibula that it is replacing. However, as seen in the cross-sectional mCT (Fig. 4F) new bone appears to be immature in nature. Although it spans the defect and is contiguous with the skeletal bone, it has not remodeled to have contiguous cortices, which suggests that this may not be well integrated at this stage. Alternatively, by 6–12 weeks a cortical bone structure begins to appear in the newly formed bone (Fig. 4H–J), suggesting that the bone is being remodeled and most likely fused. Bone healing and remodeling appears to be complete by 6 weeks (Fig. 4H) with little additional remodeling occurring at weeks 9–12. Interestingly, there appears to be additional bone attached to the skeletal bone (Fig. 4C–E), or actual residual HO that has not been resorbed. Additionally, some samples appeared to have a small amount of residual HO which was not attached to the fibula, but remained in the muscle between fibers. We next looked at the bone architecture by analyzing crosssectional cuts through the bone. The architecture appeared to change dramatically over the course of bone healing. Changes in bone architecture are a component of bone remodeling and aid in determining if the new bone has truly fused to the skeletal bone. Fusion at the defect site is a critical parameter in this system, because Fig. 3. Resultant bone formation from the introduction of adenovirus-transduced cells into the defect site. A: Representative three-dimensional surface renderings obtained from microcomputational analysis of the resultant bone repair 2 weeks after introduction of critical size defect in the rat fibula and delivery of varying numbers of AdBMP2- transduced cells; (a) 5_10^4 cells, (b) 5_10^5, (c) 5_10^6, (d) 5_10^7. B: Quantification of the bone repair using microcomputational analysis. Bone volume of the newly forming bone as depicted in (A), was calculated for each cell dose (n¼5 per group). The means and standard deviations for each group were calculated and compared using a one-way analysis of variance. the majority of the new bone is made de novo, as HO, and it must fuse to the skeletal bone to complete healing. At 2 weeks the new bone is found throughout the skeletal defect (Fig. 4F); however, it appears to be immature bone, which has not remodeled or integrated into the adjacent skeletal bone. This is in contrast to the adjacent skeletal bone, which has well-defined cortices and a hollow bone marrow cavity. Thus, although there is new bone, it does not appear to be well fused into the skeletal bone, or healed to the point such that it is one contiguous remodeled structure. However, by 6 weeks portions of the new bone appear to be remodeled with defined cortical bone and the tentative fusion site are less apparent (Fig. 4H), suggesting that the bone is integrated and almost completely healed. By 9–12 weeks, we observed integrated structures with the only abnormality being the additional small amounts of bone on the outer cortex (Fig. 4I,J). We next examined the bone healing through histological analysis to confirm the remodeling and fusion of the newly formed bone with the skeletal bone. This requires bone remodeling to replace the woven bone and lamellar bone junction with integrated remodeled bone. Photomicrographs from representative samples of the healing fibulas show substantial immature bone that completely fills and surrounds the defect (Fig. 5). Over time however, the bone remodels considerably and new cartilage is no longer present in the tissues (Fig. 5B). By 6 weeks, the bone appears to be considerably more mature, with thicker cortical area that are contiguous with the skeletal cortical bone (Fig. 5C). Interestingly, the adjacent cortical bone appears to have a significant gap, which may represent either an area where the bone is vascularized, as evidenced by the pooling of blood or alternatively, a defect introduced during healing (Fig. 5C). However, this defect was not observed through radiograph analysis (Fig. 4C), suggesting that it comprises a relatively small region of the new bone. It is also of interest to note that in the serial sections where this cortex appears uniform and contiguous, the adjacent cortex now appears ruffled. This indicates that although it is healing, the new shape of the bone does not exactly mimic the original fibula. At 9 and 12 weeks, there is once more additional bone on the exterior of the fibula. However, the interior cortex appears uniform and similar to the normal fibula (Fig. 5D,E).

DISCUSSION

These studies are the first to introduce a cell-based gene therapy system into a rat critical size defect model and have it lead to rapid Fig. 4. Microcomputational analysis of bone healing over time. Representative three-dimensional

surface renderings (A–E) or two-dimensional reconstructions (F–J) of bone healing over time; (A,F) 2 weeks; (B,G) 4 weeks; (C,H) 6 weeks; (D,I) 9 weeks; and (E,J) 12 weeks after introduction of the AdBMP2-transduced cells in the fibula defect; n¼9 per group. replacement and repair of the bone. HO can successfully be induced and directed to heal a critical size defect even in bone conditions that favor bone resorption. The HO, once touching the skeletal bone, can prevent rapid resorption and enhance the bone formation, remodeling, and fusion. The overall complete healing occurs rapidly from 2 to 6 weeks with 100% healing and repair completed by 6 weeks. Interestingly, little remodeling or additional resorption appears to occur after this time. In many cases after the initial resorption, there are small amounts of bone either heterotopic or orthotopic that are associated with the structures and appear to persist. This may be due in part to the non-weight bearing nature of this bone. The rat fibula was selected for this model based on the unique fusion of this bone to the adjacent tibia. Thus, the tibia functions as an external support and no additional fixation is required, allowing this to be a very fast and reliable model. To our surprise, studies to determine the critical distance that would be unable to heal on its own showed even a simple fracture led to rapid resorption and nonunion of this bone. Interestingly, since this bone is non-weight bearing in the rodent due to the fusion with the tibia, the rapid resorption may be a result from the lack of forces on this bone. Similar phenomenon has been reported in cases where HO has become extensive enough to become weight bearing, leading to the almost complete resorption of the normal skeletal bone. Further, it has long been known that disuse of skeletal bone during immobilization can lead to elevated resorption. Therefore this model, beyond its versatility, becomes one of the most challenging of all bone repair models for the investigation of bone healing. With bone remodeling favoring resorption, contribution to new bone formation is challenging and thus may be even more difficult to obtain fusion and complete repair. Complete bone healing could be reliably achieved using a minimal dose of 5_10^6 AdBMP2-transduced cells. This number of cells yields approximately 93 ng of total BMP2 protein within culture supernatant over a 5-day period. Although lesser numbers of AdBMP2-transduced cells (5_10^5) or BMP2 (9 ng) did result in heterotopic bone formation, it was not enough to reliably heal the fibula defect. Smaller doses, such as 1 ng, were unable to induce HO. Delivery of additional cells beyond 5_10^6 resulted in a similar volume of bone, suggesting that there is an upper threshold at which BMP2 receptors are saturated and no additional response will occur. Further, the volume of bone obtained when 5_10^6 AdBMP2- transduced cells were delivered to the defect was larger than required for complete healing, and substantial resorption was observed within the first 2–4 weeks as the fibula regained its physiological shape. Fig. 5. Representative photomicrographs of the fibula defect at various times after introduction of the AdBMP2-transduced cells. Tissues were formalin fixed decalcified, paraffin embedded and serial sectioned (5 mm) through the entire fibula region. Every fifth section was hematoxylin and eosin stained, and images taken which were representative of the defect region in particular the junction with the fibula at various times, (A) 2 weeks, (B) 4 weeks, (C) 6 weeks, (D) 9 weeks, and (E) 12 weeks. The appearance of bone is identified with (B).

 Interestingly, recombinant BMP2 studies in rat shows that minimal bone formation is detected at protein levels less than 10 mg [Vogelin et al., 2005], which is 130 times more BMP2 than we require for complete healing (Figs. 2 and 3). This indicates that the BMP2 protein produced by the adenovirus-transduced cells is likely more active or potent than the purified recombinant protein. In addition, this concentration is roughly in the range of physiological concentrations of BMP2, revealing that this system is very unique and perhaps should not be compared to systems employing the recombinant protein [Sciadini and Johnson, 2000; Vogelin et al., 2000, 2005]. The ability to generate, in vivo, biologically active BMP2 in the physiological range similar to what would be expected during bone fracture [Kloen et al., 2002, 2003; Kugimiya et al., 2005] or reduction of blood flow [Yao et al., 2010] suggests that the BMP2 produced in vivo in the eukaryotic cells may be mimicking physiological scenarios that lead to repair of fractures. The kinetics of bone healing appears to be similar to fracture callus, with a large disorganized structure within the defect area initially formed and successive remodeling and resorption to produce a structure similar to the original fibula. The initial new bone was observed within 10 days of delivery, with the first emergence of a remodeled bone with cortical appearance and inner marrow cavity appearing at 6 weeks. However, approximately half of the samples at 6 weeks still had one cortical bone interface that did not appear contiguously remodeled yet (Fig. 4H), suggesting that the bone had not completely remodeled yet. However, at 9 weeks, all samples appeared to be well remodeled with visible contiguous cortical bone, suggesting that at this point all defects were reliably healed. We observed little change from 9 to 12 weeks; although there was additional bone observed associated with the newly formed skeletal bone. The majority of the bone remodeling and resorption occurred within the first 4 weeks, where the callus-like structure resorbs and begins to form bone in the shape of the original fibula. Histological analysis of the bone healing within the defect supports the subsequent findings. A large amount of mature bone and cartilage that extend away from the defect site are observed at 2 weeks (Fig. 5A). By 6 weeks and beyond, the bone was more restricted to the defect region (Fig. 5C–E). Although substantial immature woven bone was observed at 4 weeks, by 6 weeks remodeled bone with defined cortical structures could be seen

(Fig. 5B,C), suggesting that substantial remodeling and maturation was occurring between 4 and 6 weeks. Again little change occurs histologically between 9 and 12 weeks, suggesting that the bone was maintained and healing was complete. Interestingly, in these tissues the cortical bone appeared to be contiguous. Since the exact shape of the original fibula was not achieved, this may suggest that the signals which would direct and define the exterior cortices may be lacking in this model. In conclusion, bone healing of a critical size defect in the rat fibula could be rapidly achieved through injection of a cell-based gene therapy system. This system delivered 130 times less BMP2 protein compared to studies using recombinant protein as the osteoinductive agent and was able to induce bone within a physiological range of BMP2 concentration. Thus, this cell-based approach is reliable, efficacious, and importantly has additional safety in that no free virus or infectious agents of any kind would be delivered to patients. These studies are the first step in developing a cell-based gene therapy which effectively harnesses the capacity of BMP2 to generate bone at target locations and rapidly repair skeletal bone.

ACKNOWLEDGMENTS This work was supported in part by grants from Department of Defense (DAMD) W81XWH-07-1-0215 and Defense Advanced Research Agency (DARPA) W911NF-09-1-0040 (to E.A.O).

REFERENCES

Baltzer AW, Lattermann C, Whalen JD, Ghivizzani S, Wooley P, Krauspe R, Robbins PD, Evans CH. 2000. Potential role of direct adenoviral gene transfer in enhancing fracture repair. Clin Orthop Relat Res (379 Suppl):S120–S125. Blum JS, Li RH, Mikos AG, Barry MA. 2001. An optimized method for the chemiluminescent detection of alkaline phosphatase levels during osteodifferentiation by bone morphogenetic protein 2. J Cell Biochem 80:532–537. DeCoster TA, Simpson AH, Wood M, Li G, Kenwright J. 1999. Biologic model of bone transport distraction osteogenesis and vascular response. J Orthop Res 17:238–245. DeCoster TA, Gehlert RJ, Mikola EA, Pirela-Cruz MA. 2004. Management of posttraumatic segmental bone defects. J Am Acad Orthop Surg 12:28–38. Endo M, Kuroda S, Kondo H, Maruoka Y, Ohya K, Kasugai S. 2006. Bone regeneration by modified gene-activated matrix: Effectiveness in segmental tibial defects in rats. Tissue Eng 12:489–497. Finkemeier CG. 2002. Bone-grafting and bone-graft substitutes. J Bone Joint Surg Am 84-A:454–464. Fouletier-Dilling CM, Gannon FH, Olmsted-Davis EA, Lazard Z, Heggeness MH, Shafer JA, Hipp JA, Davis AR. 2007. Efficient and rapid osteoinduction in an immune-competent host. Hum Gene Ther 18:733–745. Gafni Y, Pelled G, Zilberman Y, Turgeman G, Apparailly F, Yotvat H, Galun E, Gazit Z, Jorgensen C, Gazit D. 2004. Gene therapy platform for bone regeneration using an exogenously regulated, AAV-2-based gene expression system. Mol Ther 9:587–595. Gelse K, Jiang QJ, Aigner T, Ritter T, Wagner K, Poschl E, von der Mark K, Schneider H. 2001. Fibroblast-mediated delivery of growth factor complementary DNA into mouse joints induces chondrogenesis but avoids the disadvantages of direct viral gene transfer. Arthritis Rheum 44:1943–1953. Giannoudis PV, Atkins R. 2007. Management of long-bone non-unions. Injury 38(Suppl 2):S1–S2. Gugala Z, Olmsted-Davis EA, Gannon FH, Lindsey RW, Davis AR. 2003. Osteoinduction by ex vivo adenovirus-mediated BMP2 delivery is independent of cell type. Gene Ther 10:1289–1296. Haidar ZS, Hamdy RC, Tabrizian M. 2009. Delivery of recombinant bone morphogenetic proteins for bone regeneration and repair. Part B: Delivery systems for BMPs in orthopaedic and craniofacial tissue engineering. Biotechnol Lett 31:1825–1835. Hollinger JO, Schmitt JM, Buck DC, Shannon R, Joh SP, Zegzula HD, Wozney J. 1998. Recombinant human bone morphogenetic protein-2 and collagen for bone regeneration. J Biomed Mater Res 43:356–364. Jeon O, Song SJ, Kang SW, Putnam AJ, Kim BS. 2007. Enhancement of ectopic bone formation by bone morphogenetic protein-2 released from a heparin-conjugated poly(L-lactic-co-glycolic acid) scaffold. Biomaterials 28:2763–2771. Kloen P, Doty SB, Gordon E, Rubel IF, Goumans MJ, Helfet DL. 2002. Expression and activation of the BMP-signaling components in human fracture nonunions. J Bone Joint Surg Am 84-A:1909–1918.

Kloen P, Di Paola M, Borens O, Richmond J, Perino G, Helfet DL, Goumans MJ. 2003. BMP signaling components are expressed in human fracture callus. Bone 33:362–371. Kugimiya F, Kawaguchi H, Kamekura S, Chikuda H, Ohba S, Yano F, Ogata N, Katagiri T, Harada Y, Azuma Y, Nakamura K, Chung UI. 2005. Involvement of endogenous bone morphogenetic protein (BMP) 2 and BMP6 in bone formation. J Biol Chem 280:35704–35712. Laurencin C, Khan Y, El-Amin SF. 2006. Bone graft substitutes. Expert Rev Med Devices 3:49–57. Lieberman JR, Le LQ, Wu L, Finerman GA, Berk A, Witte ON, Stevenson S. 1998. Regional gene therapy with a BMP-2-producing murine stromal cell line induces heterotopic and orthotopic bone formation in rodents. J Orthop Res 16:330–339. Motsitsi NS. 2008. Management of infected nonunion of long bones: The last decade (1996–2006). Injury 39:155–160. Moutsatsos IK, Turgeman G, Zhou S, Kurkalli BG, Pelled G, Tzur L, Kelley P, Stumm N, Mi S, Muller R, Zilberman Y, Gazit D. 2001. Exogenously regulated stem cell-mediated gene therapy for bone regeneration. Mol Ther 3:449–461. Olmsted EA, Blum JS, Rill D, Yotnda P, Gugala Z, Lindsey RW, Davis AR. 2001. Adenovirus-mediated BMP2 expression in human bone marrow stromal cells. J Cell Biochem 82:11–21. Olmsted-Davis EA, Gugala Z, Gannon FH, Yotnda P, McAlhany RE, Lindsey RW, Davis AR. 2002. Use of a chimeric adenovirus vector enhances BMP2 production and bone formation. Hum Gene Ther 13:1337–1347. Sciadini MF, Johnson KD. 2000. Evaluation of recombinant human bone morphogenetic protein-2 as a bone-graft substitute in a canine segmental defect model. J Orthop Res 18:289–302. Sen MK, Miclau T. 2007. Autologous iliac crest bone graft: Should it still be the gold standard for treating nonunions? Injury 38(Suppl 1):S75–S80. Sorger JI, Hornicek FJ, Zavatta M, Menzner JP, Gebhardt MC, Tomford WW, Mankin HJ. 2001. Allograft fractures revisited. Clin Orthop Relat Res (382): 66–74. Thies RS, Bauduy M, Ashton BA, Kurtzberg L, Wozney JM, Rosen V. 1992. Recombinant human bone morphogenetic protein-2 induces osteoblastic differentiation in W-20-17 stromal cells. Endocrinology 130:1318–1324. Tzioupis C, Giannoudis PV.

2007. Prevalence of long-bone non-unions. Injury 38(Suppl 2):S3–S9. Vogelin E, Brekke JH, Jones NF. 2000. Heterotopic and orthotopic bone formation with a vascularized periosteal flap, a matrix and rh-BMP- 2 (bone morphogenetic protein) in the rat model. Mund Kiefer Gesichtschir 4(Suppl 2):S454–S458. Vogelin E, Jones NF, Huang JI, Brekke JH, Lieberman JR. 2005. Healing of a critical-sized defect in the rat femur with use of a vascularized periosteal flap, a biodegradable matrix, and bone morphogenetic protein. J Bone Joint Surg Am 87:1323–1331. Vyrostek SB, Annest JL, Ryan GW. 2004. Surveillance for fatal and nonfatal injuries—United States, 2001. MMWR Surveill Summ 53:1–57. Watson JT, Anders M, Moed BR. 1995. Management strategies for bone loss in tibial shaft fractures. Clin Orthop Relat Res (315):138–152. Winn SR, Hu Y, Sfeir C, Hollinger JO. 2000. Gene therapy approaches for modulating bone regeneration. Adv Drug Deliv Rev 42:121–138. Yao Y, Bennett BJ, Wang X, Rosenfeld ME, Giachelli C, Lusis AJ, Bostrom KI. 2010. Inhibition of bone morphogenetic proteins protects against atherosclerosis and vascular calcification. Circ Res 107:485–494.

Commentary: Important considerations on bone morphogenetic protein-2 and neuroinflammation

Michael H. Heggeness, MD, PhD* Baylor College of Medicine, 6620 Main St, Houston, TX 77030, USA Received 19 May 2011; accepted 19 May 2011

COMMENTARY ON: Dmitriev AE, Lehman RA Jr., Symes AJ. Bone morphogenetic protein-2 and spinal arthrodesis: the basic science perspective on protein interaction with the nervous system. Spine J 2011;11:500–5 (in this issue).

The growth factor recombinant human bone morphogenetic protein (rhBMP-2) came into very widespread clinical use before the very complex biologic activities of the molecule were well understood. Indeed, the complex biological actions of BMP-2 are still not completely established and remain under active study. As the Dmitriev et al. [1] review article describes, the interaction of BMP-2 with neurological tissue is an important issue. At this point of time, the fact that BMP-2 induces inflammation is indisputable. We also know that along with this potent inflammatory process, BMP-2 stimulates the local formation of brown fat (with the production of heat and water via uncoupled mitochondrial activity) and ultimately leads to cartilage formation, neovascularization, and bone formation [2–4]. Very recent work has strongly suggested that there is a direct action of BMP-2 on peripheral nerves in a process that includes the direct induction of neuroinflammation. It further appears that this neuroinflammation may be basic to the process of BMP-2–induced bone formation [5]. This recent work, well summarized in the review by Salisbury et al. [5], demonstrates that the ‘‘release of BMP-2, such as during the induction of Heterotopic Ossification in soft tissue, initiates neurogenic inflammation within the local environment.’’ This process appears to involve the participation of mast cells. The frequent occurrence of new and ‘‘paradoxical’’ symptoms of leg pain, radiculitis, and sciatica in patients where BMP-2 had been applied near the spine may possibly be related to the direct interaction of BMP-2 with peripheral nerves or nerve roots within the surgical field. The Dmitriev et al. group also indicate that some of this effect may be because of direct effect on the dorsal root ganglia. Although these are currently early findings, the clinical complication involving apparent neurological effects (such as neuropathic pain, radiculitis, retrograde ejaculation, and so on) may be explained by these diverse mechanisms. In the future, the clinical use of recombinant BMP-2 may need to be carefully considered with attention to the protection of nerve roots, their dorsal root ganglia, large nerves, and autonomic plexuses from the local area of rhBMP-2 application. For now, it is important to understand that the BMP-2 interaction with neurologic tissues is complex, involves a potent inflammatory response, and that the downstream effects are not yet well understood.

References

[1] Dmitriev AE, Lehman RA, Symes AJ. Bone morphogenetic protein-2 and spinal arthrodesis: the basic science perspective on protein interaction with the nervous system. Spine J 2011;11:500–5. [2] Olmstead-Davis E, Gannon FH, Ozen M, et al. Hypoxic adipocytes pattern early heterotopic bone formation. Am J Pathol 2007;170:620–32. [3] Dilling CF, Wada AM, Lazard ZW, et al. Vessel formation is induced prior to the appearance of cartilage in BMP-2-mediated heterotopic ossification. J Bone Miner Res 2010;25:1147–56. [4] Shafer J, Davis AR, Gannon FH, et al. Oxygen tension directs chondrogenic differentiation of myelo-monocytic progenitors during endochondral bone formation. Tissue Eng 2007;13:2011–9. [5] Salisbury E, Sonnet C, Heggeness M, et al. Heterotopic ossification has some nerve. Crit Rev Eukaryot Gene Expr 2010;20:313–24. DOI of original article: 10.1016/j.spinee.2011.05.002. FDA device/drug status: not applicable. Author disclosures: MHH: Royalties: Relievant Medsystems Inc. (C), K2M (C); Stock Ownership: Relievant Medsystems Inc. (45000 Shares, 1.6%); Research Support: Investigator Salary: Department of Defense (E, Paid directly to institution/employer); Grants: Department of Defense (I, Paid directly to institution/employer). The disclosure key can be found on the Table of Contents and at www. TheSpineJournalOnline.com. * Corresponding author. Baylor College of Medicine, 6620 Main St, Houston, TX 77030, USA. Tel.: (713) 986-5730; fax: (713) 986-5731. E-mail address: heggeness@bcm.edu (M.H.

Heggeness) 1529-9430/$ - see front matter _ 2011 Elsevier Inc. All rights reserved. doi:10.1016/j.spinee.2011.05.010 The Spine Journal 11 (2011) 506

Sensory Nerve Induced Inflammation Contributes to Heterotopic Ossification

Elizabeth Salisbury,[1,2] Eric Rodenberg,[1] Corinne Sonnet,[1] John Hipp,[3] Francis H. Gannon,[3,4] Tegy J. Vadakkan,[5] Mary E. Dickinson,[1,5] Elizabeth A. Olmsted-Davis,[1,2,3,6] and Alan R. Davis[1,2,3,6]* [1]Center for Cell and Gene Therapy, Baylor College of Medicine, Houston, Texas 77030 [2]Translational Biology and Molecular Medicine, Baylor College of Medicine, Houston, Texas 77030 [3]Department of Orthopedic Surgery, Baylor College of Medicine, Houston, Texas, 77030 [4]Department of Pathology, Baylor College of Medicine, Houston, Texas 77030 [5]Department of Molecular Physiology and Biophysics, Baylor College of Medicine, Houston, Texas 77030 [6]Department of Pediatrics, Hematology-Oncology, Baylor College of Medicine, Houston, Texas 77030

ABSTRACT Heterotopic ossification (HO), or bone formation in soft tissues, is often the result of traumatic injury. Much evidence has linked the release of BMPs (bone morphogenetic proteins) upon injury to this process. HO was once thought to be a rare occurrence, but recent statistics from the military suggest that as many as 60% of traumatic injuries, resulting from bomb blasts, have associated HO. In this study, we attempt to define the role of peripheral nerves in this process. Since BMP2 has been shown previously to induce release of the neuroinflammatory molecules, substance P (SP) and calcitonin gene related peptide (CGRP), from peripheral, sensory neurons, we examined this process in vivo. SP and CGRP are rapidly expressed upon delivery of BMP2 and remain elevated throughout bone formation. In animals lacking functional sensory neurons (TRPV1 _/_), BMP2-mediated increases in SP and CGRP were suppressed as compared to the normal animals, and HO was dramatically inhibited in these deficient mice, suggesting that neuroinflammation plays a functional role. Mast cells, known to be recruited by SP and CGRP, were elevated after BMP2 induction. These mast cells were localized to the nerve structures and underwent degranulation. When degranulation was inhibited using cromolyn, HO was again reduced significantly. Immunohistochemical analysis revealed nerves expressing the stem cell markers nanog and Klf4, as well as the osteoblast marker osterix, after BMP2 induction, in mice treated with cromolyn. The data collectively suggest that BMP2 can act directly on sensory neurons to induce neurogenic inflammation, resulting in nerve remodeling and the migration/release of osteogenic and other stem cells from the nerve. Further, blocking this process significantly reduces HO, suggesting that the stem cell population contributes to bone formation. J. Cell. Biochem. 112: 2748–2758, 2011. _ 2011 Wiley-Liss, Inc.

KEY WORDS: HETEROTOPIC OSSIFICATION; NEUROGENIC INFLAMMATION; BONE MORPHOGENETIC PROTEIN TYPE 2; NEURAL CREST STEM CELLS

Bone morphogenetic proteins, named for their original isolation from ground bone [Urist, 1965], are a family of factors involved in patterning of the bone, vessels [Smadja et al., 2008], nerves [Anderson et al., 2006], blood [Bhatia et al., 1999], and, most recently, fat [Sottile and Seuwen, 2000; Tseng et al., 2008] of the early embryo. The BMPs appear to serve a similar role in the adult, where they have been shown to regulate the expansion and differentiation of progenitors for these same tissues [Yanagita, 2009]. One of the best studied of the BMPs, BMP2, is a highly conserved protein that has been shown to be the only common link between the various forms of heterotopic ossification (HO) [Kaplan et al., 2009a; Kaplan et al., 2009b; Shore and Kaplan, 2010]. HO, or bone formation at non-skeletal sites, is a disorder resulting from traumatic injury [Vanden Bossche and Vanderstraeten, 2005],

Cellular Biochemistry 112:2748–2758 (2011)

Additional supplementary information may be found in the online

version of this article. Grant sponsor: US Department of the Army; Grant numbers: DAMD W81XWH-07-1-0214, DAMD W81XWH-07-1- 0215; Grant sponsor: NBIB; Grant number: EB005173; Grant sponsor: NIH; Grant number: T-32 HL092332-06; Grant sponsor: American Heart Association; Grant number: AHA 10815339F; Grant sponsor: Kirschstein-NRSA; Grant number: T32 HL092332-08. *Correspondence to: Alan R. Davis, Baylor College of Medicine, One Baylor Plaza, Alkek N1010, Houston, TX 77030. E-mail: ardavis@bcm.edu Received 1 June 2011; Accepted 3 June 2011 _ DOI 10.1002/jcb.23225 _ _ Published online 15 June 2011 in Wiley Online Library (wileyonlinelibrary.com). with approximately 5% of all traumatic injuries leading to HO. HO has been linked specifically to the nervous system, as it appears after injury of the central nervous system (CNS) [Baird and Kang, 2009]. Maintenance of skeletal bone has been demonstrated to involve the CNS, through hypothalamic control of a number of neuroendocrine factors believed to directly regulate osteoblast function [Fu et al., 2005; Takeda and Karsenty, 2008; Ducy and Karsenty, 2010; Oury et al., 2010; Shi et al., 2010]. However, it is unclear that this mechanism results in the formation of ectopic bone. Some of the most compelling data linking HO formation to changes in the peripheral (PNS) or central nervous system come from recent statistics from the military, which suggest that 60% of all combat injuries have associated HO [Forsberg et al., 2009]. This is presumably because these are mostly blast or burn injuries, both having a significant impact on the PNS and CNS. Little is known about the causes of HO, beyond the common link to changes in BMP signaling. BMP2 has been shown to be elevated upon muscle injury and changes in blood flow, and BMP2 is released during bone injury [Beiner and Jokl, 2002; Johnson et al., 2006; Kwong and Harris, 2008; Sucosky et al., 2009]. Recently, BMP2 has also been shown to directly induce release of neuroinflammatory proteins from sensory neurons. Studies revealed the rapid upregulation of substance P (SP) and calcitonin gene related peptide (CGRP) in sensory neuron cultures, after addition of recombinant BMP2 [Bucelli et al., 2008]. The afferent, sensory fibers of the PNS release SP and CGRP leading to the induction of neuroinflammation. These sensory neurons are stimulated by noxious mechanical, thermal, or chemical stimuli, providing feedback on pain and temperature [Schaible et al., 2005], both locally and centrally through electrical signaling. The vanilloid (capsaicin) receptor TRPV1 (transient receptor potential cation channel V1) is a nociceptive ion channel located on sensory nerve endings that is activated by some of these noxious stimuli and involved in the mediation of pain [Szallasi et al., 2007; Khairatkar- Joshi and Szallasi, 2009]. Capsaicin, the compound in hot chili peppers, is one chemical stimulus, which can activate this channel, causing it to open, leading to an influx of calcium and sodium ions into the sensory neuron and triggering its depolarization. At normal levels, capsaicin binding transmits the sensation of pain. However, high doses of capsaicin lead to a massive influx of ions, resulting in death of sensory neurons expressing TRPV1. TRPV1 sensory neurons have been linked to a number of activities involving tissue regeneration and maintenance [Razavi et al., 2006], including repair of bone fractures, which were shown to be significantly inhibited when these nerves were ablated with capsaicin [Apel et al., 2009]. Morrison et al. [1999] isolated cells indistinguishable from neural crest stem cells from fetal peripheral nerves. Recently [Adameyko et al., 2009], such cells have been shown to be the origin of melanocytes in the skin in the adult. In addition, the bone tumor Ewing's sarcoma is composed of poorly differentiated cells that bear no relationship to mesenchymal cells, but show a definite relationship to neural crest stem cells [Cavazzana et al., 1987; Hu-Lieskovan et al., 2005]. This, coupled with the fact that some of the bones of the skull have been shown, using tracking techniques, to originate from the neural crest [Jiang et al., 2002], opens the question of whether the nerve may be an alternative niche for osteogenic progenitors. We provide evidence in these studies that suggest that the local peripheral nerves may indeed be an additional site for such progenitors. We developed a model of rapid, de novo bone formation, or heterotopic ossification, which relies on expression of physiological levels of BMP2 at the site of bone formation [Olmsted-Davis et al., 2002; Gugala et al., 2003; Fouletier-Dilling et al., 2005; Fouletier- Dilling et al., 2007]. Upon delivery of adenovirus-transduced cells expressing BMP2 within the muscle, a cascade of endochondral bone formation occurs over 7 days, resulting in mature bone and bone marrow [Olmsted-Davis et al., 2007; Dilling et al., 2010]. Using this heterotopic bone assay, we reliably produce mature bone when cells transduced with BMP2 adenovirus are delivered, but not when cells transduced with an empty cassette, control adenovirus are delivered, showing this bone formation is linked to BMP2. In addition, we have previously found that the transduced cells do not incorporate into any structures of the newly forming heterotopic bone and are only serving to deliver the BMP2

[Gugala et al., 2003; Fouletier-Dilling et al., 2007]. In the studies described here, we have used this model to elucidate the manner in which peripheral nerves participate in HO.

MATERIALS AND METHODS

CELL CULTURE A murine C57BL/6-derived fibroblast cell line was grown in a modified essential medium (a-MEM) supplemented with 10% fetal bovine serum, 100 U/ml penicillin, 100 mg/ml streptomycin, and 0.25 mg/ml amphotericin B and cultured, as previously described [Dilling et al., 2010]. All cell types were grown at 378C and 5% CO_2 in humidified air. The mouse fibroblast cell line was used only as a delivery cell for BMP2, and experiments repeated with multiple fibroblast cell types have yielded the same pattern of bone formation [Gugala et al., 2003; Olabisi et al., 2010]. ADENOVIRUSES AND CELL TRANSDUCTION Replication defective E1–E3 deleted first generation human type 5 adenovirus (Ad5) were constructed to contain cDNAs for BMP2 in the E1 region of the virus [Olmsted-Davis et al., 2002] or did not contain any transgene in this region, Adempty. Mouse fibroblasts (1_10^6) were transduced with Ad5-BMP-2 or Ad5-empty control virus at a concentration of 5,000 vp/cell with 1.2% GeneJammer, as described previously [Fouletier-Dilling et al., 2005]. HETEROTOPIC BONE ASSAY The transduced cells were resuspended at a concentration of 5_10^6 cells/100 ml of PBS and then delivered through intramuscular injection into the hind limb quadriceps muscle of C57BL/6 or TRVP1 _/_ mice (8–12 weeks old; Jackson Laboratories, Bar Harbor, ME). Sample sizes are indicated in figure legends. Animals were euthanized, as indicated in the text, either at daily intervals, or 10 days after injection of the transduced cells. Hind limbs were harvested and either placed in formalin or quick frozen and stored at _808C. All animal studies performed were in accordance with standards of the Baylor College of Medicine, Department of Comparative Medicine, after review and approval of the protocol by the Institutional Animal Care and Use Committee (IACUC). CROMOLYN ADMINISTRATIONS Intraperitoneal injections of sodium cromoglycate (C0399; Sigma- Aldrich, St. Louis, MO) were administered daily (8 mg/kg/day) for 5 days prior to intramuscular injection of transduced cells, and then continued daily throughout the time course of the heterotopic bone assay. Control animals were given intraperitoneal injections of the vehicle, phosphate buffered saline (PBS), following the same treatment regimen as experimental animals. Animals were euthanized at specified time points following injection of transduced cells. IMMUNOHISTOCHEMICAL ANALYSIS Mouse hind limbs were isolated, formalin fixed, and cut in half prior to decalcification, processing, and paraffin embedding. The tissues were serial sectioned (5 mm), and every fifth slide subject to hematoxylin and eosin staining as previously described [Olmsted-Davis et al., 2007]. Serial unstained slides were used for immunohistochemical staining (either single- or double-antibody labeling), using methods outlined previously. For double-antibody labeling, samples were treated with both primary antibodies simultaneously, followed by washing and incubation with respective secondary antibodies, used at 1:500 dilution, to which Alexa Fluor 488, 594, or 647 (Invitrogen, Carlsbad, CA) was conjugated. Primary antibodies were used as follows: Substance P, rat monoclonal, used at 1:250 dilution (Santa Cruz Biotechnology, Inc, Santa Cruz, CA) and CGRP, rabbit polyclonal, used at 1:250 dilution (Biomol/Enzo LifeSciences, Plymouth Meeting, PA), neurofilament, mouse monoclonal, (Sigma, St Louis, MO) used at 1:200 dilution, Klf4, goat polyclonal (R&D Systems, Minneapolis, MN) used at 1:200 dilution, nanog, goat polyclonal (Novus Biologicals, Littleton, CO) used at 1:250, osterix, goat or rabbit polyclonal (Santa Cruz Biotechnology, Inc, Santa Cruz, CA) used at 1:200, and VWF, rabbit polyclonal, (Chemicon, Billerica, MA) used at 1:250. Primary antibodies were either diluted in PBS and 10% serum of the species in which the secondary antibody was generated, or for mouse primary antibodies, staining was performed using the M.O.M. Kit (Vector Labs, Burlingame, CA). Tissues were mounted and counterstained using Vectashield mounting medium containing DAPI (Vector Laboratories, Burlingame, CA). Stained tissue sections were examined using an Olympus BX41 microscope equipped with a reflected fluorescence system, using a 20_/0.75 NA objective lens 10_, 20_, 40_, 100_. TOLUIDINE BLUE STAINING Decalcified, paraffin embedded tissue sections were stained with toluidine blue, to specifically identify mast cells. Toluidine blue O (Sigma, Chemical Company, St Louis, MO) was reconstituted in 70% ethanol, and then diluted at a ratio of 1:10 in 1% sodium chloride (pH¼2.3) for subsequent staining. After deparaffinization and hydration, sections were stained in the working solution of toluidine blue for 10 min, washed, dehydrated, and cover-slipped with resinous mounting medium. The number of toluidine blue (TB) positive cells in an area of the tissue was calculated by adding the number of positive cells counted in each of the fields taken within the area. The area fraction of TB þ cells was defined as the total number of TB þ cells within the area divided by the number of fields taken in that area. The TIFF images of the histological sections were first inverted using ADOBE Photoshop. In the inverted images, the mast cells appeared as bright spots. The number of mast cells in each inverted image was counted by segmenting the cells using FARSIGHT (RPI, Troy, New York). The area fraction was measured for five different fields, and the average area fraction was calculated for control and BMP-treated tissues for every fifth slide sectioned throughout the entire hind limb. The area fractions of TB þ cells in

the control and the BMP-treated tissues on day 2 were 3 and 8.33, respectively. Based on the Student's t test, the P value for the day 2 data was 0.02. PROTEIN EXTRACTION AND ANALYSIS Protein from the entire quadriceps muscle, injected with either Ad5BMP2 or Ad5empty transduced cells, was isolated using the Total Protein Extraction Kit (Millipore, Billerica, MA), following manufacturer's instructions. Muscle samples (n¼4) were collected every day, for 6 days following injection. Total protein concentrations of each sample were determined using the BSA Protein Assay Kit (Pierce/ThermoScientific, Rockford, IL). Quantification of protein levels of both Substance P and CGRP were assayed by Enzyme Immunoassay (EIA) (EK-061-05 and EK-015-09; Phoenix Pharmaceuticals, Inc., Burlingame, CA). For each EIA assay, samples were equally loaded based on the total protein concentration, and measured in duplicate. Results from each day were averaged, and the difference in protein levels in control and BMP2 samples assessed by standard t-test analysis. The differences in protein levels over time were analyzed by one-way analysis of variance tests (ANOVA) and post-hoc Bonferroni multiple comparisons tests comparing time points, using Stata Ver II (College Station, TX). MICROCOMPUTED TOMOGRAPHY Micro-CT exams were obtained of the left and right legs at 15 mm resolution (eXplore Locus SP; GE Healthcare, London, ON, Canada). A hydroxyapatite phantom was scanned alongside each specimen and was used to convert the scan data from arbitrary units to units of equivalent bone density. The scans were thresholded to exclude any tissue with a density less than 100 mg/cc, and the tissue volume within the region of interest was calculated as a measure of the total amount of mineralized tissue. The resulting data were analyzed by one-way analysis of variance to identify differences.

RESULTS

INDUCTION OF SUBSTANCE P AND CGRP THROUGH DELIVERY OF AdBMP2 TRANSDUCED CELLS To determine if BMP2 directly activates expression of the neuroinflammatory proteins SP and CGRP during heterotopic ossification, proteins were isolated from tissues at daily intervals, starting 24 h after delivery of AdBMP2 or Adempty (control virus) transduced cells, through the appearance of heterotopic bone. Quantification of protein levels of SP and CGRP within the tissues, through ELISA, is shown in Figure 1A and B, respectively. Both proteins appear to be significantly elevated (P_0.0005), compared 2750 NEUROGENIC INFLAMMATION AND BONE FORMATION JOURNAL OF CELLULAR BIOCHEMISTRY to controls, within 24 h after induction of HO, and again at 72 h (P_0.005) and 6 days (P_0.05) after induction. Expression, therefore, appeared somewhat cyclical, and statistical analyses, using a one-way ANOVA with a post-hoc Bonferroni test for comparison between time points, verified a significant drop in SP and CGRP between days 1 and 2 (P_0.005). This was followed by a significant rise between days 2 and 3 (P_0.005). The data suggests that BMP2 induced a substantial and immediate release of these proteins, which was attenuated, but then continued for the remainder of endochondral bone formation, through the appearance of mineralized bone (Fig. 1). Tissues were next immunostained for the presence of SP and CGRP and analyzed to determine if the expression of these factors was indeed associated with nerves. Figure 2 shows representative images of the expression of CGRP (red) and SP (green) within the tissues isolated 3 days after receiving either AdBMP2 or Adempty transduced cells. We observed a small amount of positive CGRP (red) and SP (green) expression associated with a mature nerve structure within control tissues, but expression was not found within the muscle itself (Fig. 2F and G). In contrast, in tissues receiving BMP2, CGRP and SP expression was found either within and adjacent to the nerve (CGRP, Fig. 2B) or adjacent to the nerve (SP, Fig. 2C). This suggests that the expression of these factors is associated with BMP2, as predicted [Bucelli et al., 2008]. INHIBITION OF HO IN ANIMALS LACKING TRPV1 The induction of neuroinflammatory mediators occurs through activation of sensory neurons by localized stimulus, or, in this case, secretion of BMP2. To determine if induction of neuroinflammation is contributing to HO, bone formation was quantified in animals that lacked TRPV1 (TRPV1 _/_), resulting in a functional loss of activity of sensory neurons. These TRPV1 _/_ animals lack a functional Fig. 1. Quantitation of substance P and CGRP protein by ELISA. Soft tissues, which encompass the site of new bone formation, were isolated at daily intervals from animals receiving either AdBMP2 (BMP2) or Adempty (control) transduced cells, and protein extracts were generated. A: Substance P total protein was quantified and statistically significant changes between the groups, as denoted by an asterisk, determined using a standard t-test; n¼4. B: CGRP total protein was quantified and statistically significant changes between the groups, as denoted by an asterisk, determined using a standard t-test; n¼4. _Denotes statistical significance. Error bars represent _SEM (standard error of the mean). Fig. 2. Photomicrographs of substance P and CGRP protein expression in tissues isolated 3 days after induction of HO. Tissues receiving cells transduced with AdBMP2 (BMP2) or Adempty cassette (control) were isolated 3 days after induction and immunostained with antibodies against substance P and CGRP. Expression of these factors was found within and adjacent to the nerves in tissues receiving BMP2, but was minimal in tissues receiving the Adempty cassette transduced cells. Hematoxylin and eosin stained serial sections, adjacent to the section used for immunostaining, 3 days after receiving AdBMP2 transduced cells (A) or Adempty cassette transduced cells (E). Arrows mark the nerves. Positive staining by the nerves in tissues receiving BMP2 (B and C) or by the nerves in control tissues (F and G) for CGRP (B and F; red color) or substance P (C and G; green color). D: A merged image of (B) and (C). H: A merged image of (F) and (G). JOURNAL OF CELLULAR BIOCHEMISTRY NEUROGENIC INFLAMMATION AND BONE FORMATION 2751 cationic channel on peripheral, sensory nerve terminals, which regulate neurogenic inflammation [Patapoutian et al., 2009]. We quantified the changes in SP and CGRP protein expression within tissues isolated from these knockout animals, and observed a significant suppression compared to the wild

type counterpart (Supplemental Fig. S1), although we did observe a slight increase in their expression upon delivery of BMP2. HO was induced in both TRPV1 _/_ and wild type mice (n¼7), and, after 10 days, the resultant bone formation was quantified through micro-computed tomography (mCT). Figure 3A shows a representative three dimensional reconstruction of the bone formation. Heterotopic bone volume within TRPV1 _/_ mice was inhibited significantly (P_0.05), as compared to wild type mice (Fig. 3B). NEUROINFLAMMATORY ASSOCIATED CHANGES IN MAST CELLS The reduction of HO when there is a lack of functional TRPV1 signaling suggests that this pathway may be functionally important to the process of HO. The next step in neuroinflammatory signaling involves recruitment of mast cells and their resultant degranulation, for the release of key enzymes involved in processing proteins essential for inflammatory signaling and recruitment. To determine whether mast cells were recruited to the site of new bone formation, muscle tissues from the hind limbs of wild type mice injected with AdBMP2 or Adempty transduced cells were isolated at daily intervals and then serially sectioned in entirety for quantification. There appears to be a trend toward more mast cells within the tissues undergoing HO, as compared to the control tissues (Fig. 4A). However, only day 2 shows a statistically significant increase in the number of mast cells. Since mast cells are known to migrate throughout the tissues, colocalization with specific tissue structures was also noted. As seen in Figure 4C, mast cells appeared to be scattered throughout the control tissues. However, within the tissues receiving AdBMP2 transduced cells, mast cells associated only with the nerves (Fig. 4B), in tissues isolated 2 days after induction of bone formation. As bone formation continues, the mast cells within the tissues receiving BMP2 continue to be localized within the nerve itself; however, a subset also appear within the vessel structures (data not shown). We did not see mast cells localizing within the nerve structures in control tissues at any time point. Mast cell degranulation leads to the release of degradative enzymes, such as tryptase and chymase. These enzymes are known to degrade or process other proteins, leading to their activation. Many of the enzymes are involved in tissue remodeling, including the nerve structure itself. To determine if mast cell degranulation could be a factor in heterotopic ossification, animals were pretreated with the drug sodium cromoglycate (cromolyn), which has been shown to prevent mast cell degranulation [Cox, 1967]. Following the pre-treatment with either cromolyn or a vehicle control (PBS), HO was induced and the resultant bone formation quantified 10 days later. Figure 5A shows representative images of three dimensional reconstructions of the resultant HO formation after cromolyn or vehicle control, PBS treatment. As can be seen in Figure 5B, quantification of bone volume of the HO shows a significant (P_0.05) decrease in animals after cromolyn treatment. The data collectively suggest a molecular model in which sensory neurons signal to induce neuro-inflammatory mediator expression and mast cell migration and degranulation, which ultimately facilitate HO. Since others have shown that progenitors reside within the nerve sheath [Adameyko et al., 2009] and can expand upon nerve remodeling after injury, we analyzed the nerves isolated in hind limb tissues from cromolyn or vehicle (PBS) treated animals after induction of HO by delivery of AdBMP2 transduced cells. We hypothesized cromolyn treatment would block nerve remodeling, and thus, the ultimate release of progenitors perhaps residing within the nerve. The tissues were immunostained for expression of a variety of stem cell markers, and, intriguingly, we observed changes in the subset of markers related to pluripotency. Figure 6A–F shows representative photomicrographs of tissues immunostained for expression of Nanog and Kru¨ ppel-like family of transcription factor 4 (Klf4) within the tissues isolated 2 days after induction of HO. As seen in Figure 6, in animals that received cromolyn, cells positive for these factors were observed throughout the nerve (Fig. 6B and C), as demonstrated by neurofilament (NF) staining. However, in tissues isolated from animals that received vehicle alone, these markers were significantly reduced, to completely absent, throughout the nerve (Fig. 6E and F), when compared to animals receiving cromolyn. We observed nanog þ and Klf4 þ cells within tissues isolated from animals injected with BMP2 producing cells without cromolyn treatment, but such cells were rare and often did not colocalize with the nerve. In addition, control tissues from animals Fig. 3. Microcomputational analysis of heterotopic ossification 10 days after induction with AdBMP2 transduced cells, in C57/BL6, wild type or TRVP1 _/_ mice. A: Three-dimensional reconstructions of representative samples for each group. B: Quantitation of bone volume. Statistically significant changes between the groups was determined using a one-way analysis of variance; n¼7; P <0.05. Error bars represent _SEM. receiving Adempty transduced cells, which were either cromolyn or vehicle treated, did not express these stem cell markers in the nerve (Fig. 6G–L), indicating that the observed changes in marker expression can be attributed to an effect of both cromolyn and BMP2. Both nanog and Klf4 have been implicated in maintenance of the pluripotential phenotype observed in embryonic stem (ES) cells [Hanna et al., 2009], with Klf4 actually enhancing the expression of the nanog gene in ES cells [Nakatake et al., 2006; Jiang et al., 2008]. Interestingly, the osteoblast specific transcription factor osterix was also found associated with the nerve sheath (Fig. 7). Osterix expression was observed in the nerve by co-staining with the neural marker neurofilament (Fig. 7G, H, and I), in tissues isolated 2 days after BMP2 induction, in the presence of cromolyn. These osterix positive cells also appeared to co-localize with

a portion of the primitive stem cell factors, suggesting that a subset of the cells may be undergoing differentiation (Fig. 7A–F).

DISCUSSION

Heterotopic ossification is a disorder involving rapid bone formation within muscle, tendon, and ligaments, adjacent to skeletal bone, and it has been linked to an elevation in BMP2 signaling [Shore and Kaplan, 2010]. Further, the incidence of HO appears to be dramatically increased in individuals who have sustained traumatic injury to the nervous system [Forsberg et al., 2009]. Here we determined whether localized changes in BMP signaling, which lead to heterotopic bone formation, can also alter peripheral nerve signaling through induction of neuroinflammation. Our results suggest that in the presence of BMP2, sensory neurons express mediators of neuroinflammation, resulting in the recruitment of mast cells and remodeling of the nerve structure. BMP2 has been shown previously to induce the expression of the neuroinflammatory mediators, substance P and CGRP, in sensory neuron cultures [Bucelli et al., 2008]. Here we quantified changes in these mediators, in vivo, after delivery of cells expressing BMP2. We found a significant and immediate elevation of both proteins, in relation to the control, which received the same cells transduced with an Adempty virus. Interestingly, we observed a strong correlation in elevation of these mediators, immediately following our delivery of BMP2. However, as the process continued over time, we observed a cyclical pattern in the expression of these mediators, with a significant decline in expression on day 2, followed by a significant rise in expression on day 3, and a trend towards another increase in expression by day 6. Although BMP2 would presumably be expressed for the first 3–4 days, prior to the rapid clearance of the

Fig. 4. Quantitation of mast cells in tissues surrounding the area of new bone formation. Tissue sections were stained with the mast cell stain, toluidine blue. Photomicrographs of random fields (five per section) were taken at 10_ magnification, for every fifth slide, throughout the entire hindlimb. Each field equals 5.2mm2. A: Quantitation of the average number of mast cells within the tissues at daily intervals after induction of HO. Statistically significant changes were determined using a standard t-test; n¼3 biological replicates. Seven slides were analyzed per tissue, and five fields per slide (35 images quantified per sample/time point). _Denotes statistical significance. Error bars represent _SEM. B: Representative photomicrographs of tissues isolated 2 days after receiving AdBMP2 (BMP2) or Adempty (control) transduced cells, stained with toluidine blue. Positive cells are highlighted with arrows.

cells [Fouletier-Dilling et al., 2007], the kinetics of BMP2 receptor signaling in this model is unclear. Intriguingly, one of the first steps is the rapid formation of brown adipocytes within the tissues [Olmsted-Davis et al., 2007]. We have previously shown brown adipocytes to be necessary for patterning of the new bone, by their unique capacity to regulate the oxygen microenvironment, not only by stimulation of new vessels, but also by uncoupling of aerobic respiration and ''burning'' of oxygen [Olmsted-Davis et al., 2007]. The result of this uncoupling is a release of energy as heat, which could potentially re-stimulate sensory neurons to respond and release substance P and CGRP. This could potentially explain the observed cyclical nature of the response, suggesting secondary or tertiary signaling events. Performing the assay in animals lacking TRPV1, we saw a significant decrease in the volume of heterotopic bone formed, compared to animals with functional TRPV1. The suppression, rather than complete ablation, suggests that other TRPV family members present on sensory neurons may also contribute to the induction of HO. Although we do not rule out alterations in other peripheral nerve signaling to the central nervous system in these animals, both substance P and CGRP were found to be significantly decreased in the TRPV1 _/_ mice. We still observed a trend towards an increase in substance P and CGRP upon addition of the AdBMP2 transduced cells. However, this was not above the normal background levels observed in wild type mice, nor was it statistically significant for CGRP, and the induction was over three folds lower for SP, so it is unclear whether this contributes to HO. The result that BMP2 does not induce SP or CGRP in TRPV1 _/_ mice is not surprising, as it has been previously shown that TRPV1 induces SP in response to capsaicin [Theriault et al., 1979] and that TRPV1 also controls heat- and acid-induced CGRP release from sensory nerves [Kichko and Reeh, 2009]. In addition, previous studies have revealed decreased injury-induced neuropeptide release in TRPV1 _/_ mice [Wang and Wang, 2005]. While TRPV1 is unquestionably involved in pain and neuroinflammation, TRPV has also been found to be involved in diabetes [Razavi et al., 2006] and obesity [Motter and Ahern, 2008]. Whether this is by the same mechanism proposed here, or by alternative mechanisms, remains undetermined. Consequently, deletion of TRPV1 could have additional pleiotropic effects. TRPV1 _/_ mice receiving Adempty transduced cells did not produce heterotopic bone, which is in line with our previous findings that Adempty transduced cells have not produced HO in any animal model we have tested [Olmsted-Davis et al., 2002]. Mast cells are known to be recruited to nerves during times of neuroinflammation. Upon degranulation, mast cells release a number of digestive factors, chymases, tryptases, and other enzymes, which can cleave proproteins, leading to their activation. These factors appear to be essential for tissue remodeling of not only the nerve, but also other surrounding tissues, including the vasculature [Johnson et al., 1988; Richardson and Vasko, 2002; Kleij and Bienenstock, 2005; Schaible et al., 2005; Kulka et al., 2008]. Nerve remodeling is thought to be part of neurite outgrowth, or the ability to remodel and extend neurons. Perhaps this process is utilized to innervate the newly forming HO. Alternatively, Adameyko et al. [2009] recently

demonstrated the presence of a stem cell population residing within peripheral nerves that would migrate from the nerve to undergo melanocyte differentiation. We quantified the number of mast cells after induction of HO and found a significant elevation in this population within 48 h, when compared to tissues receiving the control cells. We observed an upward trend in the number of mast cells on all days. However, perhaps due to the immune response evoked to clear the injected cells, there was also an increase in mast cell numbers in the control tissues, leading to a significant difference only on day 2. Further, we observed the mast cells, within the first 48 h, associating with the nerves and within the nerves, as compared to control tissues where the mast cells were usually located randomly throughout the tissues. It is intriguing that we observed the most significant difference at these early stages, since this appears to parallel our findings for the release of SP and CGRP within the tissues, suggesting mast cells may be recruited after release of these factors. Although not shown here, we did observe the mast cells associating with vessels, as well as nerves, later in the time course, suggesting that there is also a secondary vascular remodeling that may be triggered through this process. In line with these results, mast cells have been observed in the human, genetic disease of HO, fibrodyplasia ossificans progressiva [Gannon et al., 2001]. Also consistent with our observations, mast cells have previously been shown to be recruited by SP and CGRP [Yano et al., 1989; Itoh et al.,

Fig. 5. Microcomputational analysis of heterotopic ossification 10 days after induction with AdBMP2 transduced cells, in mice pre-treated with either cromolyn or vehicle control (PBS). A: Three-dimensional reconstructions of representative samples for each group. B: Quantitation of bone volume. Statistically significant changes between the groups was determined using a one-way analysis of variance; n¼9; P <0.05. Error bars represent _SEM.

 2010] and indeed have multiple receptors that bind to these inflammatory mediators [Kulka et al., 2008]. However, other modulators can bind and recruit mast cells, including neurokinin A, derived from pre-protachykinin 1, which is also the precursor for SP [Itoh et al., 2010]. Additionally, mast cells, like platelets, store serotonin, presumably derived from the gut, and release it in an active form upon degranulation [Theoharides et al., 1982]. Serotonin, which has recently been linked to skeletal bone remodeling [Ducy and Karsenty, 2010], is then capable of stimulating sympathetic neurons, which can ultimately regulate adipose production. Serotonin released by the gut has been reported to favor bone resorption during bone remodeling, whereas serotonin released in the hypothalamus appears to enhance bone formation and increase osteogenesis. Although it is still unclear how serotonin release contributes to HO, we have previously reported that brown adipocytes are made rapidly in the local tissues, presumably through activation of sympathetic neurons [Salisbury et al., 2010]. Thus, it seems likely that serotonin release may aid in the production and activation of adipocytes necessary for creating a microenvironment conducive for formation and patterning of bone. We next looked at whether the nerve remodeling was releasing cells that were essential to bone formation. As noted above, it has been previously demonstrated that precursors in peripheral nerves are the origin of skin melanoctyes. Therefore, mast cell degranulation, and subsequent nerve remodeling, was blocked using cromolyn, and we observed a significant decrease in HO. We next analyzed the nerves from these animals and found an increase in cells expressing markers of early stem cells (nanog and Klf4). These primitive markers were sporadic in the nerves of untreated animals, but completely covered the nerve in the cromolyn treated animals. This not only suggests that the early tissue changes lead to expansion of these cells, but also that the pool size of these cells within the nerve of untreated animals is extremely low, due to concomitant and rapid migration and differentiation. However, blockade of these latter steps with cromolyn leads to accumulation of these cells expressing primitive markers within the nerve. We note here, however, that the mechanisms of cromolyn action are incompletely understood. Although cromolyn is widely characterized as a "mast cell-stabilizer" (i.e., an agent that blocks the release of mast cell mediators following appropriate activation of the cell) that can suppress mouse mast cell function in vivo, its molecular targets are neither fully defined nor restricted to mast cells [Galli et al., 2008]. Moreover, while the mechanism of action of cromolyn mainly involves mast cell degranulation [Cox, 1967], other mechanisms, such as inhibition of neutrophils and eosinophil

Fig. 6. Peripheral nerves contain primitive stem cell markers after BMP2 induction in the presence of cromolyn. Photomicrographs of tissues isolated 2 days after induction of HO. Tissues from animals receiving cells transduced with AdBMP2 (BMP2) and pre-treated with either cromolyn (A–C) or vehicle, PBS (D–F) were isolated 2 days after induction, and immunostained with antibodies against stem cell markers, Klf4 and Nanog. Expression of these factors was found to co-localize to nerves residing within the area of new bone formation, upon cromolyn treatment. Tissues from animals receiving cells transduced with Adempty cassette (control) and pre-treated with either cromolyn (G–I) or vehicle (J–L) were isolated and immunostained the same. Nerves were identified by neurofilament (NF) staining (A, D, G, J; green color). Positive staining for Klf4 (B; red color) or Nanog (C; red color) was observed throughout the nerves in tissues isolated from animals receiving cromolyn at 2 days after BMP2 induction. In comparison, the nerves in BMP2 treated animals receiving vehicle appeared to lack positive staining for either Klf 4 (E; red color) or Nanog (F; red color). The nerves in animals receiving Adempty transduced cells also appeared to lack positive staining for either Klf4 (H, K) or Nanog (I, L), under both conditions. Tissues were counterstained with DAPI (B, C, E, F, H, I, K, L; blue color), which stains the nucleus of cells.

 induced chemotaxis [Bruijnzeel et al., 1990], have also been described. To our surprise, we observed osterix positive cells on the nerve as early as day 2, in the presence of cromolyn. There were also cells that expressed primitive stem cell factors, which appeared to simultaneously express

osterix, suggesting that these cells are osteoblast precursors. The majority of osterix positive expression was associated with the nerve. We also observed Klf-4 þ and nanog þ cells that were not associated with osterix, suggesting that these cells may have other potentials. Besides osteoblasts, another possible fate of these cells may be brown adipocytes, which we have shown previously to be critical for reduction of the oxygen tension in the microenvironment for cartilage formation [Olmsted-Davis et al., 2007] and for secreting VEGF for vessel formation [Dilling et al., 2010]. It has recently been noted that the Misty mouse phenotype [Sviderskaya et al., 1998], which is deficient in brown fat, is caused by a mutation in dock 7 [Blasius et al., 2009], a neuronal factor that regulates Schwann cell migration and neuronal polarity. It is intriguing to speculate that brown fat progenitors may also reside in peripheral nerves, particularly since TRPV1 responds to heat [Szallasi et al., 2007]. Additionally, it is interesting that the mutation in a single neuronal protein, dock7, not only dramatically increases HO in the Misty mouse [Olmsted-Davis et al., 2007], but also causes severe osteoporosis in the skeletal bone (Rosen C., unpublished). Further, we previously demonstrated the rapid formation of new vessels early after BMP2 induction [Dilling et al., 2010], suggesting that several types of tissues are being assembled simultaneously during this period. Osterix has previously been suggested to play a role in osteoblast lineage commitment of progenitors, suppressing the adipose phenotype [Cheng et al., 2003]. Perhaps the early osterix expression, 4 days prior to the appearance of osteoid matrix, may be part of a regulatory mechanism to preserve these cells for future osteogenic fate. Finally, although not highlighted in this manuscript, we did observe osterix positive cells,

Fig. 7. Peripheral nerves contain osterix-expressing cells after BMP2 induction in the presence of cromolyn. Photomicrographs of osterix expression within tissues isolated 2 days after BMP2 induction in the presence of cromolyn. Images of osterix expression (G; osterix red color, DAPI blue color) associated with the nerve (H; neurofilament, NF, green color). I: Osterix and NF, is a merger of (G) and (H). Images of the expression of osterix (A, D; osterix green color, DAPI blue color) and Klf4 (B; red) or nanog (E; red). C: Osterix and Klf4, is a merger of (A) and (B). F: Osterix and nanog, is a merger of (D) and (E).

at later times, in vessel-like structures that co-aligned with early endothelial markers, such as flk 1, which we have previously identified as characteristic of this early vasculogenesis [Dilling et al., 2010]. This notion supports the work of Lounev et al. [2009], suggesting that osteoblast progenitors reside within the newly forming vessels, have a Tie 2 marker, and are not derived from marrow [Kaplan et al., 2007]. Other investigators have also provided evidence for this concept of osteoblast progenitors being associated with the vasculature [Kolf et al., 2007; Medici et al., 2010]. This study is the first step in identifying a potential direct role for the peripheral nervous system in the induction of heterotopic ossification. The data suggest that early neuroinflammation, elicited in the presence of BMP2, may be capable of expanding a population of cells within the nerve, which can migrate and potentially contribute to a number of structures, rapidly assembling to produce HO. Suppression of these steps significantly decreases HO formation. Although it is unclear what affects this may have on the adjacent skeletal bone, the data suggest that there is direct communication with the hypothalamus, which could, in part, signal to impact bone remodeling. Understanding these earliest steps of HO will, for the first time, provide us novel targets for therapeutic intervention, which may ultimately lead to effective treatments. Finally, it is conceivable that such a mechanism could play a role in many other disease states, including neurofibromatosis and vascular calcification.

ACKNOWLEDGMENTS

This work was supported by grants from the US Department of the Army, Orthopedic Trauma to ARD (DAMD W81XWH-07-1-0214) and EAOD (DAMD W81XWH-07-1-0215), as well as a grant from NBIB (EB005173) and from the NIH (T-32 HL092332-06) to ER, and a Pre-doctoral fellowship from the American Heart Association (AHA 10815339F) and Kirschstein-NRSA (T32 HL092332-08) to ES. The authors thank Hua Chen of the Vector Development Laboratory, Baylor College of Medicine for vector preparation.

REFERENCES

Adameyko I, Lallemend F, Aquino JB, Pereira JA, Topilko P, Muller T, Fritz N, Beljajeva A, Mochii M, Liste I, Usoskin D, Suter U, Birchmeier C, Ernfors P. 2009. Schwann cell precursors from nerve innervation are a cellular origin of melanocytes in skin. Cell 139:366–379. Anderson RM, Stottmann RW, Choi M, Klingensmith J. 2006. Endogenous bone morphogenetic protein antagonists regulate mammalian neural crest generation and survival. Dev Dyn 235:2507–2520. Apel PJ, Crane D, Northam CN, Callahan M, Smith TL, Teasdall RD. 2009. Effect of selective sensory denervation on fracture-healing: An experimental study of rats. J Bone Joint Surg Am 91:2886–2895. Baird EO, Kang QK. 2009. Prophylaxis of heterotopic ossification - an updated review. J Orthop Surg Res 4:12. Beiner JM, Jokl P. 2002. Muscle contusion injury and myositis ossificans traumatica. Clin Orthop Relat Res S110–S119. Bhatia M, Bonnet D, Wu D, Murdoch B, Wrana J, Gallacher L, Dick JE. 1999. Bone morphogenetic proteins regulate the developmental program of human hematopoietic stem cells. J Exp Med 189:1139–1148. Blasius AL, Brandl K, Crozat K, Xia Y, Khovananth K, Krebs P, Smart NG, Zampolli A, Ruggeri ZM, Beutler BA. 2009. Mice with mutations of Dock7 have generalized hypopigmentation and white-spotting but show normal neurological function. Proc Natl Acad Sci USA 106:2706–2711. Bruijnzeel PL, Warringa RA, Kok PT, Kreukniet J. 1990. Inhibition of neutrophil and eosinophil induced chemotaxis by nedocromil sodium and sodium cromoglycate. Br J Pharmacol 99:798–802. Bucelli RC, Gonsiorek EA, Kim WY,

Bruun D, Rabin RA, Higgins D, Lein PJ. 2008. Statins decrease expression of the proinflammatory neuropeptides calcitonin gene-related peptide and substance P in sensory neurons. J Pharmacol Exp Ther 324:1172–1180. Cavazzana AO, Miser JS, Jefferson J, Triche TJ. 1987. Experimental evidence for a neural origin of Ewing's sarcoma of bone. Am J Pathol 127:507–518. Cheng SL, Shao JS, Charlton-Kachigian N, Loewy AP, Towler DA. 2003. MSX2 promotes osteogenesis and suppresses adipogenic differentiation of multipotent mesenchymal progenitors. J Biol Chem 278:45969–45977. Cox JS. 1967. Disodium cromoglycate (FPL 670) ('Intal'): A specific inhibitor of reaginic antibody-antigen mechanisms. Nature 216:1328–1329. Dilling CF, Wada AM, Lazard ZW, Salisbury EA, Gannon FH, Vadakkan TJ, Gao L, Hirschi K, Dickinson ME, Davis AR, Olmsted-Davis EA. 2010. Vessel formation is induced prior to the appearance of cartilage in BMP-2-mediated heterotopic ossification. J Bone Miner Res 25:1147–1156. Ducy P, Karsenty G. 2010. The two faces of serotonin in bone biology. J Cell Biol 191:7–13. Forsberg JA, Pepek JM, Wagner S, Wilson K, Flint J, Andersen RC, Tadaki D, Gage FA, Stojadinovic A, Elster EA. 2009. Heterotopic ossification in highenergy wartime extremity injuries: Prevalence and risk factors. J Bone Joint Surg Am 91:1084–1091. Fouletier-Dilling CM, Bosch P, Davis AR, Shafer JA, Stice SL, Gugala Z, Gannon FH, Olmsted-Davis EA. 2005. Novel compound enables high-level adenovirus transduction in the absence of an adenovirus-specific receptor. Hum Gene Ther 16:1287–1297. Fouletier-Dilling CM, Gannon FH, Olmsted-Davis EA, Lazard Z, Heggeness MH, Shafer JA, Hipp JA, Davis AR. 2007. Efficient and rapid osteoinduction in an immune-competent host. Hum Gene Ther 18:733–745. Fu L, Patel MS, Bradley A, Wagner EF, Karsenty G. 2005. The molecular clock mediates leptin-regulated bone formation. Cell 122:803–815. Galli SJ, Grimbaldeston M, Tsai M. 2008. Immunomodulatory mast cells: Negative, as well as positive, regulators of immunity. Nat Rev Immunol 8:478–486. Gannon FH, Glaser D, Caron R, Thompson LD, Shore EM, Kaplan FS. 2001. Mast cell involvement in fibrodysplasia ossificans progressiva. Hum Pathol 32:842–848. Gugala Z, Olmsted-Davis EA, Gannon FH, Lindsey RW, Davis AR. 2003. Osteoinduction by ex vivo adenovirus-mediated BMP2 delivery is independent of cell type. Gene Ther 10:1289–1296. Hanna J, Saha K, Pando B, van Zon J, Lengner CJ, Creyghton MP, van Oudenaarden A, Jaenisch R. 2009. Direct cell reprogramming is a stochastic process amenable to acceleration. Nature 462:595–601. Hu-Lieskovan S, Zhang J, Wu L, Shimada H, Schofield DE, Triche TJ. 2005. EWS-FLI1 fusion protein up-regulates critical genes in neural crest development and is responsible for the observed phenotype of Ewing's family of tumors. Cancer Res 65:4633–4644. Itoh S, Nakae S, Velotta JB, Kosuge H, Connolly A, Tsai M, Adachi H, Galli SJ, Robbins RC, Fischbein MP. 2010. The role of recipient mast cells in acute and chronic cardiac allograft rejection in C57BL/6-KitW-sh/W-sh mice. J Heart Lung Transplant 29:401–409. Jiang J, Chan YS, Loh YH, Cai J, Tong GQ, Lim CA, Robson P, Zhong S, Ng HH. 2008. A core Klf circuitry regulates self-renewal of embryonic stem cells. Nat Cell Biol 10:353–360. Jiang X, Iseki S, Maxson RE, Sucov HM, Morriss-Kay GM. 2002. Tissue origins and interactions in the mammalian skull vault. Dev Biol 241:106– 116. Johnson D, Weiner HL, Seeldrayers PA. 1988. Role of mast cells in peripheral nervous system demyelination. Ann NY Acad Sci 540:727–728. Johnson RC, Leopold JA, Loscalzo J. 2006. Vascular calcification: Pathobiological mechanisms and clinical implications. Circ Res 99:1044–1059. Kaplan FS, Glaser DL, Shore EM, Pignolo RJ, Xu M, Zhang Y, Senitzer D, Forman SJ, Emerson SG. 2007. Hematopoietic stem-cell contribution to ectopic skeletogenesis. J Bone Joint Surg Am 89:347–357. Kaplan FS, Pignolo RJ, Shore EM. 2009a. The FOP metamorphogene encodes a novel type I receptor that dysregulates BMP signaling. Cytokine Growth Factor Rev 20:399–407. Kaplan FS, Xu M, Seemann P, Connor JM, Glaser DL, Carroll L, Delai P, Fastnacht-Urban E, Forman SJ, Gillessen-Kaesbach G, Hoover-Fong J, Koster B, Pauli RM, Reardon W, Zaidi SA, Zasloff M, Morhart R, Mundlos S, Groppe J, Shore EM. 2009b. Classic and atypical fibrodysplasia ossificans progressiva (FOP) phenotypes are caused by mutations in the bone morphogenetic protein (BMP) type I receptor ACVR1. Hum Mutat 30:379–390. Khairatkar-Joshi N, Szallasi A. 2009. TRPV1 antagonists: The challenges for therapeutic targeting. Trends Mol Med 15:14–22. Kichko TI, Reeh PW. 2009. TRPV1 controls acid- and heat-induced calcitonin gene-related peptide release and sensitization by bradykinin in the isolated mouse trachea. Eur J Neurosci 29:1896–1904. Kleij HP, Bienenstock J. 2005. Significance of conversation between mast cells and nerves. Allergy Asthma Clin Immunol 1:65–80. Kolf CM, Cho E, Tuan RS. 2007. Mesenchymal stromal cells. Biology of adult mesenchymal stem cells: Regulation of niche, self-renewal and differentiation. Arthritis Res Ther 9:204. Kulka M, Sheen CH, Tancowny BP, Grammer LC, Schleimer RP. 2008. Neuropeptides activate human mast cell degranulation and chemokine production. Immunology 123:398–410. Kwong FN, Harris MB. 2008. Recent developments in the biology of fracture repair. J Am Acad Orthop Surg 16:619–625. Lounev VY, Ramachandran R, Wosczyna MN, Yamamoto M, Maidment AD, Shore EM, Glaser DL, Goldhamer DJ, Kaplan FS. 2009. Identification of progenitor cells that contribute to heterotopic skeletogenesis. J Bone Joint Surg Am 91:652–663. Medici D, Shore EM, Lounev VY, Kaplan FS, Kalluri R, Olsen BR. 2010. Conversion of vascular endothelial cells into multipotent stem-like cells. Nat Med 16:1400–1406. Morrison SJ, White PM, Zock C, Anderson DJ. 1999. Prospective identification, isolation by flow cytometry, and in vivo self-renewal of multipotent mammalian neural crest stem cells. Cell 96:737–749. Motter AL, Ahern GP. 2008. TRPV1-null mice are protected from dietinduced obesity. FEBS Lett 582:2257–2262. Nakatake Y, Fukui N, Iwamatsu Y, Masui S, Takahashi K, Yagi R, Yagi K, Miyazaki J, Matoba R, Ko MS, Niwa H. 2006. Klf4 cooperates with Oct3/4 and Sox2 to activate the Lefty1 core promoter in embryonic stem cells. Mol Cell Biol 26:7772–7782. Olabisi RM, Lazard ZW, Franco CL, Hall MA, Kwon SK, Sevick-Muraca EM, Hipp JA, Davis AR, Olmsted-Davis EA, West JL. 2010. Hydrogel microsphere encapsulation of a cell-based gene therapy system increases cell survival of injected cells, transgene expression, and bone volume in a model of heterotopic ossification. Tissue Eng Part A 16:3727–3736. Olmsted-Davis E, Gannon FH, Ozen M, Ittmann MM, Gugala Z, Hipp JA, Moran KM, Fouletier-Dilling CM, Schumara-Martin S, Lindsey RW, Heggeness MH, Brenner MK, Davis AR. 2007. Hypoxic adipocytes pattern early heterotopic bone formation. Am J Pathol 170:620–632. Olmsted-Davis EA, Gugala Z, Gannon FH, Yotnda P, McAlhany RE, Lindsey RW, Davis AR. 2002. Use of a chimeric adenovirus vector enhances BMP2 production and bone formation. Hum Gene Ther 13:1337–1347. Oury F, Yadav VK, Wang Y, Zhou B, Liu XS, Guo XE, Tecott LH, Schutz G, Means AR, Karsenty G. 2010. CREB mediates brain serotonin regulation of bone mass through its

expression in ventromedial hypothalamic neurons. Genes Dev 24:2330–2342. Patapoutian A, Tate S, Woolf CJ. 2009. Transient receptor potential channels: Targeting pain at the source. Nat Rev Drug Discov 8:55–68. Razavi R, Chan Y, Afifiyan FN, Liu XJ, Wan X, Yantha J, Tsui H, Tang L, Tsai S, Santamaria P, Driver JP, Serreze D, Salter MW, Dosch HM. 2006. TRPV1þ sensory neurons control beta cell stress and islet inflammation in autoimmune diabetes. Cell 127:1123–1135. Richardson JD, Vasko MR. 2002. Cellular mechanisms of neurogenic inflammation. J Pharmacol Exp Ther 302:839–845. Salisbury E, Sonnet C, Heggeness M, Davis AR, Olmsted-Davis E. 2010. Heterotopic ossification has some nerve. Critical reviews in eukaryotic gene expression 20:313–324. Schaible HG, Del Rosso A, Matucci-Cerinic M. 2005. Neurogenic aspects of inflammation. Rheum Dis Clin North Am 31:77–101 ix. Shi Y, Oury F, Yadav VK, Wess J, Liu XS, Guo XE, Murshed M, Karsenty G. 2010. Signaling through the M(3) muscarinic receptor favors bone mass accrual by decreasing sympathetic activity. Cell Metab 11(3): 231–238. Shore EM, Kaplan FS. 2010. Inherited human diseases of heterotopic bone formation. Nat Rev Rheumatol 6(9): 518–527. Smadja DM, Bieche I, Silvestre JS, Germain S, Cornet A, Laurendeau I, Duong-Van-Huyen JP, Emmerich J, Vidaud M, Aiach M, Gaussem P. 2008. Bone morphogenetic proteins 2 and 4 are selectively expressed by late outgrowth endothelial progenitor cells and promote neoangiogenesis. Arterioscler Thromb Vasc Biol 28:2137–2143. Sottile V, Seuwen K. 2000. Bone morphogenetic protein-2 stimulates adipogenic differentiation of mesenchymal precursor cells in synergy with BRL 49653 (rosiglitazone). FEBS Lett 475:201–204. Sucosky P, Balachandran K, Elhammali A, Jo H, Yoganathan AP. 2009. Altered shear stress stimulates upregulation of endothelial VCAM-1 and ICAM-1 in a BMP-4- and TGF-beta1-dependent pathway. Arterioscler Thromb Vasc Biol 29:254–260. Svíderskaya EV, Novak EK, Swank RT, Bennett DC. 1998. The murine misty mutation: Phenotypic effects on melanocytes, platelets and brown fat. Genetics 148:381–390. Szallasi A, Cortright DN, Blum CA, Eid SR. 2007. The vanilloid receptor TRPV1: 10 years from channel cloning to antagonist proof-of-concept. Nat Rev Drug Discov 6:357–372. Takeda S, Karsenty G. 2008. Molecular bases of the sympathetic regulation of bone mass. Bone 42:837–840. Theoharides TC, Bondy PK, Tsakalos ND, Askenase PW. 1982. Differential release of serotonin and histamine from mast cells. Nature 297:229– 231. Theriault E, Otsuka M, Jessell T. 1979. Capsaicin-evoked release of substance P from primary sensory neurons. Brain Res 170:209–213. Tseng YH, Kokkotou E, Schulz TJ, Huang TL, Winnay JN, Taniguchi CM, Tran TT, Suzuki R, Espinoza DO, Yamamoto Y, Ahrens MJ, Dudley AT, Norris AW, Kulkarni RN, Kahn CR. 2008. New role of bone morphogenetic protein 7 in brown adipogenesis and energy expenditure. Nature 454:1000–1004. Urist MR. 1965. Bone: Formation by autoinduction. Science 150:893– 899. Vanden Bossche L, Vanderstraeten G. 2005. Heterotopic ossification: A review. J Rehabil Med 37:129–136. Wang L, Wang DH. 2005. TRPV1 gene knockout impairs postischemic recovery in isolated perfused heart in mice. Circulation 112:3617–3623. Yanagita M. 2009. BMP modulators regulate the function of BMP during body patterning and disease progression. Biofactors 35:113–119. Yano H, Wershil BK, Arizono N, Galli SJ. 1989. Substance P-induced augmentation of cutaneous vascular permeability and granulocyte infiltration in mice is mast cell dependent. J Clin Invest 84:1276–1286.